2007

Stirling Convertor Control for a Lunar Concept Rover

Gina Blaze
Cleveland State University

STIRLING CONVERTOR CONTROL FOR A LUNAR CONCEPT ROVER

GINA BLAZE

Bachelor of Electrical Engineering

Cleveland State University

May, 2006

submitted in partial fulfillment of requirements for the degree

MASTER OF SCIENCE IN ELECTRICAL ENGINEERING

at the

CLEVELAND STATE UNIVERSITY

December, 2007

This thesis has been approved
for the Department of Electrical and Computer Engineering
and the College of Graduate Studies by

_____

Thesis Committee Chairperson, Dan Simon

_____

Electrical and Computer Engineering/Date

_____

Ana Stankovic

_____

Electrical and Computer Engineering/Date

_____

Charles Alexander

_____

Electrical and Computer Engineering/Date

ACKNOWLEDGEMENTS

Thank you to my advisor, Dr. Simon, for helping me with this thesis.

Thank you to my NASA technical mentor, Michael Brace, for helping me with this thesis and encouraging me.

Thank you to my family, fiancé, and ACES mentor for standing by me and encouraging me.

Thank you to the NASA Glenn Research Center Thermal Energy Conversion Branch for their support.

STIRLING CONVERTOR CONTROL FOR A LUNAR CONCEPT ROVER

GINA BLAZE

ABSTRACT

NASA Glenn Research Center is developing various circuits for a lunar concept rover powered by both a stirling convertor and lithium ion batteries. To begin, a survey of six analog, non-power factor correcting controllers was done for an Advanced Stirling Convertor (ASC) design; one was selected to control the stirling convertor. Next, a constant power circuit and lithium ion battery charger was designed, built and tested based on simulation in PSpice. The constant power circuit enables the stirling convertor to maintain a constant power when additional power is required from the batteries.

TABLE OF CONTENTS

Page

LIST OF TABLES

Table **Page**

LIST OF FIGURES

Figure **Page**

CHAPTER I

INTRODUCTION

1.1 Stirling Convertors

Figure 1 describes the operation of a stirling convertor. It describes the various configurations of stirling machines and how each configuration operates. It also shows how a free piston stirling operates and the affect of operating and initial conditions on the operation of the convertors.

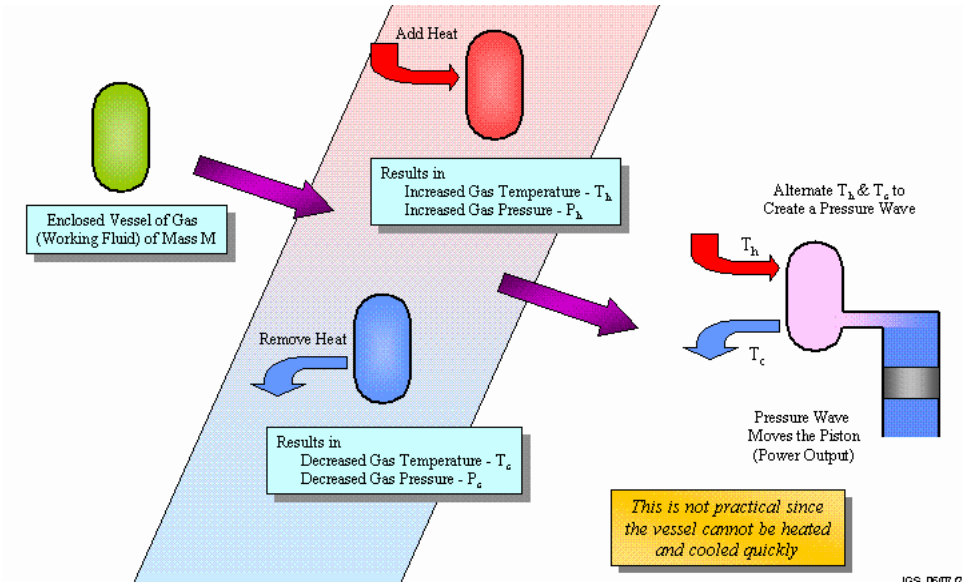

(a)

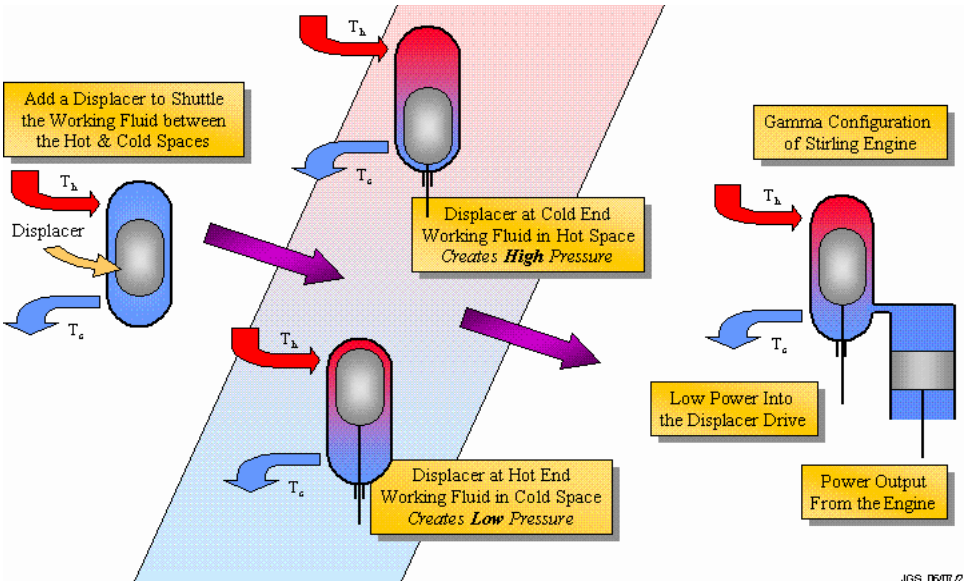
Add a Displacer to Shuttle the Working Fluid between the Hot & Cold Spaces
Displacer
Displacer at Cold End Working Fluid in Hot Space Creates High Pressure
Displacer at Hot End Working Fluid in Cold Space Creates Low Pressure
Gamma Configuration of Stirling Engine
Low Power Into the Displacer Drive
Power Output From the Engine

(b)

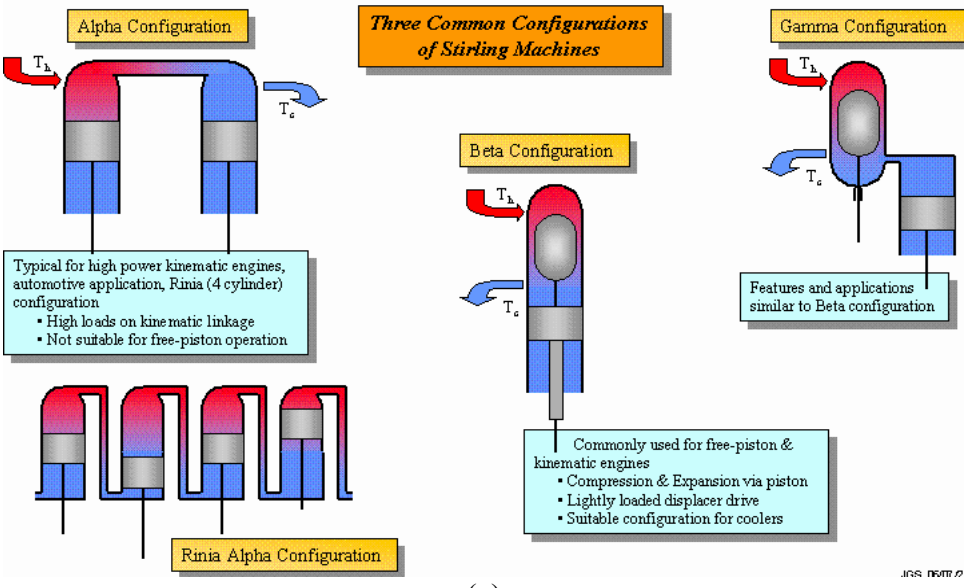
Three Common Configurations of Stirling Machines
Alpha Configuration
Typical for high power kinematic engines, automotive application, Rinia (4 cylinder) configuration
• High loads on kinematic linkage
• Not suitable for free-piston operation
Rinia Alpha Configuration
Beta Configuration
Commonly used for free-piston & kinematic engines
• Compression & Expansion via piston
• Lightly loaded displacer drive
• Suitable configuration for coolers
Gamma Configuration
Features and applications similar to Beta configuration

(c)

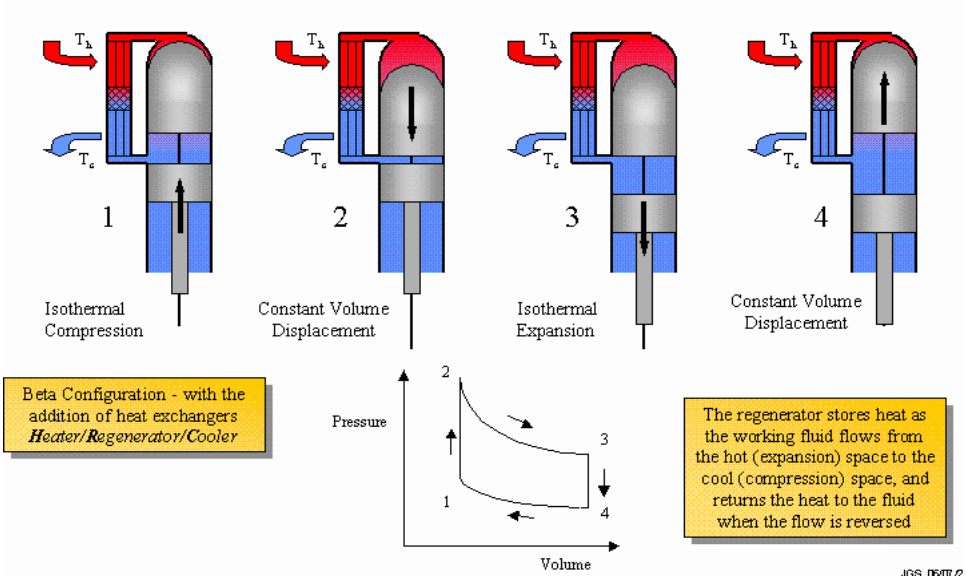
Th
Tc
1
Isothermal Compression
2
Constant Volume Displacement
3
Isothermal Expansion
4
Constant Volume Displacement
Beta Configuration - with the addition of heat exchangers Heater/Regenerator/Cooler
Pressure
Volume
The regenerator stores heat as the working fluid flows from the hot (expansion) space to the cool (compression) space, and returns the heat to the fluid when the flow is reversed

(d)

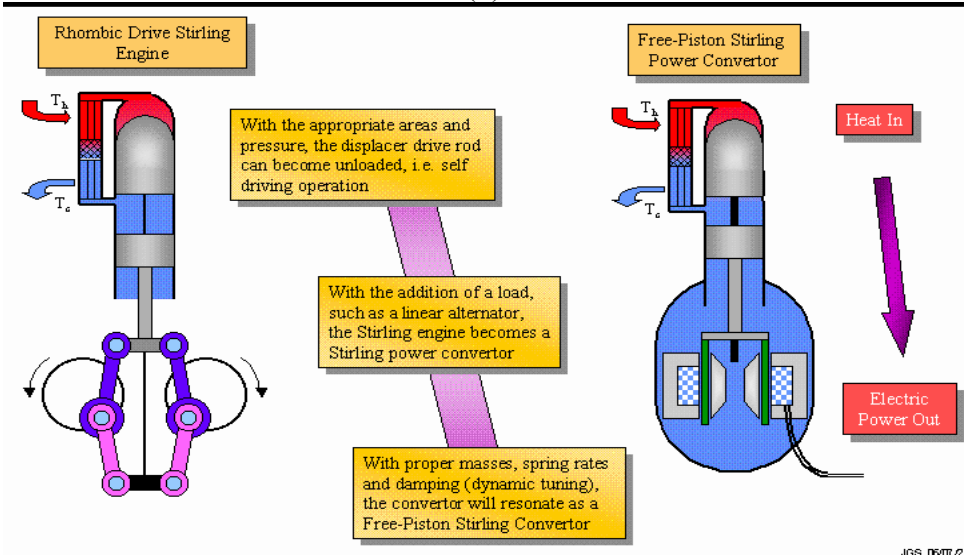
Rhombic Drive Stirling Engine
Th
Tc
With the appropriate areas and pressure, the displacer drive rod can become unloaded, i.e. self driving operation
With the addition of a load, such as a linear alternator, the Stirling engine becomes a Stirling power convertor
With proper masses, spring rates and damping (dynamic tuning), the convertor will resonate as a Free-Piston Stirling Convertor
Free-Piston Stirling Power Convertor
Heat In
Electric Power Out

(e)

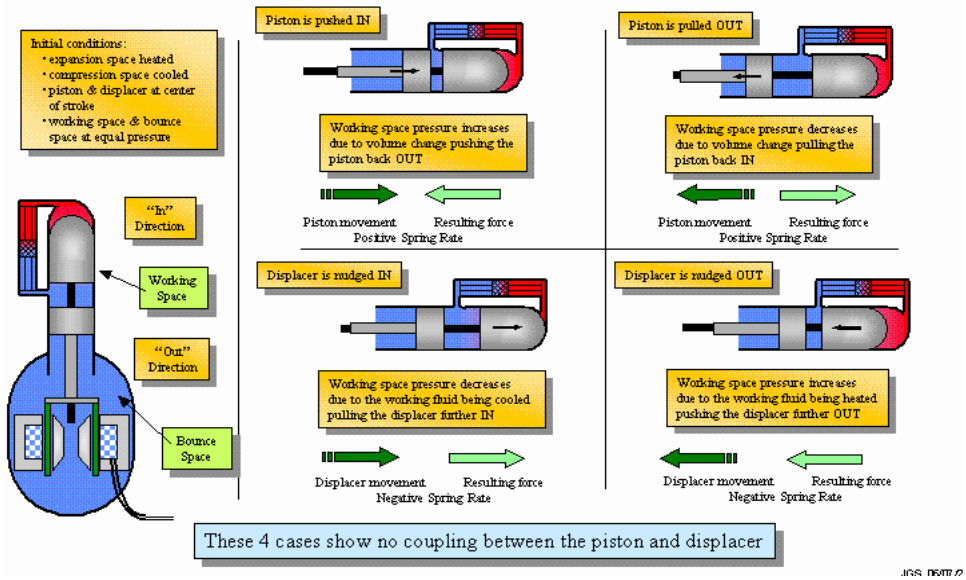

(f)

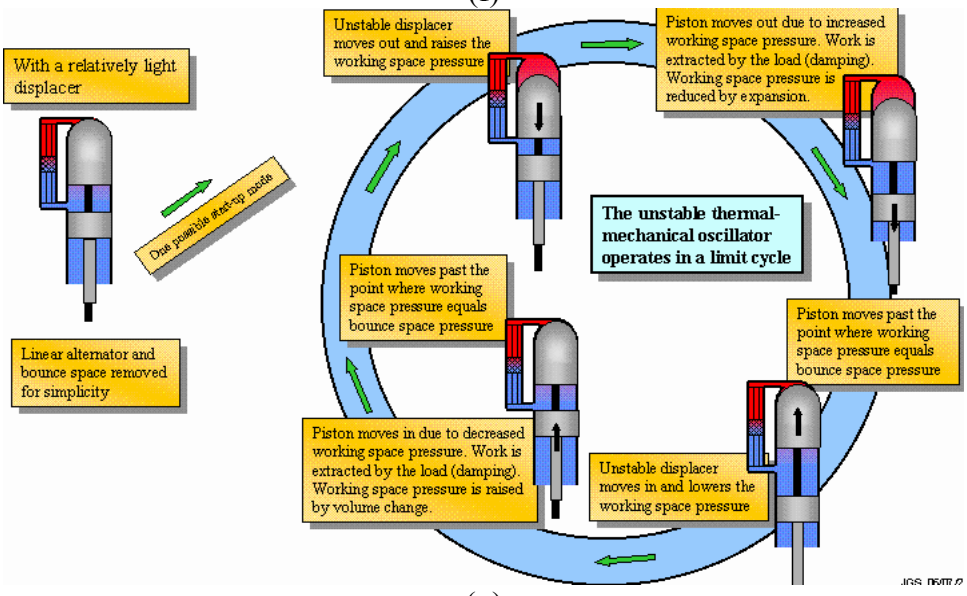

(g)

Figure 1. Operation of a Free-Piston Stirling Convertor [1]

1.2 History [2]

The stirling engine was invented by Reverend Robert Stirling and patented by him in 1816. The main subject of the original patent was a heat exchanger which Reverend Stirling called the economiser. The economiser enhanced the fuel economy in a variety of applications. The patent also described in detail the employment of one form of the economiser in air engine. This application is now known as the regenerator. An engine

built by Stirling was put to work pumping water in a quarry in 1818. The need for stirling to run at a very high temperature to maximize power and efficiency exposed limitations due to the material available in that time period. The few engines which were built in those early years had short and troublesome lives.

The stirling engine was considered as an alternative to a steam engine. Two key features made the early stirling engines attractive in the decades that followed. First, they provided greater efficiency than the steam engines. The second feature was the safety that they provided. A rigorous boiler code to guide the design of pressurized systems had not been developed. This resulted in numerous boiler failures and accidents that posed hazard to personnel as steam engines were in wide use. The Reverend Stirling was motivated to work on his engine in part due to the concern for the safety of the members of his parish. The early stirling engines were closed cycle, and operated with air as the working fluid at atmospheric pressure. This resulted in relatively large cylinders compared to steam engines. Stirling engines enjoyed commercial success and were commonly produced in the range of 0.2 to 4 kW.

Advances in the steel industry resulted in a tightly controlled product with more consistent material properties. In addition, a rigorous design code was established to guide the use of steel in pressurized systems and enhance safety. The design code used safety factors to provide uniform safety in boilers and piping, and included compensation for the known variation in material properties produced by the steel products of that era. This resulted in relatively safe, high-power steam engines being readily available from numerous manufacturers. Designers were able to push power density of steam engines to higher levels; the stirling engine became obsolete. Internal combustion engines were

developed by the mid 1800s, followed by the invention of the electric motor later that century.

By the early 1900s, the first general phase of stirling development had ended. This status did not change until the 1930's when pioneering research began at Philips Laboratories of Einhoven, Netherlands. The contributions were in several areas such as performance, the first of which was operating the cycle at elevated mean pressure. This increased the power density of the engine. The second major contribution by Philips was the use of gasses other than air as the working fluid. Significant increases in power and efficiency were found to be available in engines with helium or hydrogen as the working fluid. By 1954, they succeeded in liquefying air. Both gasses improved performance in engines but presented challenges in containment of the working fluid with hydrogen proving to be more difficult than helium since hydrogen could more easily permeate through polymer o-rings and in some cases, through high-temperature heater tubes. The third contribution by Philips was perfecting the regenerator to increase cycle efficiency. The regenerator is a porous matrix that absorbs heat from the working fluid when it flows from the hot expansion space to the relatively cool compression space, and returns the heat to the working fluid when it moves from the compression space toward the expansion space. The early engines developed by Reverend Robert Stirling more than 100 years earlier had a form of a regenerator known as an "economizer". This was one of the most important features of the invention, and was likely conceived by intuition. The work at Philips continued into the 1980's resulting in highly developed kinematic engines, which depended on linkages, seals, lubrication systems, and resulted in rotary shaft power output.

One of the applications envisioned for stirling at that time was an automotive engine. Efforts to develop automotive engines continued at low levels because of its multi-fuel capability, quiet operation, low emissions, and increased efficiency. Other features were that the engine needed no muffler, no catalytic converter, there was only one igniter, and there was no need for an oil change over the life of the engine. Interest in the automotive stirling engine increased sharply in the 1970s, motivated in the U.S. by the energy crisis. The most successful advanced heat engine effort was the Automotive Stirling engine project funded by the Department of Energy (DOE), managed by NASA, with prime contractor Mechanical Technology Incorporated (MTI) of Latham, New York. Initially, Ford Motor Company worked on a parallel effort, partnered with Philips on a four-cylinder engine designated the 4-215 that produced 127 kW. After approximately 1 year, Ford made a corporate decision to discontinue their involvement in stirling to focus their resources on a lean-burning Otto cycle engine.

By the mid-1980s, several generations of engines had been developed. The goals had been achieved of increasing power, reducing manufacturing cost, reduce start-up time, and improve throttle response. Engine efficiency was over 38 percent. A manufacturing study concluded that production cost would be less than a comparable Diesel engine. Early vehicle tests used American Motors Corporation Lerma and Spirit, which logged 2,300 and 13,763 miles respectively. Engines were integrated into three demonstration vehicles, which were put into service, two by the U.S. Air Force and one by the U.S. Postal Service. An automotive Stirling engine is shown in Figure 2 integrated into a D-150 pickup truck.

Figure 2. Automotive Stirling engine integrated into a D-150 pickup truck [2]

The engine resulted in a 10 percent improvement in fuel economy compared to spark ignition engines of the day. The D-150 pick up truck logged over 1,200 hours on the road, and more than 20,000 miles. The postal vehicle was used in daily service for a 3-month trial. Other technologies advanced during that time and the price of fuel stabilized, reducing the willingness of industry to embrace this new technology.

The invention of the free-piston stirling is accredited to William Beale, founder of Sunpower of Athens, Ohio in the 1960s. The free-piston stirling is a resonant device whereby the motions of a piston and a displacer are guided by spring-mass-damping system dynamics. Very generally, the total spring content comes from several sources including internal gas springs, mechanical springs, and other sources of spring that are inherent in the dynamic system, mass comes from the moving physical components, and damping comes from internal flow losses or the load for the power output produced. Development of early free-piston stirlings focused more on mechanical configuration, dynamics, reliability, and performance, but paid less attention to the conversion of linear motion to electricity. The potential of free-piston stirling for a range of applications was recognized by the 1970s resulting in the early research efforts for applications such as terrestrial generators, heat pumps, or space power conversion. By the 1980s, free-piston

stirling technology had evolved to the point where the intended performance of a new engine design could be achieved after a reasonable amount of development. Integration had improved and the designs were becoming more compact and more efficient. The integrated free-piston stirling engine with a linear alternator converts heat to electric power and had become known as a stirling convertor.

NASA had interest in stirling power conversion since the 1970s, envisioning that the technology could someday be developed into a long-life, high-reliability device. The emergence of free-piston technology resulted in MTI being commissioned to design the Space Power Demonstrator Engine (SPDE) and the Component Technology Power Convertor (CTPC) for the SP-100 project. The SPDE was intended to demonstrate the feasibility of free-piston Stirling power conversion for a 100-kWe system that would use multiple stirling convertors, heated by a nuclear reactor. The SPDE, shown in Figure 3, produced 25-kWe output with conversion of heat to electricity at about 20 percent efficiency.

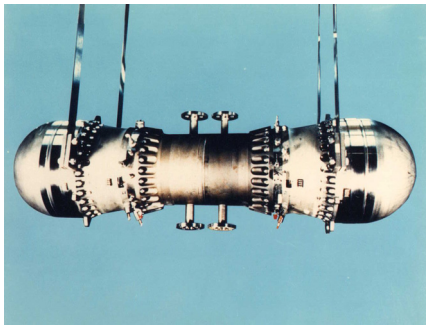

Figure 3. The Space Power Demonstration Unit [2]

It was a symmetrical design with two displacers, two power pistons, and two linear alternators, sharing a common expansion space. The SPDE was a dynamically balanced unit showing negligible vibration Since it was intended to demonstrate feasibility, the

SPDE was built with materials that limited the hot-end temperature to about 630 K (357 °C).

Convertors were being built that were more compact, operated more reliably, and achieved intended performance with minimal development. This can be viewed as a third phase of stirling development whereby free-piston stirling power conversion is able to operate at the intended level of performance, sometimes needing a little refinement following initial operation to achieve full performance, but to a great extent still lacking in system integration.

1.3 Technology Demonstrator Convertor (TDC) [2]

The Technology Demonstration Convertor (TDC) was developed by Infinia Corporation to convert heat from one General Purpose Heat Source (GPHS) module to electric power, and by 1999 had demonstrated efficiency greater than 20 percent from heat input to AC electric power output. The TDC had a mass of about 6 kg with anticipated mass reduction if flight development were undertaken. In support of DOE, Orbital Sciences Corporation (OSC) investigated several generator designs to assess feasibility of the integrated system. Some concepts included three GPHS modules and four Stirling convertors such that each convertor would operate at derated power, and in the event of failure of one convertor, the remaining three convertors would change their operating points to allow the generator to maintain full power.

The status of free-piston stirling for potential use in a radioisotope power system in space had changed measurably by mid-1999. Some of the features previously identified as “potentials” were demonstrated. A 10-W convertor based on non-contacting operation had operated for over 50,000 hr at Infinia with no change in performance. The

convertors operate to this day. Four pairs have operated in the past 4 years accumulating over 125,000 hours.

1.4 EE-35 Stirling Convertor [2]

Advances have been made in the pursuit of improved performance. The most common metric considered for convertors for space power applications is the specific power of the fully integrated system. The TDC that was used in the SRG110 design had specific power of the stirling convertor of about 15 W per kg. Through Small Business Innovative Research (SBIR), and an advanced technology effort at GRC, many of the technologies necessary for significant increase in specific power were developed. The first example of the increase in specific power was shown in the EE-35 developed by Sunpower. The EE-35 was sized for half of the heat from a GPHS module and achieved approximately 90 W/kg. High levels of specific power were projected to be possible in the past; however, development of the EE-35 has demonstrated this in hardware. With the higher specific power of the stirling convertor, it appears that a radioisotope generator could achieve approximately 8 W per kg, potentially enabling radioisotope electric propulsion missions. Further advances may be achievable through the use of ceramics or refractory alloys, but it would bring some amount of developmental risk. The most recent designs appear to be able to withstand even higher levels of random vibration than earlier designs. At the onset of the SRG110 project, stirling convertors had been tested to 12.3 random vibration. The EE-35 was tested at GRC in 2004 and survived nearly 24 g vibration. The only failures noted were breakage of a fill tube that would not be attached in a space mission, and failure of a controller, of the type that would not be used in a space mission. The EE-35's have operated over 3,000 hours.

1.5 Advanced Stirling Convertor (ASC) [3]

The objective of the Radioisotope Power Conversion Technology (RPCT) project is to advance the development of power-conversion technologies to provide higher efficiencies and specific power than the state-of-the-practice general-purpose heat source Radioisotope Thermoelectric Generator (RTG). Other goals include safety, long life (>14 year with well-understood degradation), reliability, scalability, multimission capability (in Mar's atmosphere or in the vacuum of space), resistance to radiation (from the GPHS or potential mission environments), and minimal interference with the spacecraft payload.

The ASC consists of the free-piston stirling engine integrated with a linear alternator to produce electricity. The ASC is pictured in Figure 4.

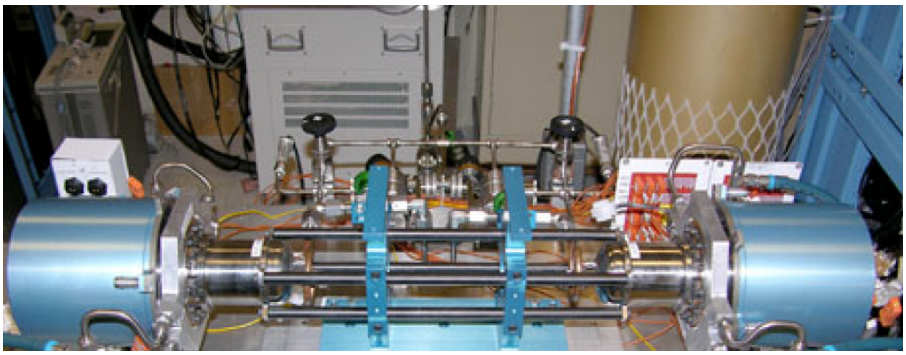

Figure 4. ASC in GRC Stirling Lab [3]

The key technologies in the ASC that enable high efficiency and low mass are the hydrostatic gas bearings, a moving-magnet linear alternator, high-frequency operation (>100 Hz), high-temperature heater head materials and fabrication processes, and high-temperature, high-porosity regenerators. The charge pressure of the ASC is 3.5 MPa, and the frequency is about 105 Hz. The four pairs of ASCs at NASA GRC have operated over 14,000 hours.

1.6 Advanced Stirling Radioisotope Generator (ASRG) Simulator [4]

An ASRG (Advanced Stirling Radioisotope Generator) simulator was designed for demonstrating stirling power conversion outside the laboratory environment. The setup is depicted in Figure 5. Two FTB (Frequency Test Bed) units were mounted in the dual-opposed configuration. FTBs are the initial ASCs designed before others are manufactured. Fins were placed on the rejection zone to allow air cooling. The mounting structure supports the convertors and provides containment for the air flow from the cooling fans. The outer panels of the containment allow observation of the convertors inside. Two fans located on the top of the container draw air in from the environment and discharge into the containment through the top panel. The cooling fins and fans were sized for operation in ambient air temperatures up to 110 °F.

Thermal energy is supplied to each hot end by an array of cartridge heaters inserted into a nickel heat collector. The hot end and regenerators sections were insulated using Kaowool^{TM} ceramic blanket. The inner insulation containment functions to direct the air flow exiting the cooling fins along the radial direction.

A helium management system made up of a pressure gauge, isolation valve and fill port was integrated into the container for charge pressure adjustment.

The ASRG simulator system was designed to require as little support equipment as possible, with the intended application being integration onto a rover. The ASRG Simulator has support equipment such as a tuning capacitor bank, control electronics, and ground support equipment (Figure 6). The tuning capacitor bank is necessary for power factor correction, and is connected in series with the alternator outputs. The control electronics contain the linear AC controller, protection circuit, constant power circuit, and

Li-Ion battery charger. Power is supplied to the user by one of the connectors on the front of the control electronics. The controller's parasitic load is located on the sides of the container, and dissipates full power while being air-cooled by natural convection. Any power not required by the user is dissipated in the parasitic load. The ground support equipment requires a connection to a 120 V_{AC}, 60 Hz source. It provides heater power and temperature control, cooling fan power, and centering and starting circuits. PID controllers maintain the hot-end temperature set-points. Over temperature protection is accomplished by using the alarm relay integrated into each PID controller. When either upper temperature limit is exceeded, the relay opens both heater circuits, removing power from the heaters.

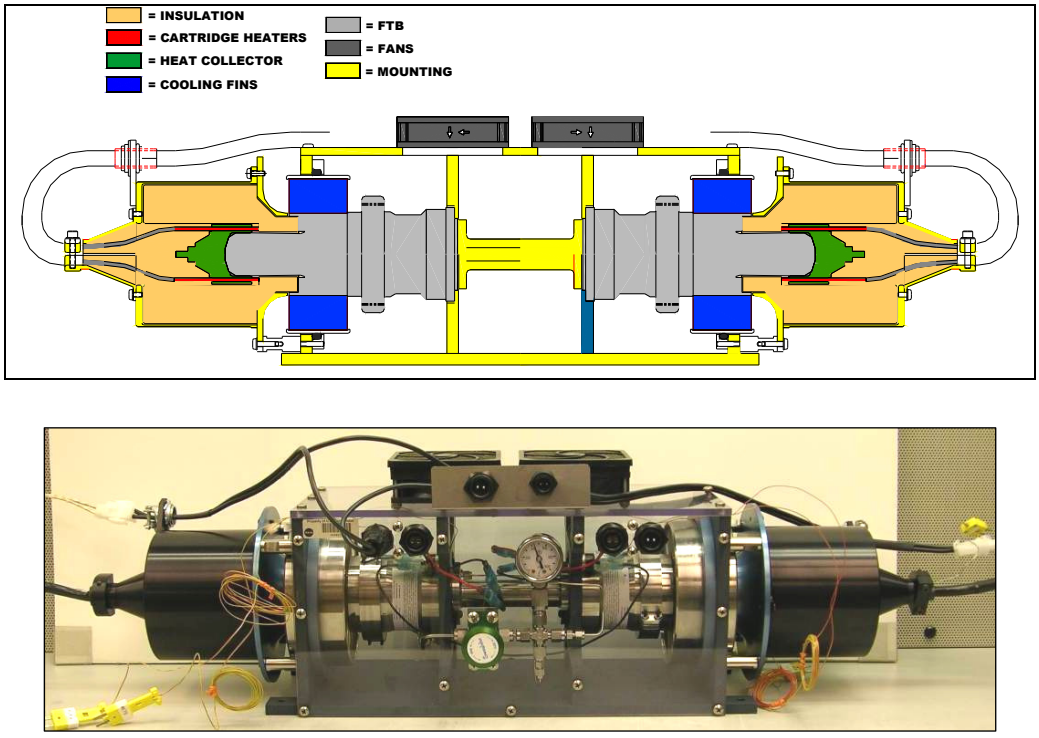

Figure 5. ASRG Simulator Setup [4]

Figure 6. Ground Support Equipment [4]

Figure 7 represents the total system used to operate, control, and power the rover. The stirling controller, constant power circuit, and Li-Ion battery charger will be the focus of this thesis. The smart block to control charging, protect stirling, and communicate state will be completed by another engineer. When the rover power exceeds that of the stirling convertors then the batteries supply the additional power needed. When the constant power circuit detects that more power is required then the diode becomes forward biased and the batteries start supplying power. The constant power circuit enables the stirling convertors to continue to maintain full power while the batteries supply the additional power required by the rover. The FTBs in the ASRG simulator supply 20 V, 6.5 A and 130 W at a frequency of 106 Hz. The linear AC controller, constant power circuit, and battery charger will be discussed in more detail in the following sections.

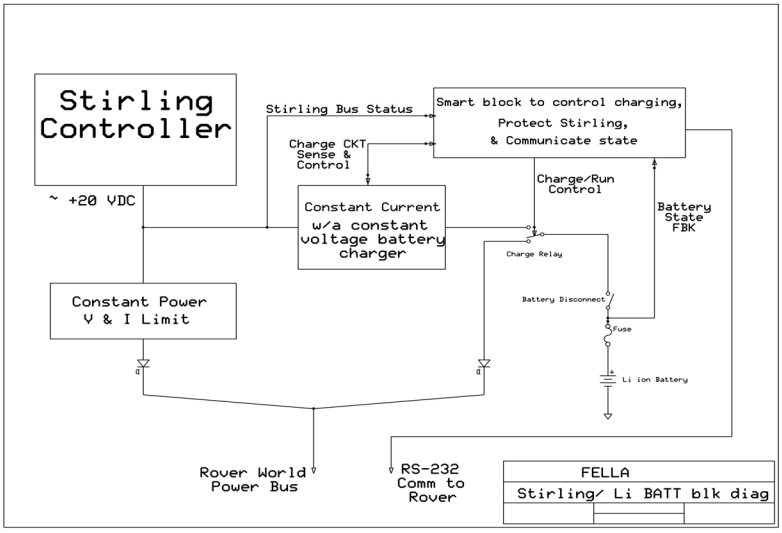

Figure 7. Electronic Support Equipment Block Diagram

1.7 Stirling Convertor Controller Development

In 1999, there were no designs for a flight controller. A flight controller must have high reliability over the life of the mission, and be able to operate in an autonomous manner, in addition to meeting specific requirements of a mission such as operating temperature and radiation tolerance. Since that time, there have been fully autonomous controllers designed for space and terrestrial applications, however, none of the designs for space have been built and tested. Results of the designs have indicated that a flight-worthy controller is possible, yet none exists and therefore, none of the extended operation tests is making use of a flight-like controller. An advanced controller is presently being developed at GRC that will make use of active power factor correction (APFC) to eliminate the need for tuning capacitors. The controller will be used in a future test that will be conducted in the thermal vacuum facility at GRC, and is intended to operate a pair of Advanced Stirling Convertors (ASC) in the dual-opposed configuration in extended operation. Work on the APFC is still in progress.

Previous controllers used tuning capacitors between the linear alternator and the controller to compensate for the inherent inductance of the coil of the linear alternator. Compensation of the inductance would force current through the linear alternator in phase with the velocity and the electromotive force generated, thereby minimizing reactive current and the associated resistive losses. A relatively new technique to minimize reactive current without the need for tuning capacitors is with power electronics. This technique senses the piston position or velocity, and uses a switching technique to force current to flow in the phase desired. Tuning capacitors were found to occupy significant volume, and with requirements for mounting, wiring, shielding, and the mass of the tuning capacitors themselves, resulted in controller mass greater than desired. GRC has studied the various options for configuring APFC controllers, and is developing controllers for use in air and in vacuum. Current APFC controllers being designed and tested at GRC are a part of the mass savings that enable the generator with specific power of 8 W/kg. Controllers of this type have been operated successfully at GRC in addition to a few other organizations.

A development effort of a power electronics controller for advanced stirling radioisotope generators was initiated by NASA Glenn Research Center and various contractors. According to [5] the power electronics controller is beneficial because it eliminates the tuning capacitors. The power electronics controller synchronizes dual-opposed convertors and maintains a fixed frequency operating point. The controller is single-fault tolerant and uses high-frequency pulse width modulation to create the sinusoidal currents that are nearly in phase with the piston velocity, eliminating the need for large series tuning capacitors. Based on a system-level trade study, mission planners

said that single-fault tolerance is the baseline for meeting space mission requirements. Several features of the controller design were identified. These include:

- Single Point Fault Tolerant
- Provide Controller and ASC telemetry and status
- Commandable ASC hot end temperature set point
- Compatible with battery or capacitor dominated spacecraft bus with a voltage range of 22 to 36 volts.
- Space and Source Radiation TID to 126 krad
- 17-year design life
- Controller Efficiency > 93%

These requirements are achieved through the use of three Field Programmable Gate Arrays (FPGA), use of H-switch design, and life and radiation requirement met via the proper parts selection.

According to [6] a free-piston stirling convertor end-to-end modeling effort produced a software-based test bed in which free-piston stirling convertors can be simulated and evaluated. The simulation includes all the components of the convertor. Three controllers have been studied using this model. It has aided in developing control engineering techniques for the free-piston stirling convertor. The three styles of controllers studied with this model are controllers with parasitic DC loading, controllers with parasitic AC loading, and controllers that maintain a reference current.

A controller with parasitic DC loading makes use of a rectifier circuit. Rectifier diodes allow current to flow in only one direction. The output voltage of the rectifier resembles the absolute value of the sinusoidal input voltage. The increasing portion of the

rectifier voltage is used to charge the filter capacitor. DC loads draw their energy from the filter capacitor. A rectifier circuit makes a good load for the stirling convertor as long as the input voltage signal is in phase with the piston velocity. The fixed DC load is not a practical controller unless it allows the user loads to be drawn from the DC bus.

Controllers with parasitic AC loading also make use of a tuning capacitor to bring load current in phase with piston velocity. The resulting DC voltage is converted to a binary number in an analog-to-digital converter. The binary number at the output is used to close or open relays which connect/disconnect resistors at the AC bus. The original space power research engine application fitted the controller with a PID front-end that operated to automatically adjust the horizontal position of the characteristic to maintain set point amplitude under various conditions of end-use loading. A 2^{nd} generation digital controller was tested at GRC. It makes use of the zero-switched discrete parasitic resistors but the controller switches them not to synthesize a specific voltage controlled resistance characteristic but to directly maintain a voltage setpoint. The analog-to-digital converter is again used but it looks at the difference between terminal voltage and the setpoint voltage. The resulting binary representation of the error present at the ADC output is added to a binary register containing the representation of the connected parasitic resistance. Thus the error adds or subtracts from the connected load.

Controllers that maintain a reference current do not require tuning capacitors. This control method uses a position sensor to generate a position signal in order to bring the current into phase with the piston velocity. This controller uses power electronics techniques to synthesize the required current waveform. A control loop varies the current amplitude in order to maintain a certain operating point. The usual connection for dual

opposed stirling convertors is to connect the two alternator outputs together through tuning capacitors. Unless they are locked together electrically, it has been found they drift out of synchronization. Using this type of controller, it may be possible to run without electrically connecting the two outputs. The signals must have identical frequencies and they must provide a load that satisfies the basic stability criterion.

1.8 Stirling Convertor Applications

Future application of NASA multi-kilowatt free-piston stirling convertors have been considered according to [7]. These applications began when President Bush in January 2004 announced a NASA vision for exploration. He proposed an ambitious program that plans to return astronauts to the moon by the 2018 time frame. The mission plan looks much like the Apollo missions. They start with a 4-day mission and gradually grow to 12+ days. The exact details of the landers and other structures on the moon are not available. The power levels are expected to rise from the level of a few kilowatts to anywhere from 25 to 50 kW. Past studies have shown that a solar array/regenerative fuel cell system is exceptionally massive for a 20 kW system. Dynamic conversion systems powered from thermal sources have been shown to be potentially lighter. There is an opportunity to develop new, larger free-piston stirling convertor systems to meet future NASA needs.

Stirling isotope power systems for stationary and mobile lunar applications were considered according to [8]. A significant emphasis on the development of a wide range of capabilities on the lunar surface is a stepping-stone to further space exploration. One candidate system to provide electrical power is made by coupling the General Purpose Heat Source (GPHS) with a high-performance stirling convertor. The practical power

range of the GPHS/stirling convertor system with conductively coupled hot-end designs for use on the lunar surface has been considered. Unique issues concerning stirling convertor configurations, integration of the GPHS with the stirling convertor, controller operation, waste heat rejection, and thermal protection have been explored. The evaluation process of understanding the interaction between the wide range of unique lunar environments and the selection of key systems operating characteristics and the power systems design is important. As power levels rise the interface between the GPHS and stirling and the stirling and radiator begins to dominate systems mass then material selection becomes more important.

1.9 Contributions of this Thesis

The ASRG simulator and Li-ion batteries will be used to power a lunar concept rover. This thesis discusses a survey of six controllers for the ASRG simulator. When the survey is complete, one controller is chosen to control the ASRG simulator. A constant power circuit was designed to maintain the power at the output of the controller when the Li-ion batteries are supplying additional power. A battery charger was designed to charge a Li-ion battery.

Chapter 1 of this thesis discusses past and present research on the topic of stirling convertor controllers and applications. Chapter 2 discusses the stirling convertor controller option evaluation. Chapter 3 discusses the constant power circuit design and bench testing. Chapter 4 discusses the Li-Ion battery charger design and bench testing. Chapter 5 discusses the system integration of the constant power circuit and Li-Ion battery charger.

CHAPTER II

STIRLING CONVERTOR CONTROLLER

Stable operation of a stirling convertor is maintained by a controller. A stirling convertor controller regulates the alternating current produced by the linear alternator of the convertor. The regulated current is used to power a load. The controller is designed to maintain operation at a certain piston amplitude and hot end temperature. The controller allows some adjustment so that the operating point may be adjusted; hot end temperature or piston amplitude may be adjusted up or down. The piston amplitude is maintained by the regulation stage of each controller. The load of the controller is sized to dissipate all the power being produced by the convertor. If the controller did not dissipate all the power, the excess would flow into the resonating piston motion, increasing amplitude, and ultimately resulting in damage to internal convertor components. Similarly, if the controller dissipated more power than that being produced, the balance would be extracted from the resonating piston motion, causing a stall of the engine cycle. The controller also provides a regulated user voltage at its output. The controller rectifies the alternator output, and then produces a specified output voltage based on the load sizing.

The goal of the stirling convertor controller task was to design and build a small, efficient, and reliable controller for use on the ASRG simulator. Six methods of control were considered and each of the methods was analog and used tuning capacitors for passive power factor correction. No active power factor correcting control methods were investigated. The controller uses a tuning capacitor because the stator current must be in phase with piston velocity to achieve stable operation. Load current flows as a response to terminal voltage. When a tuning capacitor is used, terminal voltage is in phase with piston velocity. The phase discrepancy is caused by the inductance of the stator. It is balanced out by a capacitance to make a resistive circuit. In a resistive circuit, the voltage and current are in phase. One important consequence of this technique is that the tuning capacitor will only cancel the effect of the alternator inductance at a single frequency. If the operating frequency deviates from this value, the power factor correction will be reduced.

Originally, each control concept was designed for TDC operation. The designs required modification to accommodate the lower alternator voltage and higher power output of the ASCs and FTB convertors. Each controller was designed for both single convertor and dual-opposed pair operation. The circuit simulation software PSpice^{TM} was used to simulate operation of an ASC convertor pair on each of the controllers. A model of each controller circuit connected to the ASC linear alternators was constructed. The linear alternator was modeled as an AC voltage source using its nominal values for resistance, inductance, frequency, and output voltage.

The linear alternator is designed with a resistance and an inductance. Through the known values of inductance and frequency, the capacitance can be calculated as follows:

$$\omega = \frac{1}{\sqrt{LC}}$$

where $\omega = 2\pi f$ and $f = 106Hz$

$$\omega = 2\pi(106Hz) = 212\pi$$

$$(212\pi)^2 = \frac{1}{(L)(C)}$$

$$(212\pi)^2 (L)(C) = 1$$

$$C = \frac{1}{(212\pi)^2 (L)}$$

Each controller will be designed with a 50 $k\Omega$ potentiometer and a 5 V reference so that a connection can be made to the Labview Interface. The Labview Interface is an SPI (Serial Peripheral Interface) interface combined with an isolator and 50 $k\Omega$ digital potentiometer; it can be interchanged with a 50 $k\Omega$ manual pot. The potentiometer is used to control the piston amplitude of the convertor.

2.1 Controller Types

Six controllers, which have either been designed for a TDC or an EE-35 convertor, have been re-designed for ASC operation. Each controller was designed by Michael Brace [1] at NASA GRC with the exception of the linear AC controller. The linear AC controller was designed by both Michael Brace and Gina Blaze at NASA GRC. Three of the six controllers considered provide AC control.

2.1.1 Zener-diode

Figure 8 shows the zener diode based controller. The motivation behind the zener diode controller was to improve the reliability of the controller. The controller

accomplished this through staged loads. The AC from both alternators is converted to DC by a diode bridge and an energy storage capacitor. The loads are then applied in stages to the DC bus. The DC voltage is connected to the operational amplifiers only after it exceeds the breakdown voltage of the zener-diode. The output of each operational amplifier controls the state of a field effect transistor (FET), which functions to switch a resistance onto the DC bus. The voltage level at which each operational amplifier turns on is controlled by sensing resistors, which are sized so that the trip point of each operational amplifier is slightly higher than the previous one. As the DC voltage rises above the first trip point, the first operational amplifier will turn on, applying its associated resistance to the DC bus. If the DC voltage continues to increase, the next operational amplifier in sequence will turn on, applying more loads. This process continues until the DC voltage stops increasing or until all stages are on. As the DC voltage drops, the stages turn off one at a time in the reverse sequence.

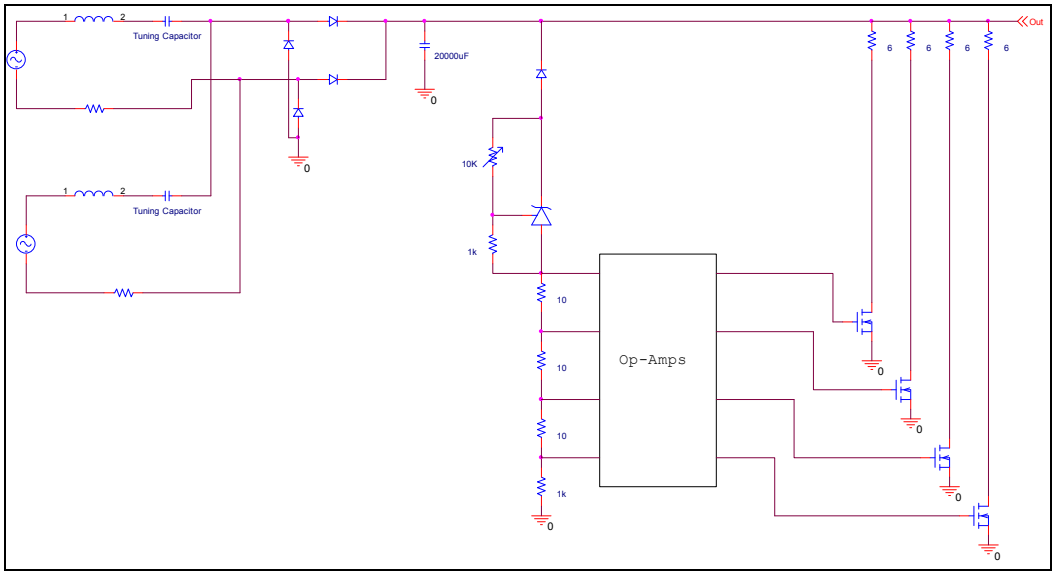

Figure 8. Circuit Model of Zener-Diode Based Controller

The load resistors are sized so that there is sufficient load available to maintain piston amplitude control at maximum convertor power output. The user may change the piston

amplitude by adjusting the breakdown voltage of the zener-diode. The piston amplitudes can be increased by increasing the DC voltage. This control method was considered the baseline for the evaluation effort. The zener-diode controller has been used to operate several convertor designs and has heritage in the GRC Stirling Research Lab.

2.1.2 Linear DC regulator

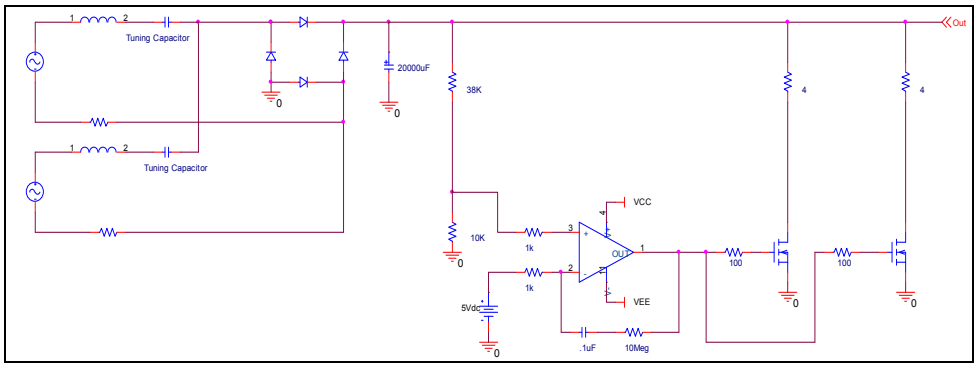

Figure 9. Circuit Model of Linear DC Controller

Figure 9 shows the linear DC regulator. The linear DC regulator method functions much the same way as the zener-diode method, but applies load in a directly proportional manner, rather than in discrete steps. As with the zener-diode controller, the AC from both alternators is converted to DC. However, the DC voltage is sensed by a voltage divider connected to a single operational amplifier. It generates a voltage proportional to the difference between the divided voltage and the reference voltage. This output is used to drive FETs in their linear range, rather than discrete on-off states. The FETs connect load resistors onto the DC bus, but also dissipate power themselves. The user may change piston amplitude by adjusting the voltage divider that controls the input to the operational amplifier. The motivation behind the design of the linear DC regulator is that is has continuously variable loads, which avoids the ON/OFF behavior of the zener diode controller, but retains the multiple redundant load stages.

2.1.3 Digital hybrid

Figure 10 shows the digital hybrid controller. The digital hybrid controller is similar to the zener-diode. The load can be adjusted in discrete steps, but not all steps are identical. Instead the resistors are sized to provide a linear change in load. Also the load is only updated once every half cycle of operation when the AC voltage crosses zero. The DC bus voltage is sensed by a voltage divider connected to an operational amplifier acting as a PID controller. The output of the PID loop is converted to a binary value by an analog-to-digital converter. The analog-to-digital converter is controlled by a zero crossing detector which generates a pulse each time the AC voltage crosses zero. The binary value controls FETs that switch resistors onto the DC bus. Any bit with a value of one will switch on the FET occupying the same position in the sequence as the bit. The resistors are sized so that each provides twice the load as the previous one. As the DC voltage increases, the binary value increases, which applies more load to the DC bus. The user may change piston amplitude by adjusting the voltage divider that controls the input to the PID loop. The digital hybrid was designed to essentially be a digital potentiometer that can dissipate power. The idea was to have something like a linear regulator, but avoid dissipating power in the MOSFETs by having them be discrete switches.

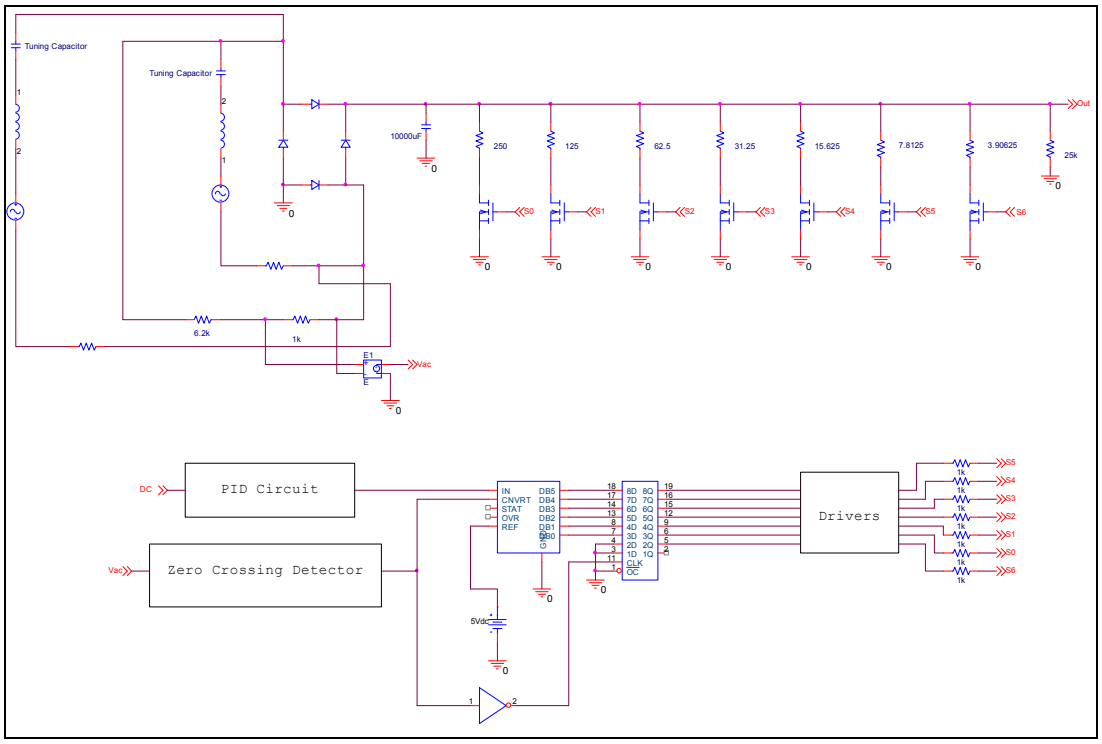

Figure 10. Circuit Model of Digital Hybrid Controller

2.1.4 Buck circuit with zener-diode

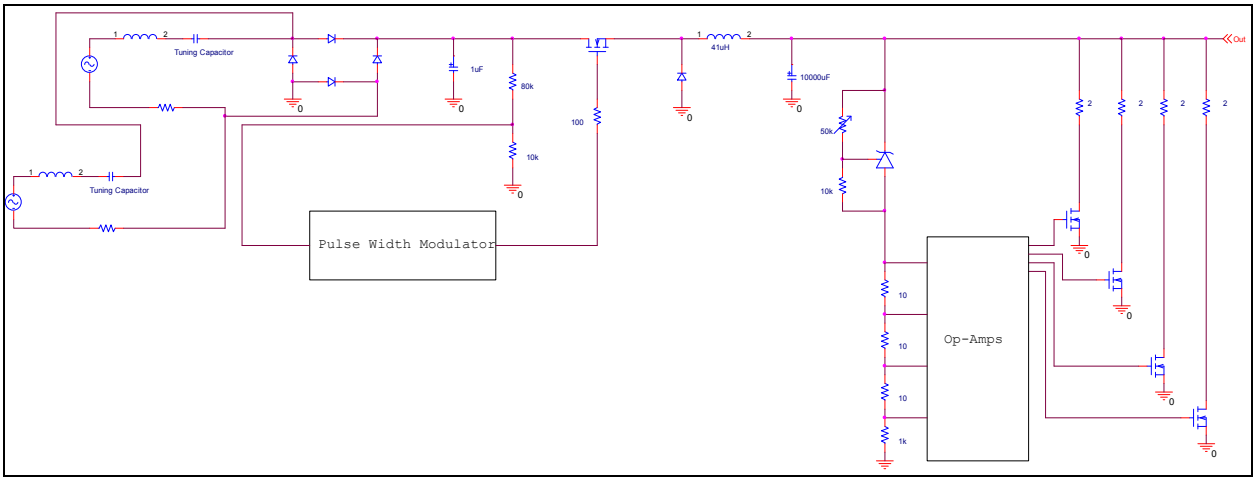

Figure 11. Circuit Model of a Buck Circuit with Zener-Diode

Figure 11 shows the buck circuit with zener-diode controller. The AC from the alternators is rectified by a diode bridge. However, the energy storage capacitor for DC conversion is not connected directly to the diode bridge. Instead, an inductor, diode, and FET are inserted between the diode bridge and energy storage capacitor. These

components, along with a pulse width modulator (PWM) comprise a buck circuit. The rectified AC voltage is sensed by a voltage divider connected to a PWM that switches the FET at 50 kHz. As the sensed voltage rises, the duty cycle of the PWM, and thus the FET, increases. When the FET is on, the AC is switched onto the buck circuit. The power flowing through the buck circuit must be dissipated and virtually any dissipative regulator will suffice. In this example, a zener-diode controller is used. The zener-diode controller functions the same as described above, but is used only to dissipate power. Coupling a buck circuit to a dissipative controller allows the load to be adjusted at a higher frequency than that of the alternator voltage. In this example, the load is adjusted 50,000 times each second. This allows the controller to respond more quickly to changes in convertor operation. One important consequence of this method is that the buck circuit reduces the output voltage below the desired range. Both the boost circuit with pulse width modulator and the buck circuit with zener diode were designed to improve the power factor.

2.1.5 Boost circuit with pulse width modulation regulator

Figure 12 shows the boost circuit with pulse width modulation regulator controller. This method operates similar to the buck circuit with zener-diode, but utilizes a boost

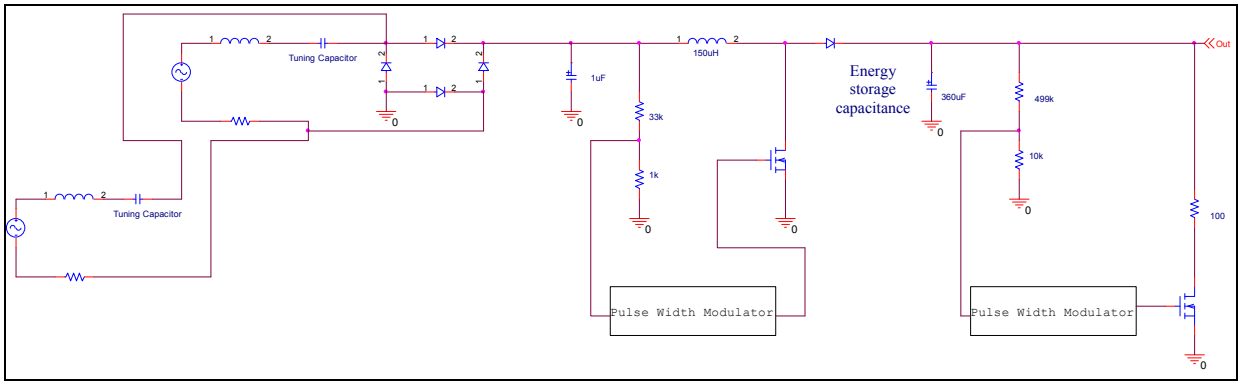

Figure 12. Circuit Model of Boost Circuit with Pulse Width Modulator

circuit. The PWM still switches a FET at 50 kHz, but the FET connects a boost circuit. Again, power must be dissipated after the boost circuit. In this example, another PWM, FET, and resistor are used to provide load. The duty cycle of the FET is adjusted by the PWM to control the amount of load applied to the DC bus. This method also permits quicker adjustment of the load. One important consequence of this method is that the boost circuit increases the output voltage above the desired range.

2.1.6 Linear AC regulator

Figure 13 shows the linear AC regulator controller. This method operates in a manner similar to the linear DC voltage regulator method, except that the rectified alternator voltage is used to control the load instead of the DC voltage. The AC voltage is passed through a separate diode bridge with no energy storage capacitor that would convert it to DC. The remainder of operation is identical to the linear DC voltage regulator method. However, in this example, four FETs and load resistor sets are used instead of two.

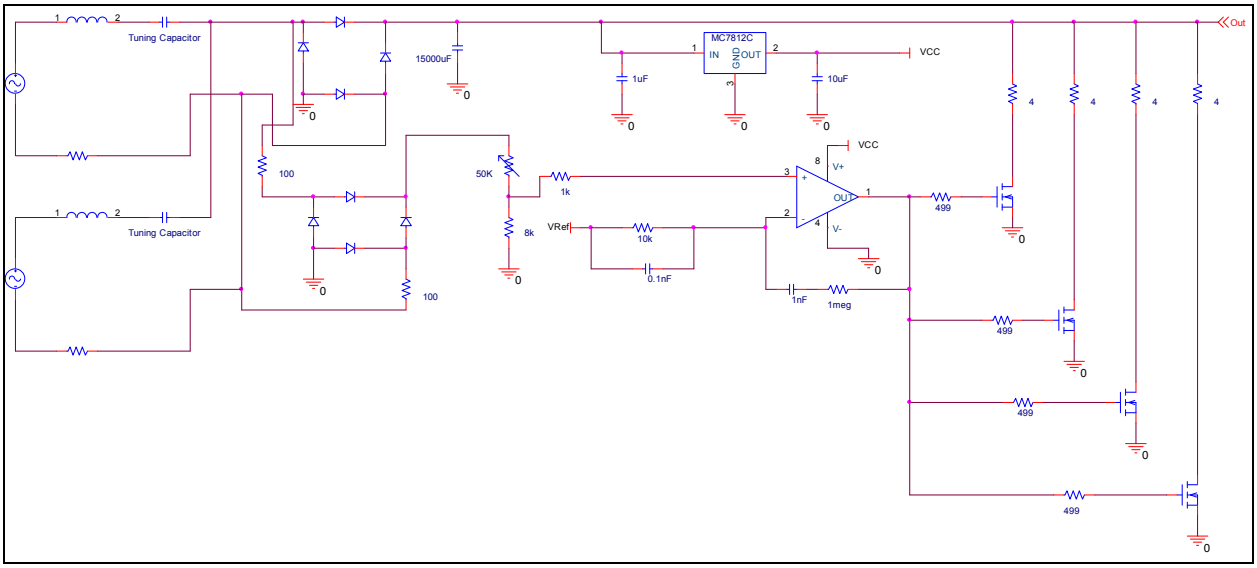

Figure 13. Circuit Model of Linear AC Controller

2.2 Initial Evaluation

The initial controller evaluation was based on results of PSpice modeling and general characteristics of each design. The circuit models were used to observe power dissipation in the loads, switching voltage, output voltage, and power flows. Observation of these items provided a first level indication of the performance of each option. Evaluation was also based on the criteria that follow.

2.2.1 Voltage Monitoring

The load can be controlled by monitoring either the AC or DC voltage. At a given frequency, the AC voltage is directly proportional to the piston amplitude. Therefore, the AC voltage is an accurate, real-time indicator of the piston amplitude. When the AC voltage is passed through the diode bridge rectifier, its full amplitude is still observable, but the waveform is altered so it occupies the positive region only. However, if the AC voltage is converted to DC by passing it through an energy storage capacitor, this amplitude is attenuated. The energy storage capacitor also has the effect of buffering changes in the alternator voltage output. For example, sudden changes in the AC voltage will be delayed because of the time constant of the capacitor. Therefore, AC bus voltage monitoring is desirable because it allows finer control of the load. The linear AC regulator, boost converter with PWM, and buck converter with zener-diode use AC bus monitoring. The zener-diode baseline, linear DC regulator, and digital hybrid use DC bus monitoring.

2.2.2. Load Staging

Staging refers to application of load in discrete increments. An example of the use of load staging can be seen in the zener-diode based controller. As the DC bus voltage

increases, each operational amplifier is activated in succession. Staging is desirable because it adds redundancy to the controller. Controllers can be designed to permit failure of at least one of the load connections while still maintaining piston amplitude at full power operation.

2.2.3. Power Dissipation Technique

Power can be dissipated in either resistors or transistors. The reliability of a transistor is reduced when used to dissipate power. For example, the power dissipating capacity of a transistor is typically reduced by 50 % for long-term, reliable operation. Because of this, use of resistors is desirable.

2.2.4. Tuning

Tuning is a process of selecting appropriate values for each parameter. The values are selected based on the design properties of the convertor. Many components in the controllers were tuned to provide a stable output, proper power dissipation, and efficient control by means of the switching of the op-amp stages. The following components were tuned in all six controllers: load resistors, filtering capacitors, gate resistors, and voltage dividers. The most complex of these components to tune was the filtering capacitor. Selecting a capacitor required careful consideration of the ESR (Effective Series Resistance) value. This value was added in the simulation. Each capacitor has its own ESR value and even amongst equivalent values of capacitance, the ESR value was variable.

The buck converter with zener and boost converter with PWM required additional tuning. The boost and buck circuits had to be redesigned. Tuning these two controllers was the most difficult. The digital hybrid was difficult to tune because the load resistors

had to be selected to give a linear change in load. The zener controller had one additional component to be tuned; the hysteresis resistor. The linear AC regulator and linear DC regulator did not require additional tuning.

The tuning process also included the addition of various components such as additional capacitors for filtering, a diode bridge, or a voltage regulator in place of a DC/DC converter. The tuning process varied amongst the six controllers. A detailed explanation of the tuning process for each controller will not be discussed. The main focus will be the advantages and disadvantages of each controller as well as the techniques used to evaluate each controller. Tuning was necessary to compare and understand each controller.

2.2.5. Necessity of DC-DC Converter

Some of the controller options required a DC-DC converter to return their output voltage to the desired range. The boost converter with PWM would normally output twice the linear alternator voltage. Similarly, the buck converter with zener-diode would normally output half the linear alternator voltage. A DC-DC converter is required on these two options to return the output voltage to 28 VDC. The digital hybrid controller also requires a DC-DC converter to compensate for the large overshoot in its output voltage. This overshoot is due to the time constant of the capacitor in the integrator of the PID circuit. Use of a DC-DC converter is undesirable because it adds a relatively large component to the controller.

2.2.6 Power Factor Controller (PFC)

The boost converter with PWM has a power factor controller. The PFC can control the follower boost allowing a drastic size reduction of both the inductor and the power

switch. It is a compact circuit that requires minimal external components. However this component does not have a PSpice model. Therefore the behavior of the PFC can not be observed before entering the lab.

Three of the six controllers were eliminated based on the advantages and disadvantages summarized in Table I. The linear DC regulator method was eliminated because a design for linear AC regulation exists, and AC voltage control is desirable. The boost convertor with PWM requires many more components than the other options, requires a DC-DC converter and has a power factor controller that can not be modeled in PSpice. The zener-diode and buck converter with zener-diode controller options both utilize load staging and dissipate power through resistors. However, the buck converter with zener-diode provides AC voltage control, making it more desirable.

Controller option	Advantages	Disadvantages	Eliminated
Zener-diode (baseline)	Resistor power dissipation Load staging	DC voltage monitoring	X
Linear DC regulator		Transistor power dissipation DC voltage monitoring	X
Digital hybrid	Resistor power dissipation Load staging	Transistor power dissipation DC voltage monitoring DC-DC converter required	
Buck converter with zener-diode	Resistor power dissipation AC voltage monitoring Load staging	DC-DC converter required	
Boost converter with PWM	AC voltage monitoring	DC-DC converter required	X
Linear AC regulator	AC voltage monitoring Load staging	Transistor power dissipation	

Table I. Controller Option Evaluation

2.3 Further Evaluation

The three remaining controllers, linear AC regulator, buck converter with zener-diode, and the digital hybrid were re-evaluated based on the following criteria.

2.3.1 Efficiency

The power required to operate the controller is supplied by the convertors, which reduces the net usable power. Internal losses may be attributed to housekeeping power. Housekeeping refers to the power required to operate the controller's resistors, op-amps, and voltage dividers. Another significant source of power loss may occur in the diode bridge during rectification. For example, the baseline zener-diode controller discussed above dissipates 26 W in the diodes at full power. The diode rectifier is a function of the current from the convertor; therefore the power dissipation in the diodes for each controller is equivalent. Schottky diodes were preferred over silicon diodes because they have a low forward voltage drop. The Schottky diode bridge significantly improves the efficiency of the controller; it dissipates 8.0 W compared to the 26 W of the silicon diode bridge. The efficiencies of the three remaining options were calculated using the circuit models. The linear AC regulator, buck converter with zener-diode, and digital hybrid efficiencies were calculated with a Schottky diode bridge. The zener-diode controller efficiency was calculated with a silicon diode bridge. These calculated values, along with the efficiency of the baseline zener-diode controller, are summarized in Table II.

2.3.2. Number of Components

The components were evaluated based on their sensitivity, size, and complexity. The number of components affects the testing of the controller. Identifying a failure during

testing is difficult in a controller which has many components. The linear AC regulator has the fewest components. The buck converter with zener has the most components.

An additional potentiometer adds to the complexity of the controller. The buck converter with zener is the only controller of the three that is designed with two potentiometers. It requires the most demands from the user because the user will have to verify two pot settings as well as adjust each of them.

The filtering capacitor and the load resistors were the most sensitive components. The filtering capacitor has a rated tolerance of +/- 20%. Each controller was tested with this specification. A 10,000 uF capacitor was tested at 8,000 uF and 12,000 uF. Changes in the filtering capacitor affect the output voltage stability and steady state value of the controller. Higher values of capacitance diminish the stability of the output voltage. This is a result of the time constant increasing with the increase of capacitance. The buck converter with zener-diode was the only controller of the three sensitive to the filtering capacitor tolerances.

The digital hybrid was the only controller of the three sensitive to changes in the load resistors. The values of the digital hybrid load resistors must decrease by 50%. The gate of the FET on each resistor and FET pair is driven by a binary number. The least significant bit corresponds to the highest resistance. If one of the FET/resistor pairs fails then the controller will act to increase the binary number during the next half cycle. This in turn decreases the stroke significantly. Then the controller will act to increase the stroke significantly. This pattern will continue as long as one of the pairs fails causing the controller to become oscillatory.

The amount of space required to house the controller increases with the parts count. The heat sink is the largest component in each controller. For the designs considered a DC/DC converter and capacitor were much larger than other components. Each controller was designed with one output filtering capacitor and in some designs a voltage regulator replaced a DC/DC converter.

2.3.3. Stability

Stability refers to the ability of the controller to maintain its output voltage at a fixed value when the convertor operating conditions change. A steady output voltage indicates the controller is able to maintain tight control of the piston amplitude. The circuit models were used to quantify the stability of each option by observing the ripple and overshoot of the output voltage.

2.3.4 Summary

Table 2 summarizes these criteria for each of the three remaining controllers and the baseline zener-diode controller. The values for voltage stability, internal power consumption, and efficiency were calculated using the circuit models. The efficiency of the controller was calculated based on the power dissipation in the diode bridge. The power dissipation was measured in PSpice.

The linear AC regulator was selected because of its exhibits the best voltage stability, requires the fewest components, and has the highest efficiency. A disadvantage of the linear AC regulator is its use of transistors for power dissipation. The reliability of these transistors is not a concern because the power dissipation is below the de-rated value.

	Zener-diode (baseline)	Linear AC regulator	Digital hybrid	Buck converter with zener-diode
DC ripple (V)	0.3	0.08	0.5	0.4
DC overshoot (V)	1	1	11.2	0
Number of components	46	42	56	62
Heat sinks required	4	4	4	5
Sensitivity	None	None	Load resistance	Energy storage capacitance
Efficiency (%)	85.1	95.4	93.4	84.7

Table II. Controller option quantitative evaluation summary

2.4 Controller Waveforms

2.4.1 Linear AC Regulator

Figure 14 represents the input power of the linear AC regulator. The convertor is designed to have an output power of 130 W based on the linear alternator voltage of 20 V. The simulation produces a power of 129.371 W.

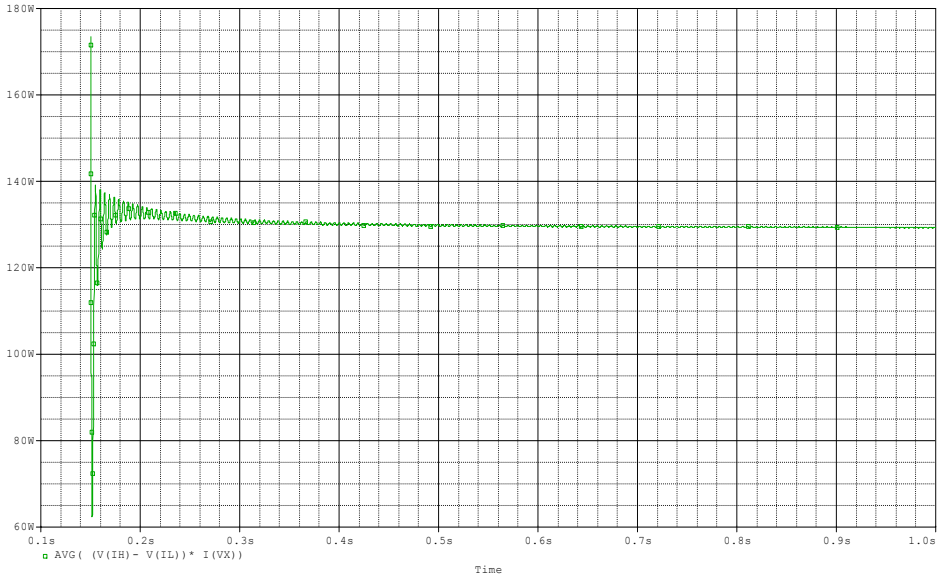

Figure 14. Linear AC Regulator Input Power

The ASRG simulator is designed with a linear alternator voltage of 20 V. As can be viewed by Figure 15, the simulation verifies that the controller produces a 20.299 V output.

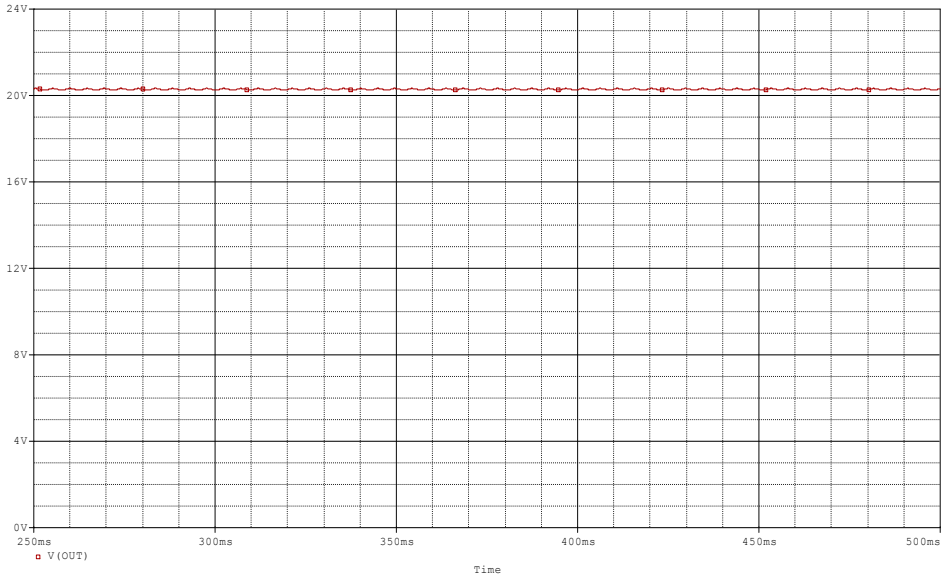

Figure 15. Linear AC Regulator DC Output Voltage

Figure 16 represents each of the four stages of the linear AC regulator. Each stage is regulating at 4.2451 V.

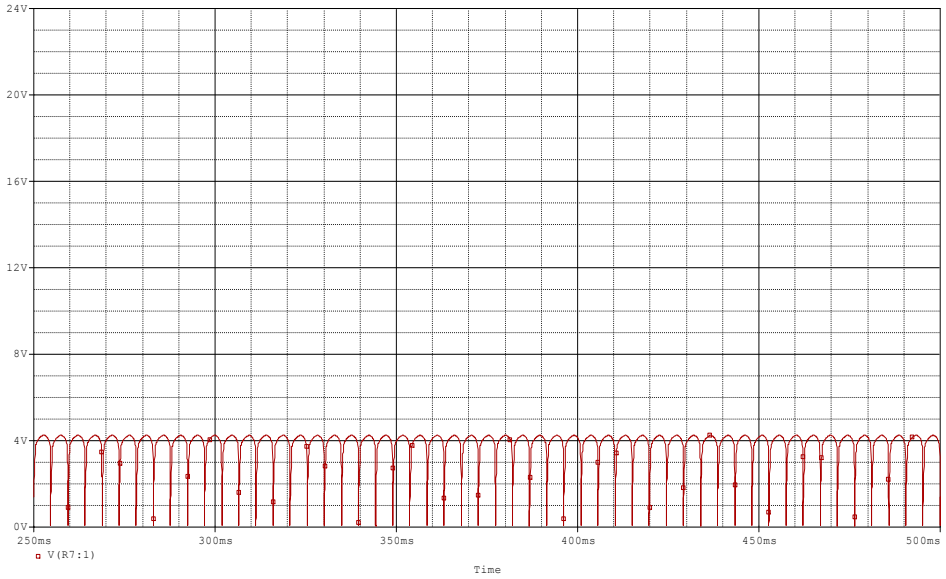

Figure 16. Linear AC Regulator Control Voltage

Figure 17 represents the power dissipated by the 2 ohm load. Power is dissipated both in resistors and MOSFET (IRFP350). Each of the eight 2 ohm loads dissipated 8.3944 W based on simulation in PSpice.

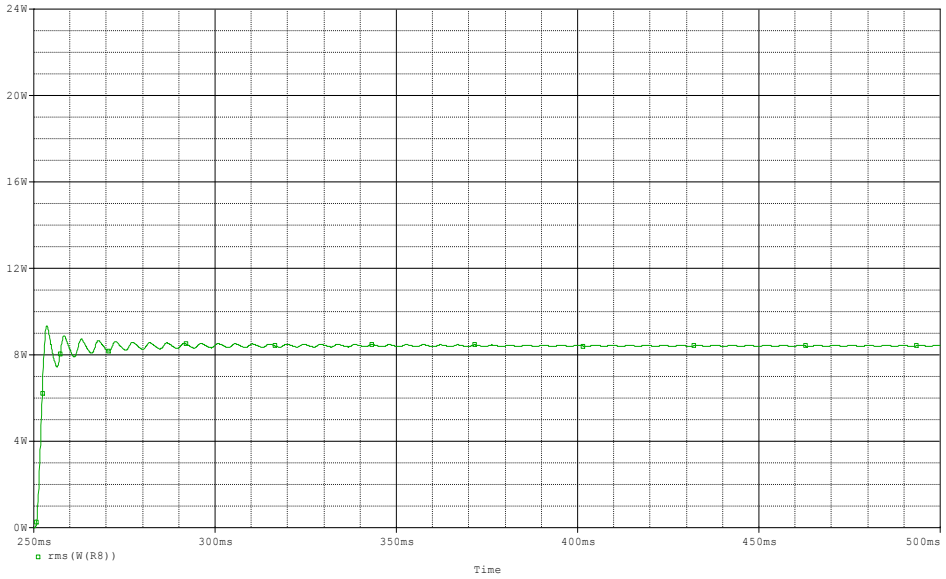

Figure 17. Linear AC Regulator 2 Ohm Load Power Dissipation

Figure 18 represents the power dissipation of the 1 ohm load. Each of the four 1 ohm loads dissipate 4.1972 W based on simulation in PSpice.

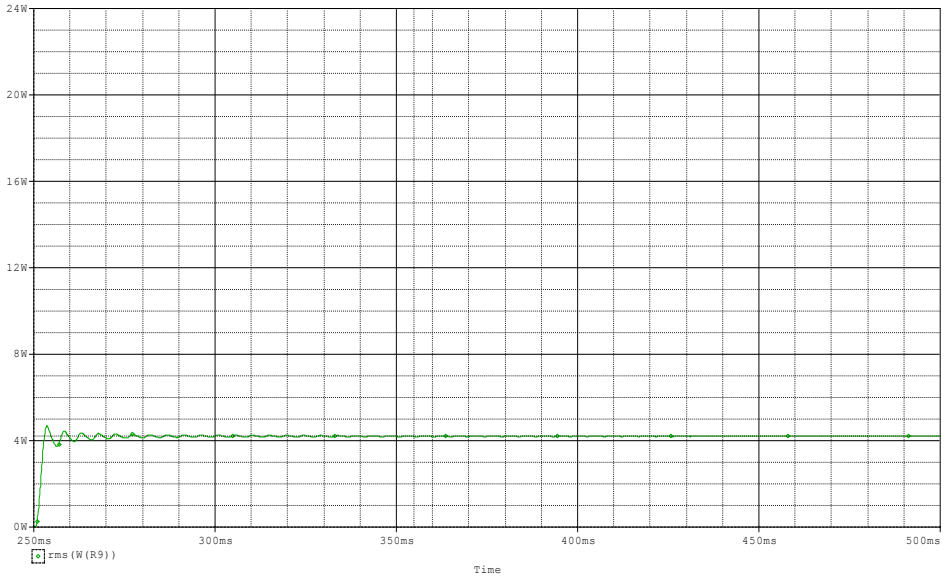

Figure 18. Linear AC Regulator 1 Ohm Load Power Dissipation

Figure 19 represents the power dissipation in each of the four MOSFET's. The power dissipation based on simulation in PSpice is 16.463 W. This is well below the de-rated value of the MOSFET, 50 W. The de-rated value was obtained from the specification sheet.

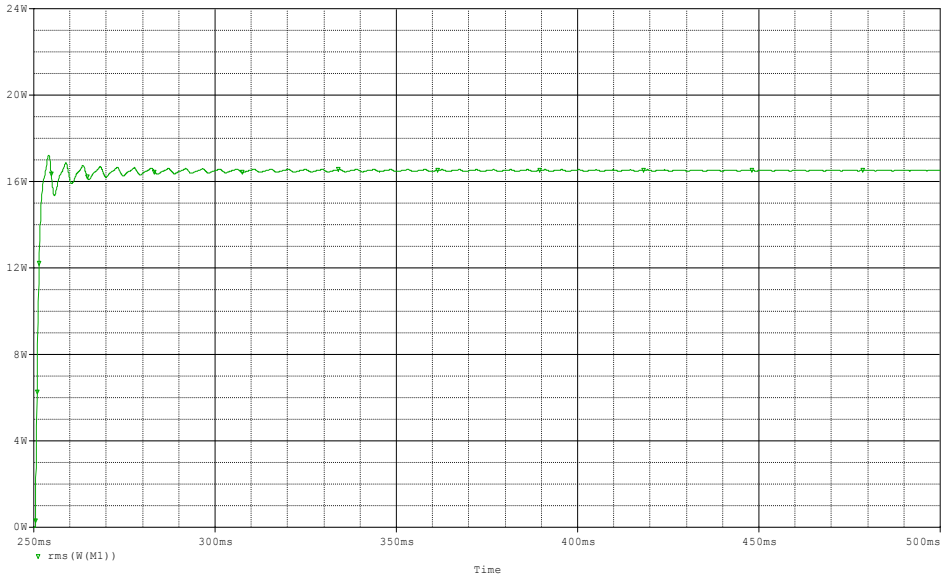

Figure 19. Linear AC Regulator MOSFET Power Dissipation

Figure 20 represents the AC input voltage of the controller; this is the voltage pre-diode bridge. The voltage is 20.818 V.

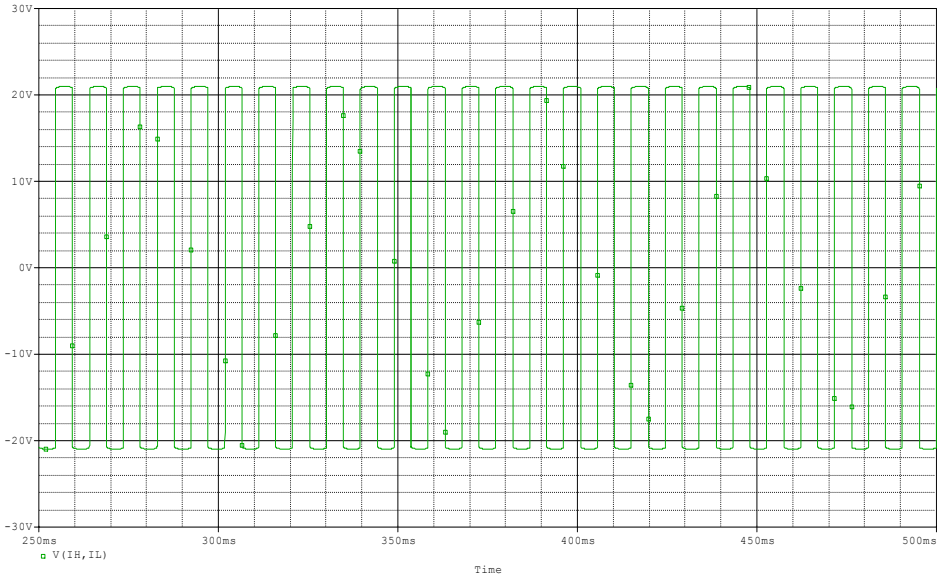

Figure 20. Linear AC Regulator AC Input Voltage

Figure 21 represents the power dissipation in each of the four schottky diodes. The power dissipation in each diode is 1.6669 W based on simulation in PSpice.

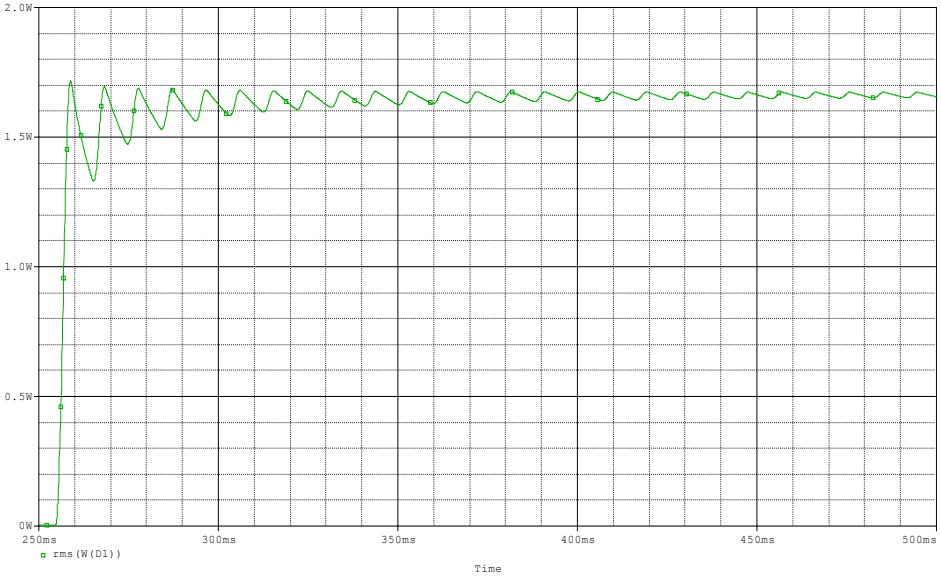

Figure 21. Linear AC Regulator Schottky Diode Power Dissipation

Figure 22 represents the capacitor ripple current. The ripple current was important when selecting the filtering capacitor. It was verified that the ripple current was within the specification listed on the datasheet. The filtering capacitor ripple current based on simulation in PSpice is 0.432875 A.

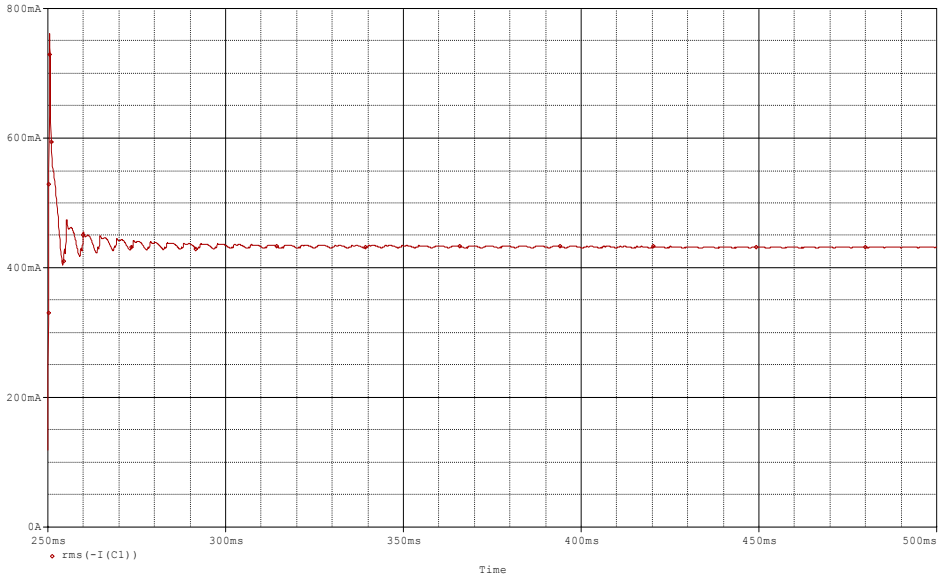

Figure 22. Linear AC Regulator Capacitor Ripple Current

2.4.2 Digital Hybrid Waveforms

Figure 23 displays the output DC regulated voltage. The steady state output voltage is approximately 23.9 V with a slight ripple on the order of a tenth of a volt and a settling time of 70 ms. The Digital Hybrid has an overshoot of 13 V and a steady state ripple voltage of 0.5 V.

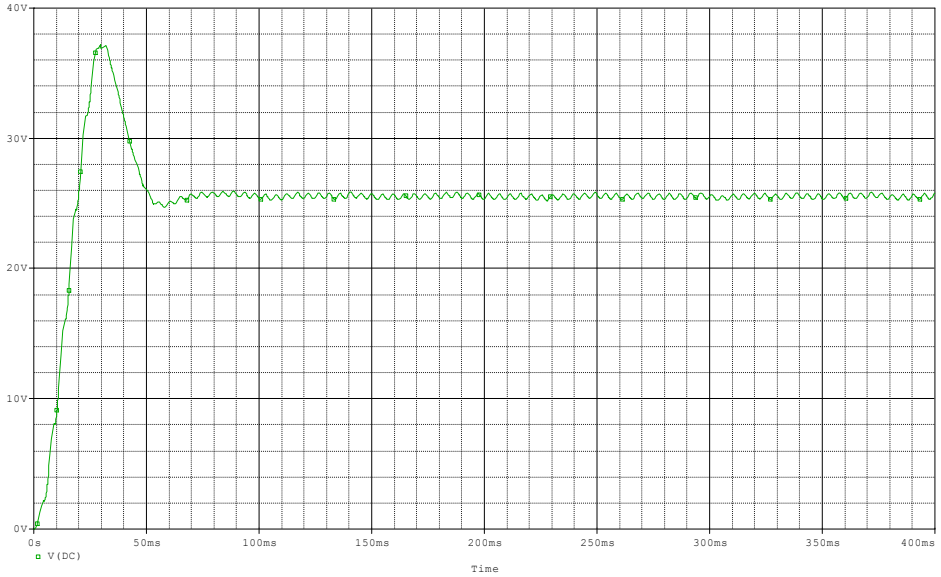

Figure 23. Digital Hybrid Regulated DC Output Voltage

Figures 24-29 display the switching of the MOSFET stages. The stages are used to regulate the DC output voltage. The switching is advantageous because not all of the MOSFET's are on all of the time. Therefore, if one stage fails, there are other stages available to compensate for this failure.

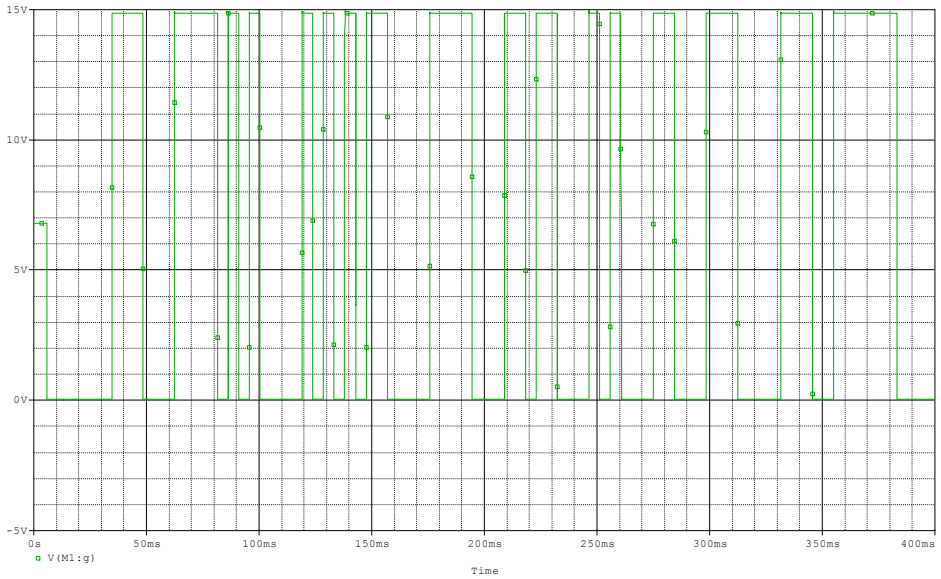

Figure 24. Digital Hybrid First Stage Switching

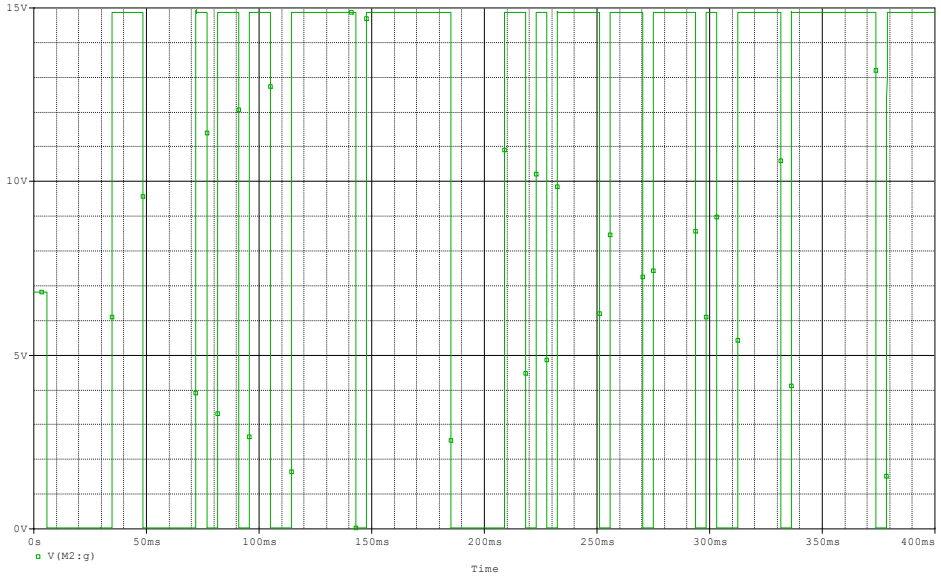

Figure 25. Digital Hybrid Second Stage Switching

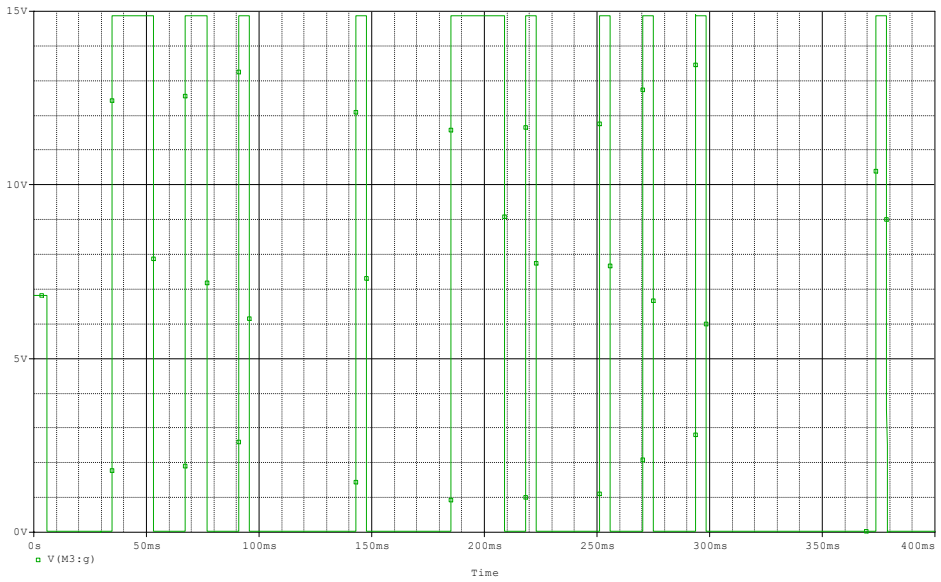

Figure 26. Digital Hybrid Third Stage Switching

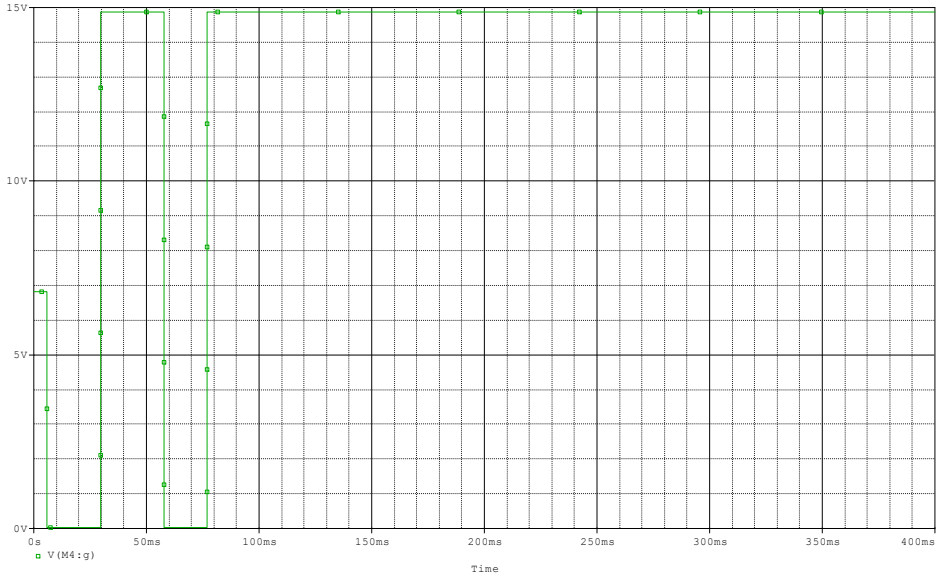

Figure 27. Digital Hybrid Fourth Stage Switching

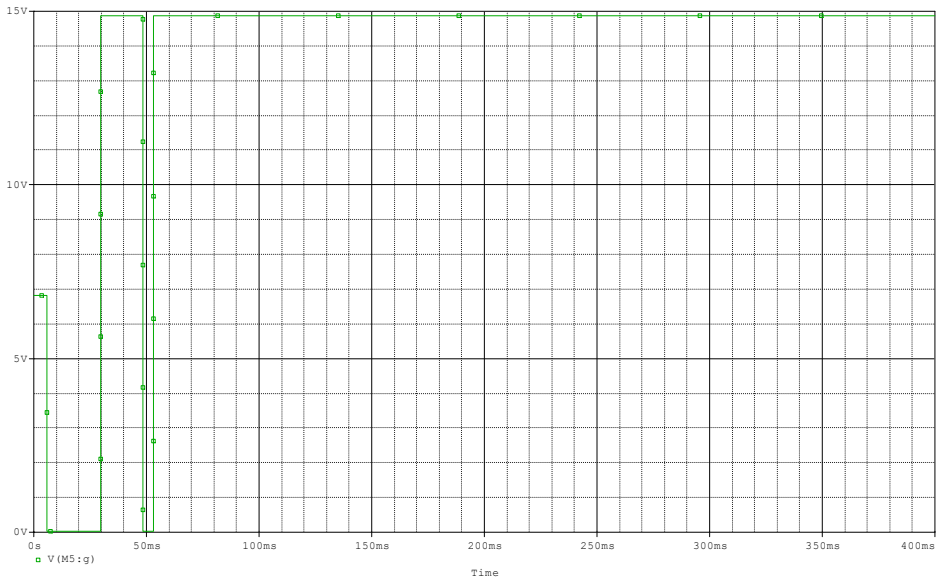

Figure 28. Digital Hybrid Fifth Stage Switching

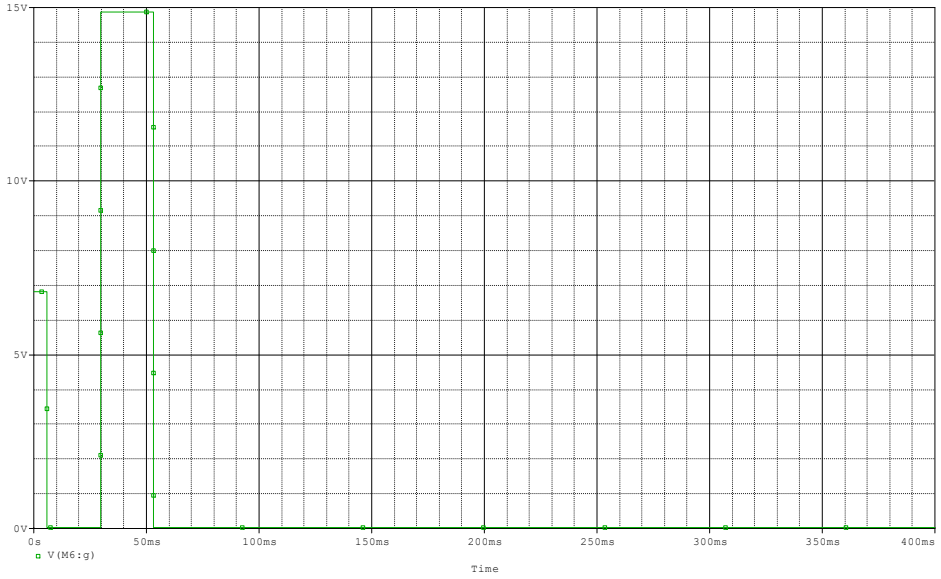

Figure 29. Digital Hybrid Sixth Stage Switching

Figures 30-41 display the waveforms corresponding to the load power dissipation in each of the seven MOSFET stages. The majority of the power dissipation is done in stages five and six; the power dissipation is not distributed evenly. If these two stages were to fail then the other stages may not be suitable to dissipate the power.

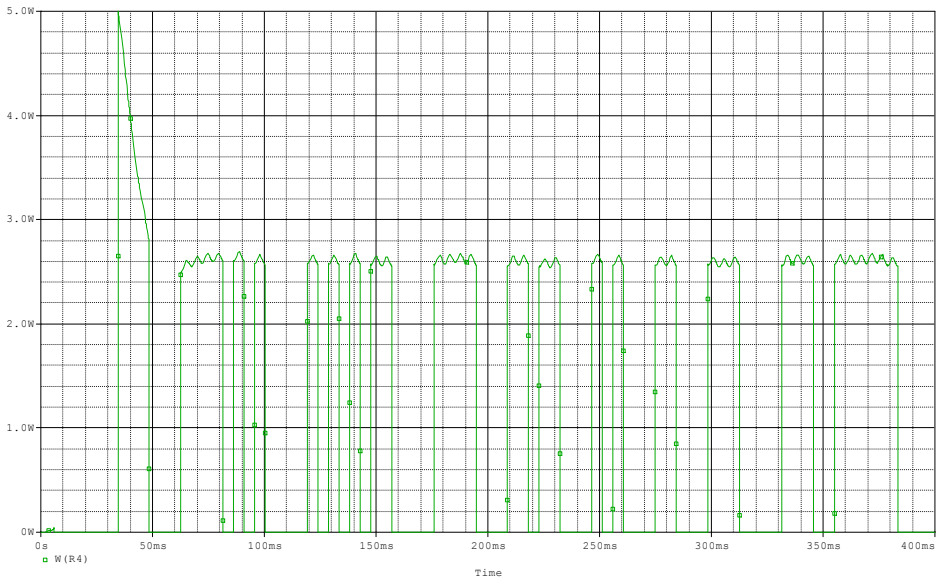

Figure 30. Digital Hybrid Stage One Load Power Dissipation

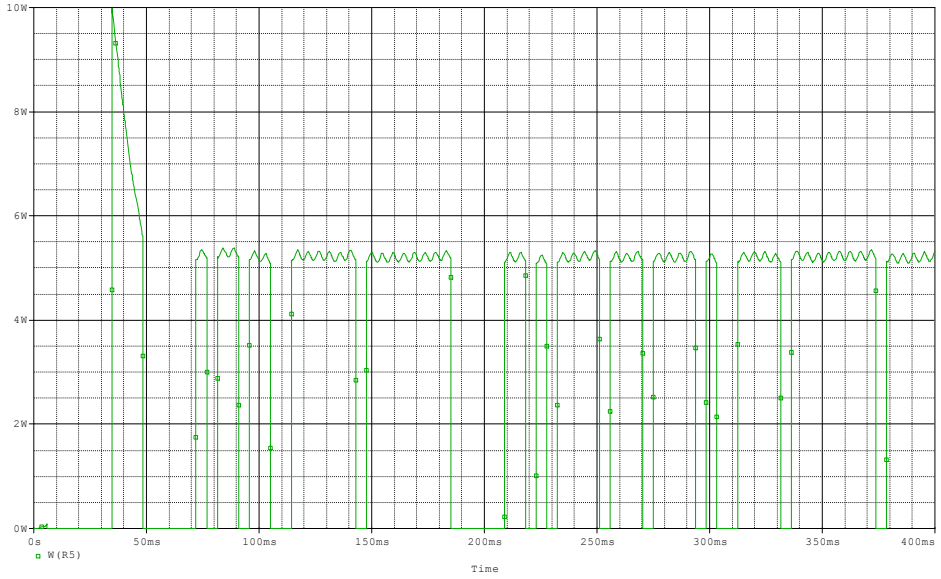

Figure 31. Digital Hybrid Stage Two Load Power Dissipation

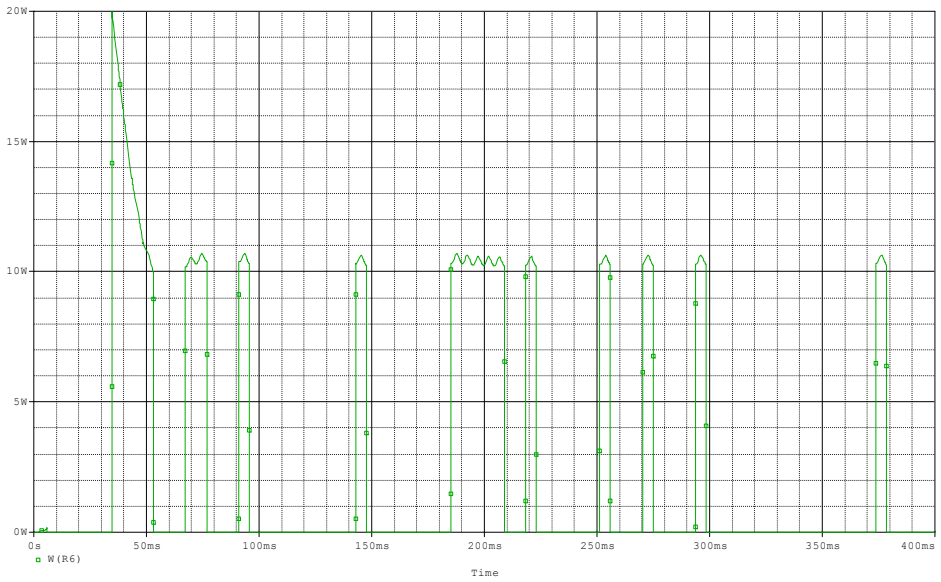

Figure 32. Digital Hybrid Stage Three Load Power Dissipation

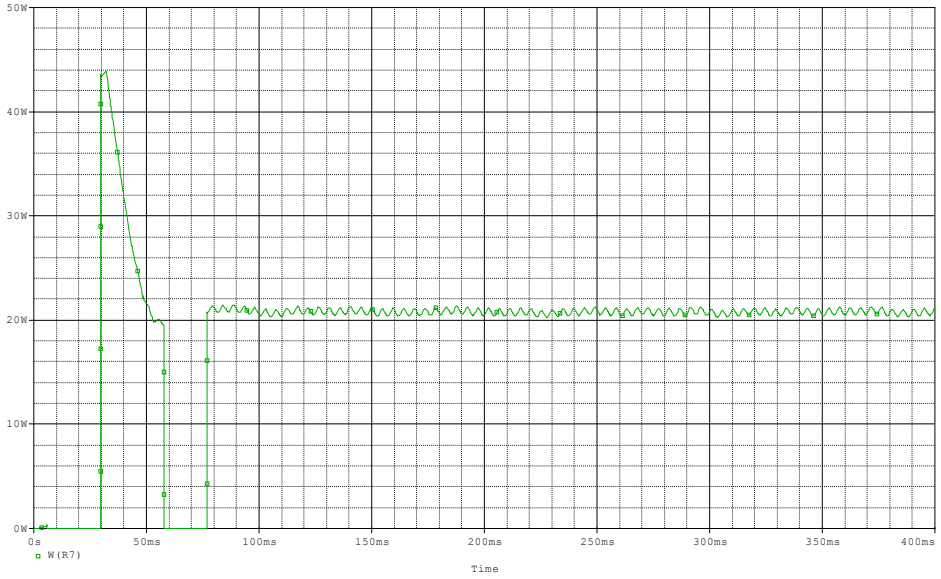

Figure 33. Digital Hybrid Stage Four Load Power Dissipation

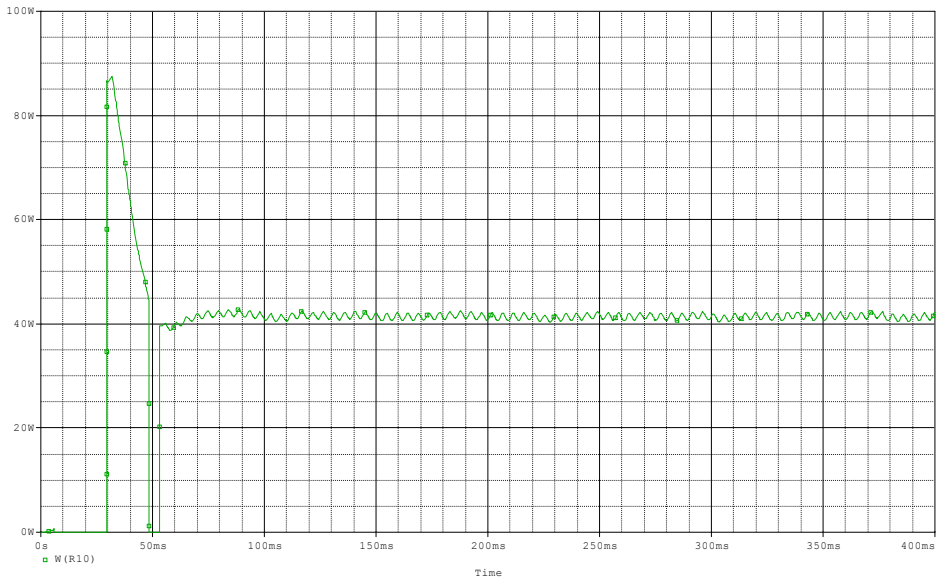

Figure 34. Digital Hybrid Stage Five Load Power Dissipation

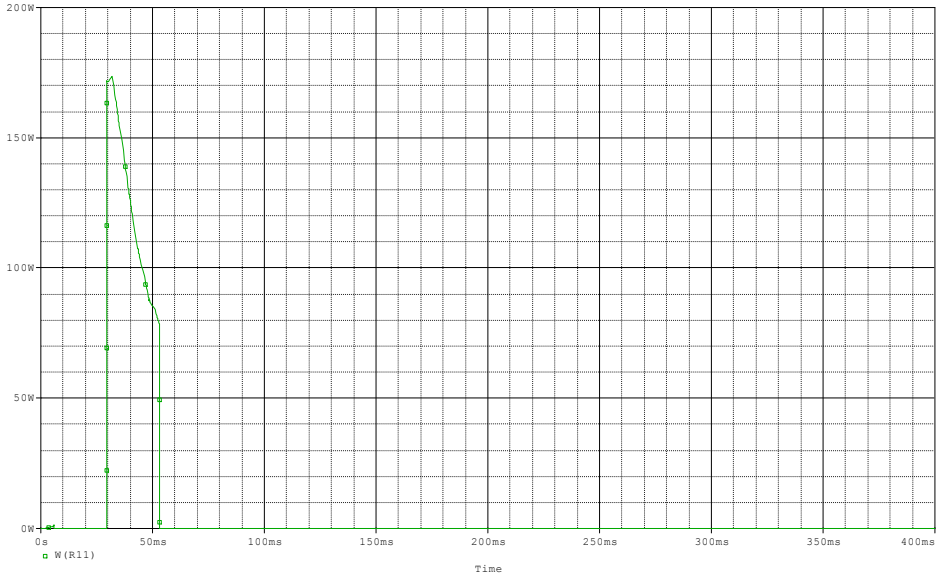

Figure 35. Digital Hybrid Stage Six Load Power Dissipation

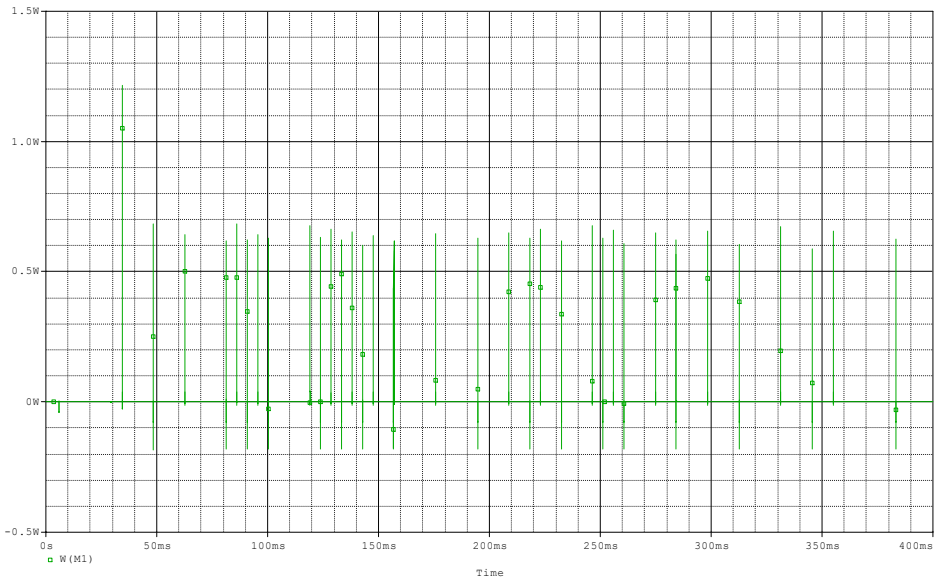

Figure 36. Digital Hybrid Stage One MOSFET Power Dissipation

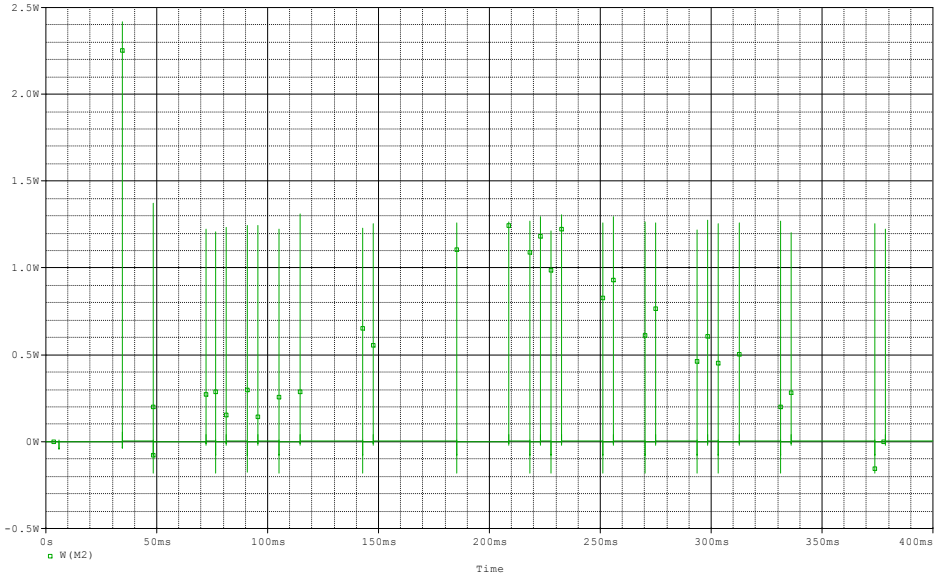

Figure 37. Digital Hybrid Stage Two MOSFET Power Dissipation

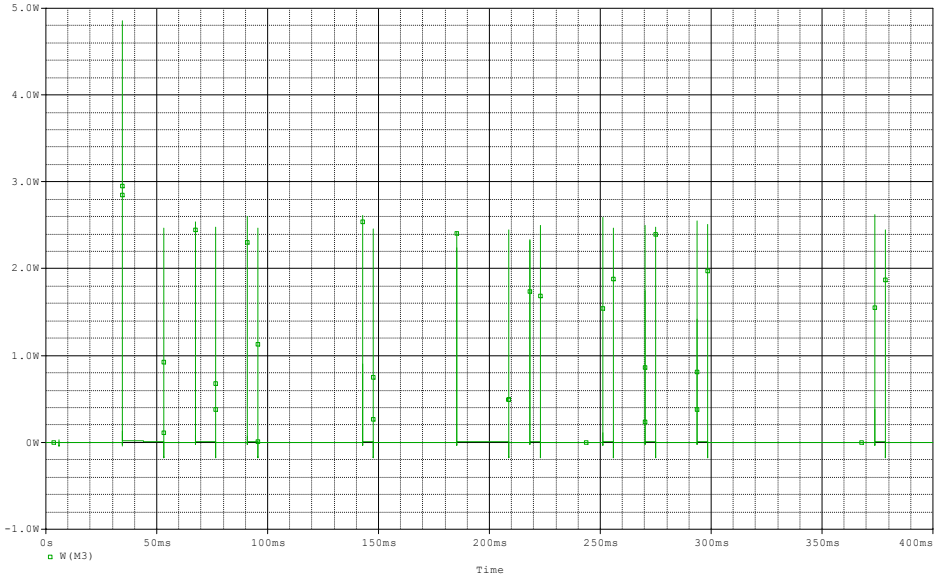

Figure 38. Digital Hybrid Stage Three MOSFET Power Dissipation

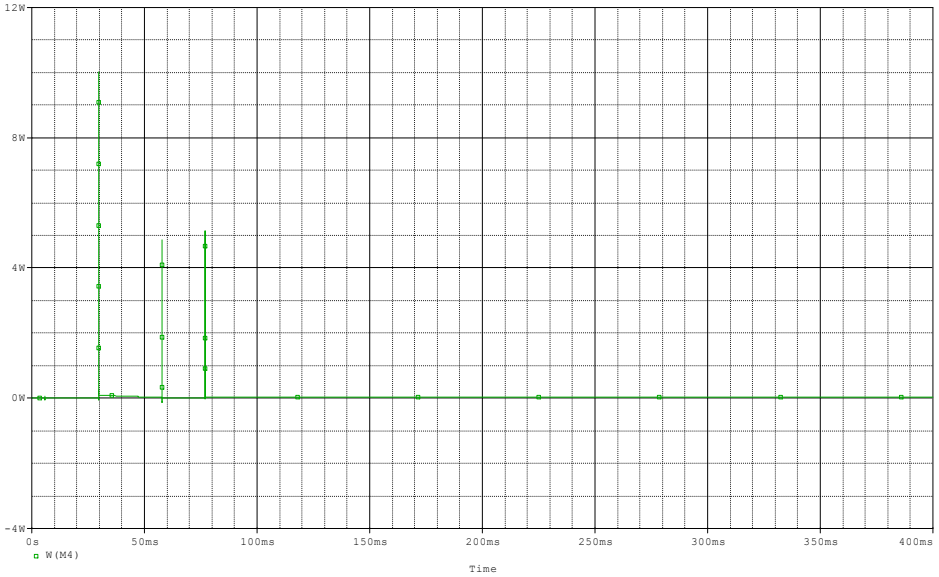

Figure 39. Digital Hybrid Stage Four MOSFET Power Dissipation

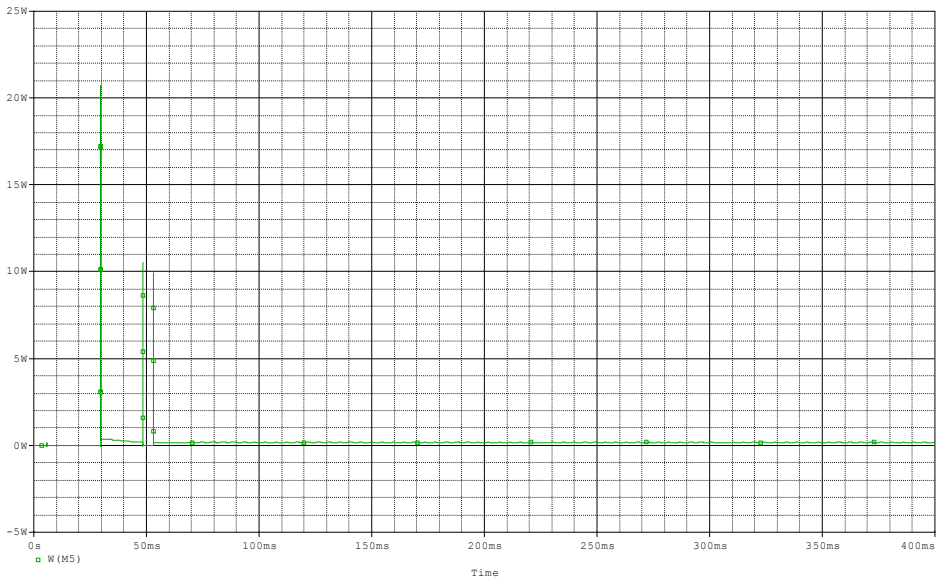

Figure 40. Digital Hybrid Stage Five MOSFET Power Dissipation

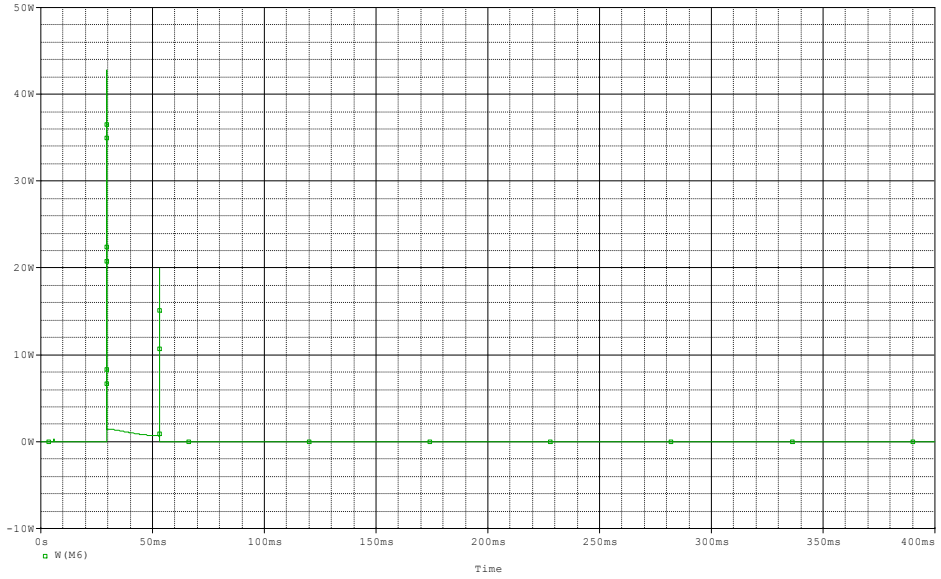

Figure 41. Digital Hybrid Stage Six MOSFET Power Dissipation

Figure 42 displays the waveform of the output ripple current of the filtering capacitor. A capacitor has been chosen that can withstand the amount of ripple current displayed in the waveform below; approximately 1.13A. It is important that the ripple current of the capacitor is not exceeded because it results in a shortened life span of the capacitor and may result in the capacitor venting or failing catastrophically.

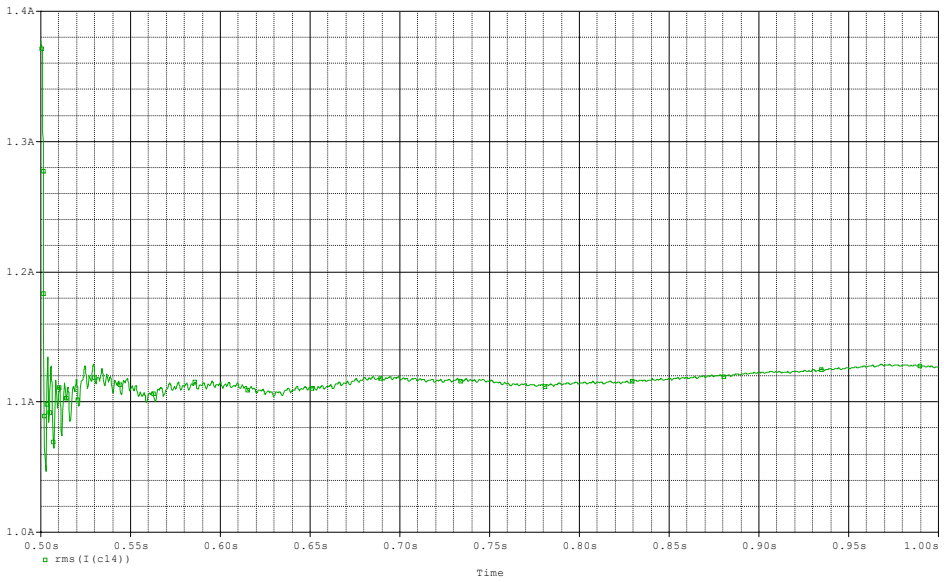

Figure 42. Digital Hybrid Capacitor Ripple Current

Figure 43 represents the AC voltage at the input of the digital hybrid controller. The AC input voltage is set to 26 V. This voltage is before the diode bridge and tuning capacitor.

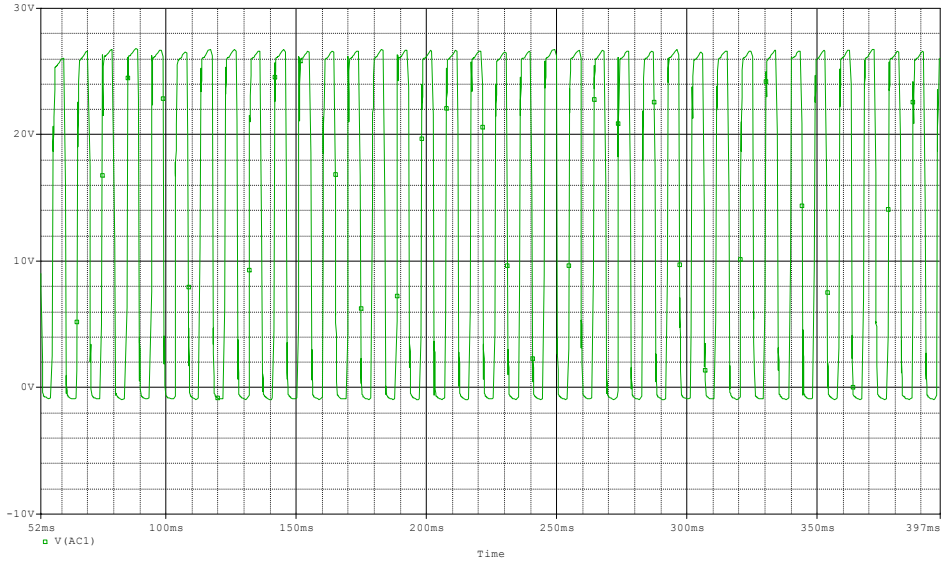

Figure 43. Digital Hybrid AC Voltage

2.4.3 Buck Converter with Zener Waveforms

Figure 44 represents the DC output voltage of the buck converter with zener. The Buck converter with zener simulations were run for 40 ms as opposed to 25 ms for the

other simulations because the file is significantly larger than the others. A simulation of 250 ms for the buck converter with zener takes approximately 30-45 minutes as opposed to less than one minute for the other controller simulations. The steady state value of the DC output voltage is viewed; not the transient. The DC output voltage reaches a steady state value of approximately 12 V; a DC/DC converter is needed at the output in order to supply the user with the desired 24 V or 28 VDC. The buck converter with zener has the most stable output voltage because the variations from the output of the buck converter are less than that of the engine.

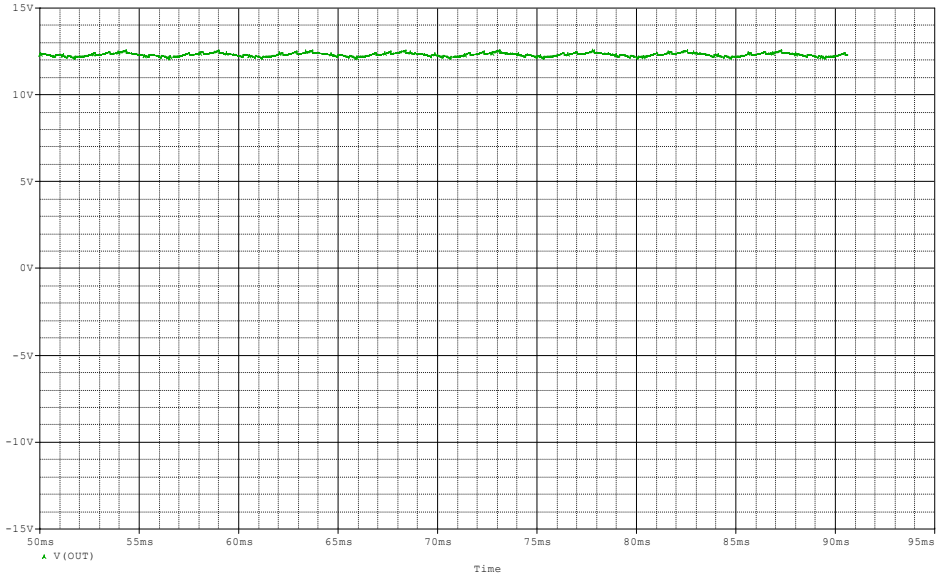

Figure 44. Buck Converter with Zener DC Output Voltage

Figure 45 represents the ripple voltage of the DC output. The ripple voltage of the buck converter with zener is approximately 0.4 V.

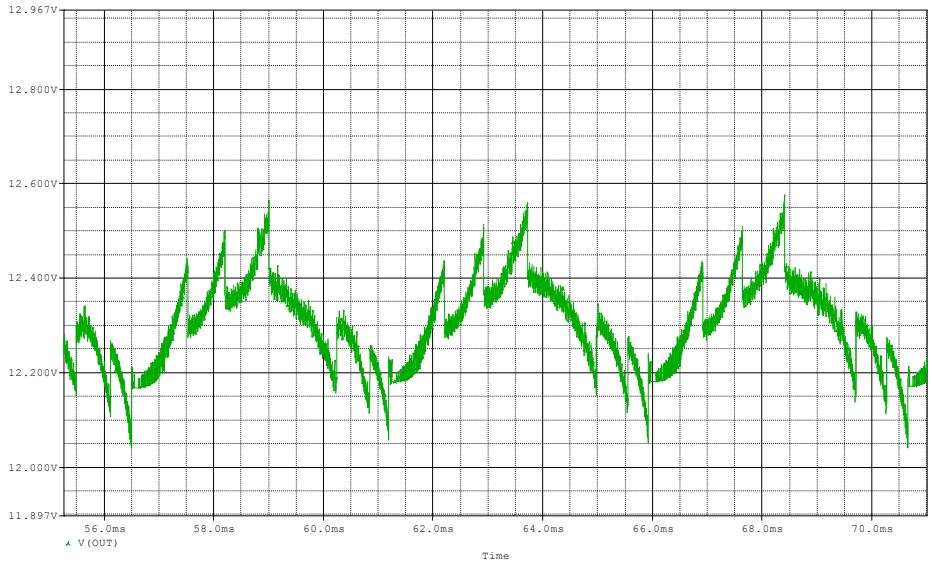

Figure 45. Buck Converter with Zener DC Output Ripple Voltage

Figures 46-48 represent the switching of each of the four op-amp stages. Each of the MOSFETs is on for a different period of time.

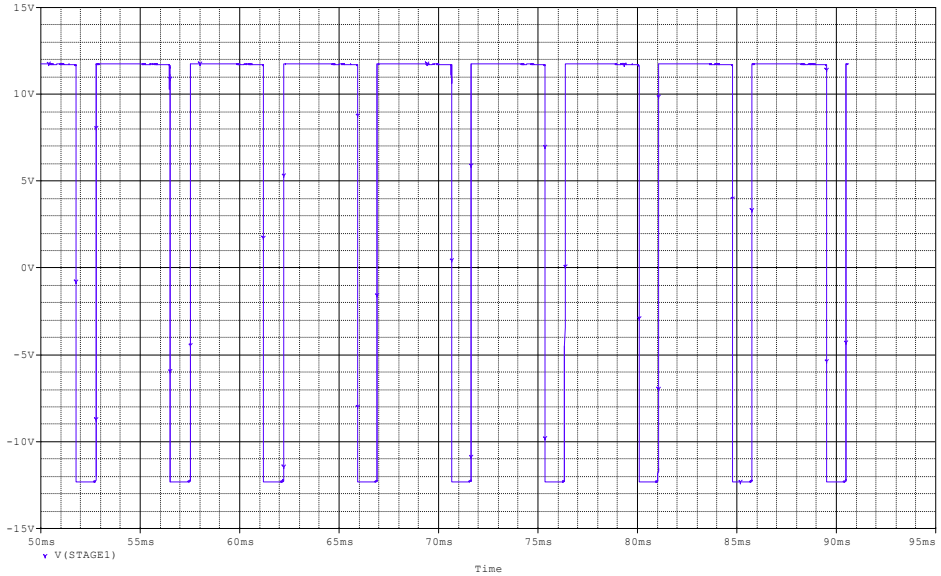

Figure 46. Buck Converter with Zener MOSFET Switching Stage One

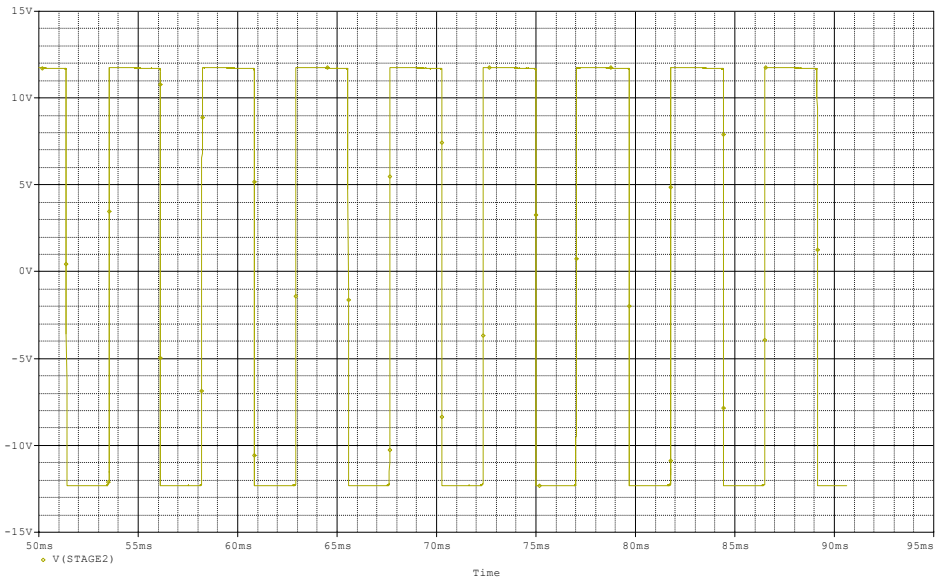

Figure 47. Buck Converter with Zener MOSFET Switching Stage Two

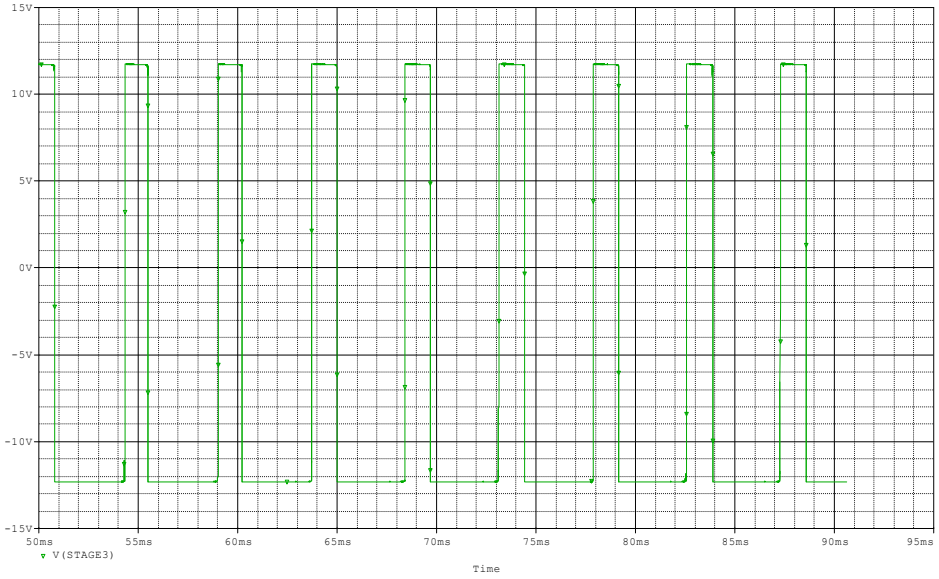

Figure 48. Buck Converter with zener MOSFET Switching Stage Three

Figure 49 represents the AC voltage from the convertor.

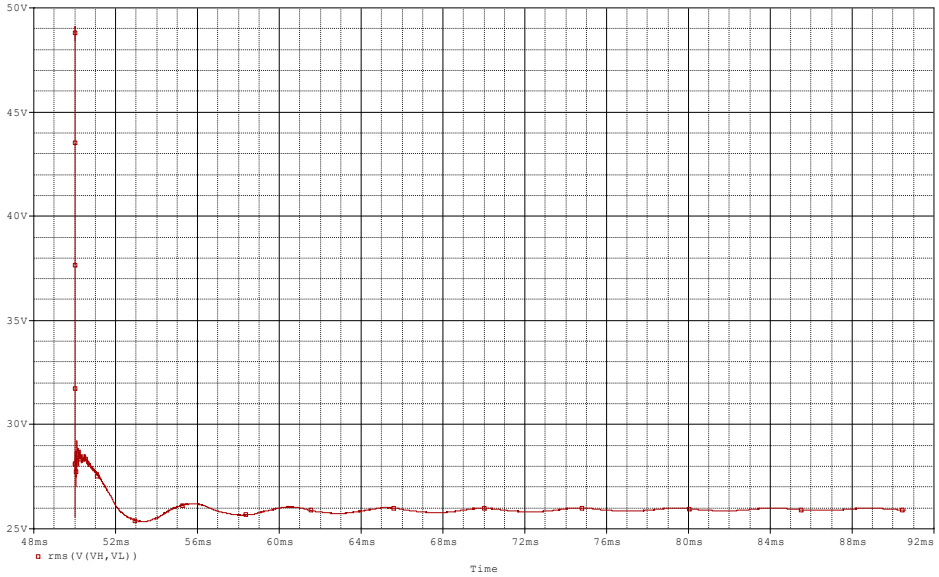

Figure 49. Buck Converter w/Zener AC Voltage

Figure 50 represents the RMS value of the power dissipation in the load resistors. The power dissipation in the load resistors is approximately 63.7 W.

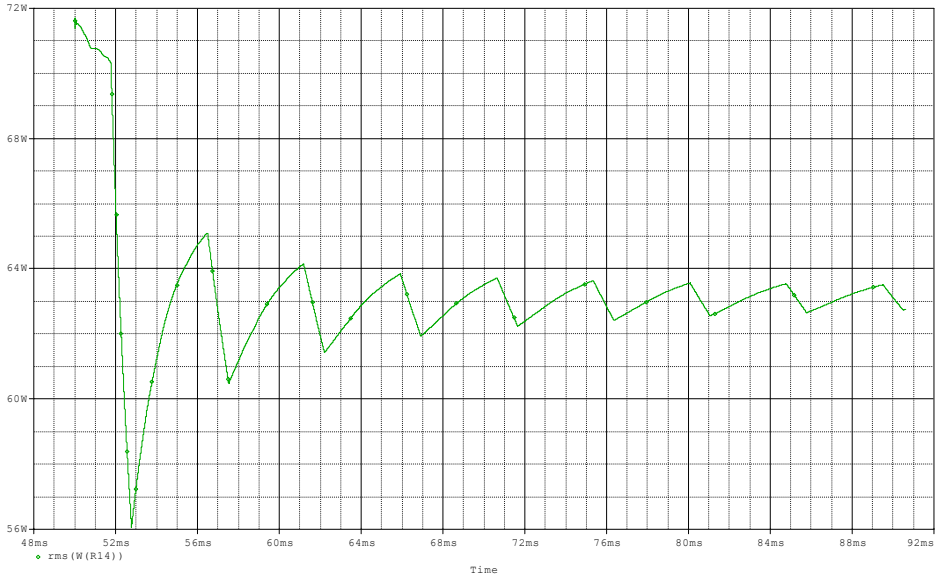

Figure 50. Buck Converter with Zener Load Resistor Power Dissipation

Figure 51 represents the power dissipation in the MOSFET. The power dissipation is approximately 2.15 W.

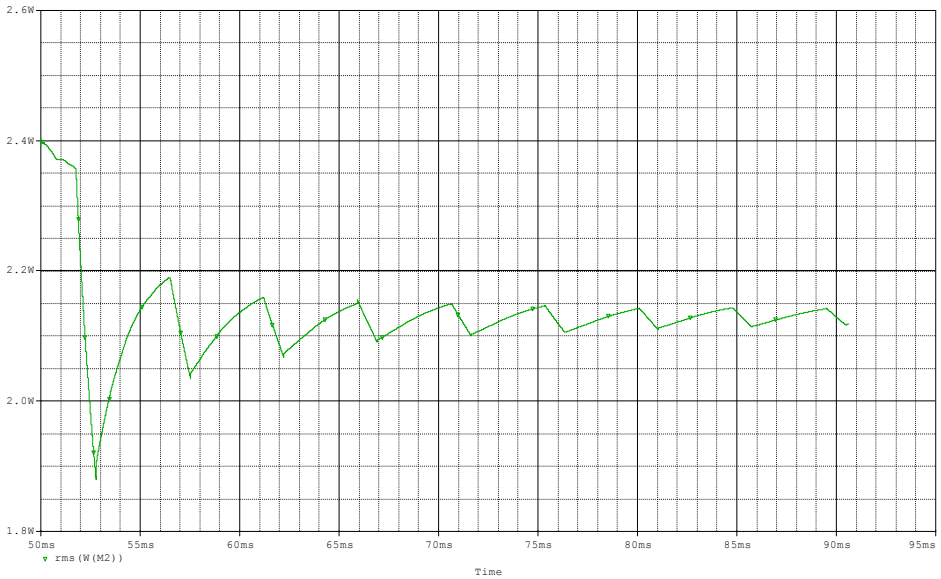

Figure 51. Buck Converter with Zener MOSFET Power Dissipation

2.5 Bench Testing

The purpose of the bench test is to verify that the controller has been assembled correctly and that the PSpice simulations, with an ASC convertor, accurately represent the performance of the controller.

2.5.1 Equipment

The following equipment was used to test the linear AC controller: BK Precision 1730A 30V/3A DC Power Supply, Chroma 6408, Agilent 34401A 6-1/2 Digit Multimeter, HP 6060B System DC Electronic Load, Clarke-Hess Model 2330 Sampling V-A-W Meter, Tektronix TDS3014 Four Channel Color Digital Phosphor Oscilloscope, High Voltage Differential Probe, 2 -1 ohm resistors.

2.5.2 Procedure

Figure 52 represents the bench test set up of the Linear AC Regulator controller.

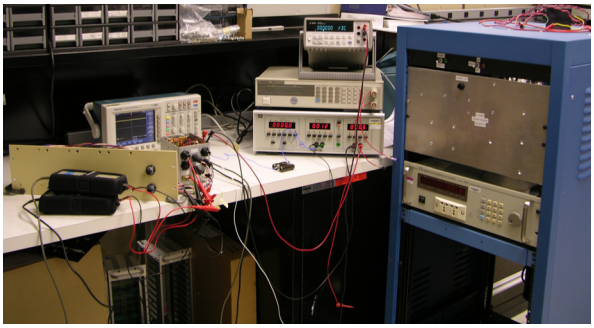

Figure 52. Linear AC Controller Bench Testing Setup

Figure 53 represents the bench test PSpice simulation. The bench test simulation differs from the original PSpice simulation for the Linear AC Regulator in that the inductor and capacitor, which represent the linear alternator, are removed.

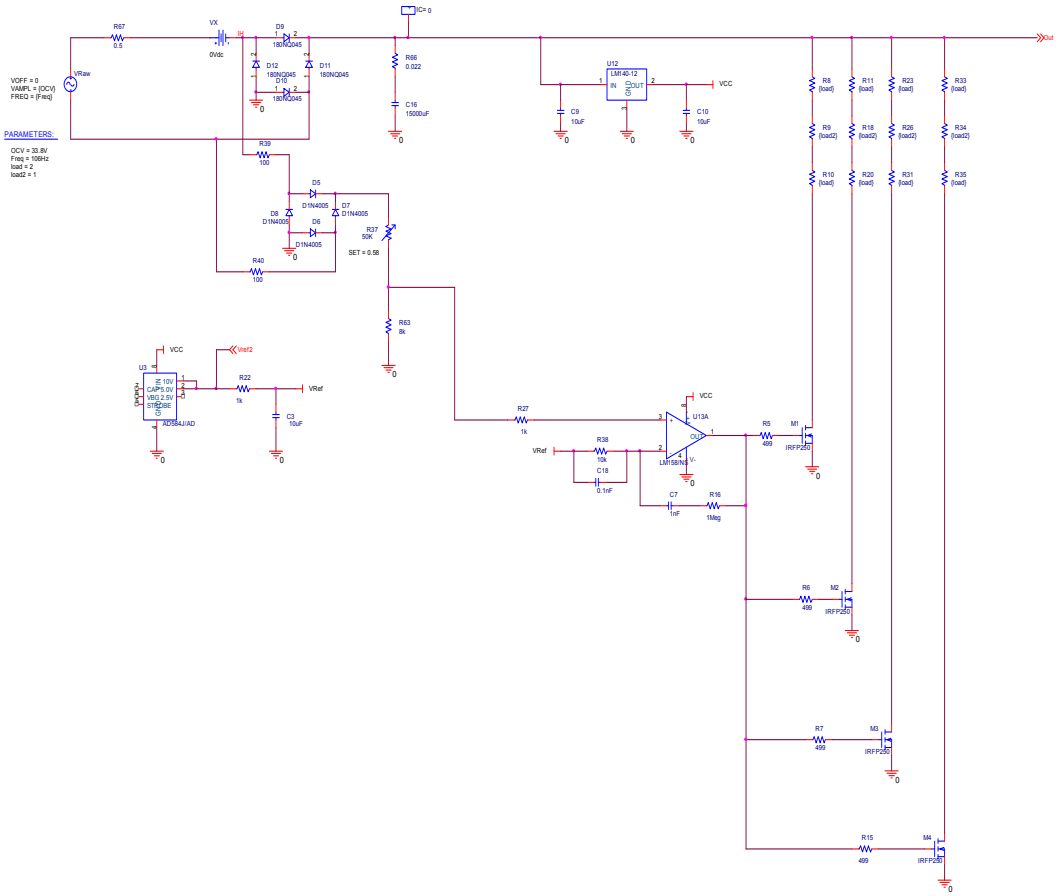

Figure 53. PSpice Simulation of Bench Testing

Initially, the controller was tested with a DC voltage input. This was used as a safety precaution in the event that a short was present in the circuit or any components were connected incorrectly. The damage to the controller would not be as significant as it would with an AC supply. Figure 54 shows the internal connections of the linear AC controller. The space inside the box is limited therefore during assembly a wrong connection could be made or two wires could be touching each other, causing a short.

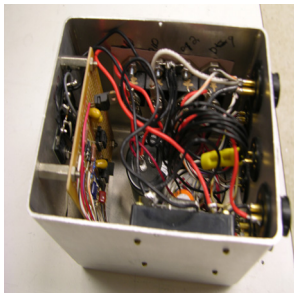

Figure 54. Linear AC Regulator Controller Internal Connections

A six ohm resistor was placed in series with the BK Precision 1730A 30V/3A DC power supply in order to produce a current through the controller. The voltage pot was set to 6.0, which corresponds to an output voltage of 24 V. The DC power supply has a built in current meter which allows the current to be monitored as the voltage is increased. If the current meter on the DC power supply increased significantly then it could be concluded that a short was present in the circuit. Once the DC input voltage was increased to 24 V the current increased slightly which indicated that the op-amp was regulating. Once the DC voltage check was complete an AC voltage was applied at the input of the controller. Figure 55 represents the controller along with the voltage and current potentiometers used during testing.

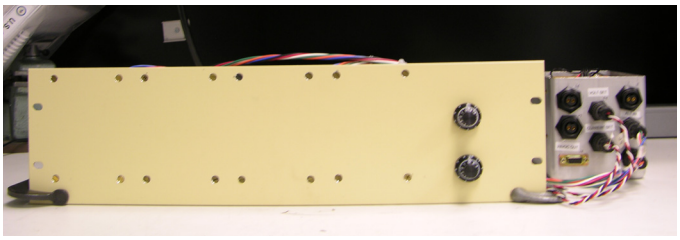

Figure 55. Linear AC Controller with Voltage and Current Potentiometers

Next, an AC voltage was applied to the input of the controller. Two 1 Ω resistors were connected in parallel to provide 0.5 Ω. The resistor value was changed in order to model the resistance of the linear alternator of the convertor. The resistor was placed in series with the AC voltage source. The Clarke-Hess V-A-W meter was used to measure the input voltage, current, and power. The Agilent multimeter was used to measure the DC output voltage. The voltage was increased slowly to 24 V; the output voltage, input voltage and regulation stages of the op-amp were monitored both on the Tektronix TDS3014 Four Channel Color Digital Phosphor oscilloscope, Agilent 34401A 6-1/2 Digit multi-meter, and the Clarke-Hess Model 2330 Sampling V-A-W meter.

2.5.3 Results

Table III represents the output voltage potentiometer dial setting corresponding to a specific output voltage.

Dial	Voltage
3.2	15.688
3.5	16.25
4	17.856
4.5	19.34
5	20.94
5.5	22.5
6	24.072

Table III. Output Voltage Potentiometer Dial Readings

Figure 56 represents the output voltage potentiometer dial readings at a range of output voltages. This graph can be used to set the output voltage to any desired value from 12-24 V. The controller is not operational below 12 V due to the voltage regulator.

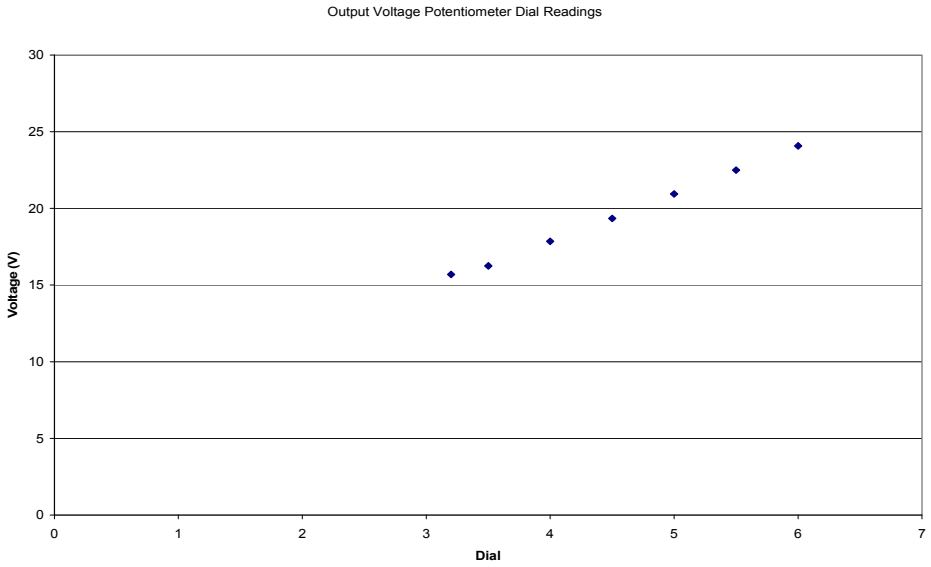

Figure 56. Output Voltage Potentiometer Dial Readings

Figure 57 represents the first two op-amp stages of the linear AC regulator controller regulating at 5 V. The inverting terminal of the op-amp was set to 5 V by a voltage reference. So the non-inverting terminal of the op-amp adjusts itself in order to match the 5 V reference of the inverting terminal. When the op-amp is regulating at 5 V then it can be concluded that the output is producing 24 V. This can be concluded because the input voltage is connected to a voltage divider which produces 5 V at a 24 V input. So as the input changes, so does the non-inverting terminal. The non-inverting terminal of the op-amp effects the output voltage regulation. Stages 3 and 4 were also monitored on the oscilloscope. Only two channels were available on the oscilloscope so all four stages could not be viewed at the same time. However, stages 3 and 4 have the same characteristics as stages 1 and 2.

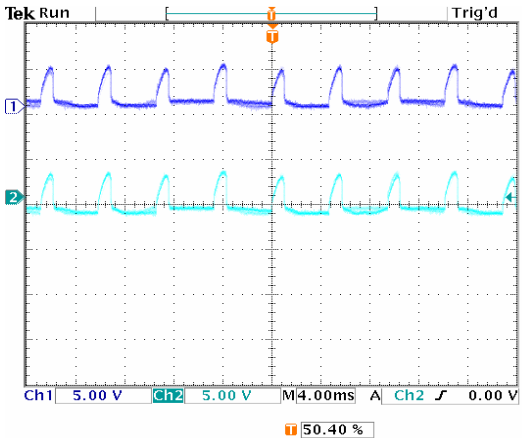

Figure 57. Op-Amp Stages: Bench Testing

Figure 58 represents the PSpice simulation waveform of the op-amp stages. As can be seen, the stages of the op-amp in the simulation match those of the experimental results.

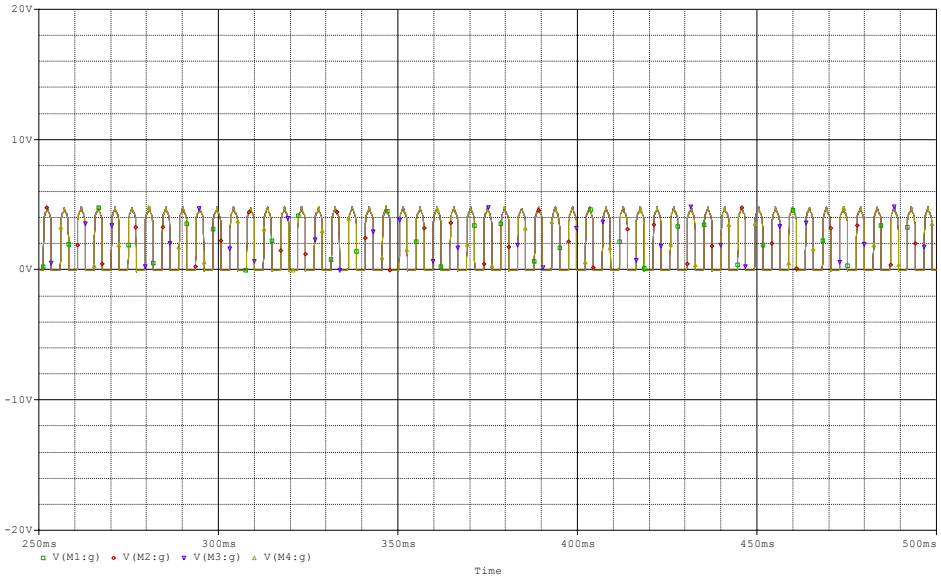

Figure 58. Op-Amp Stages: PSpice Simulation

Figure 59 represents the op-amp regulation stage and the output voltage. As shown in the figure, the output voltage is regulating at 25 VDC and the op-amp is regulating at 5 V.

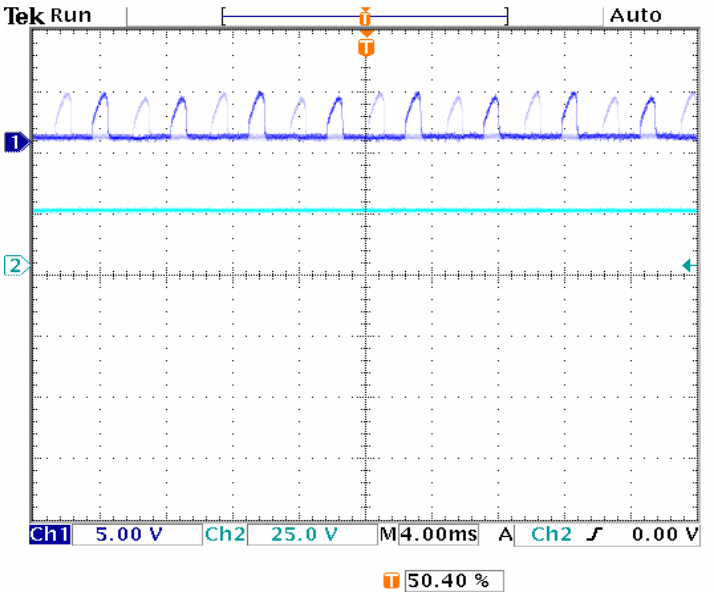

Figure 59. Op-Amp Stage and DC Output Voltage: Bench Testing

Figure 60 represents the PSpice simulation of the DC output voltage and the op-amp stages. As viewed below the DC output voltage and op-amp stages are the same as those obtained experimentally in Figure 59.

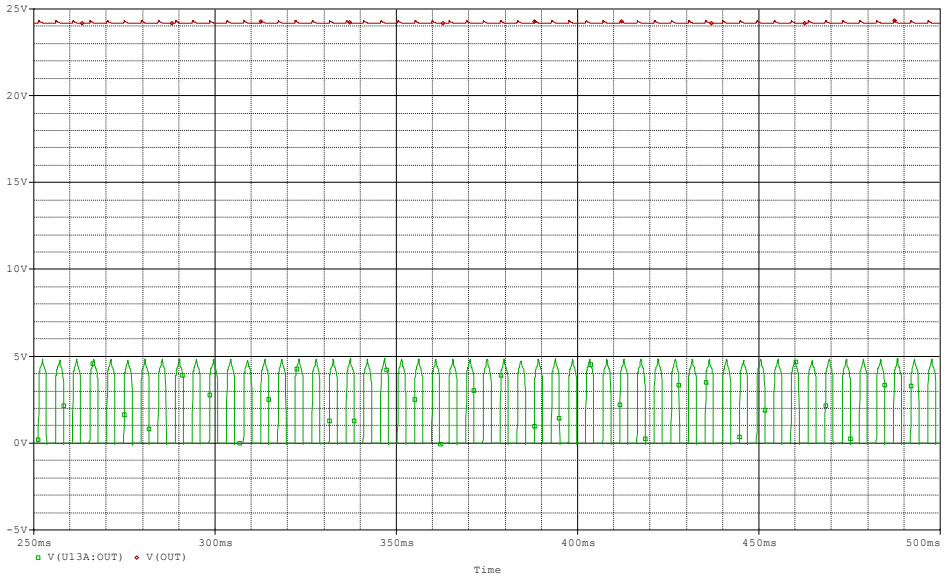

Figure 60. DC Output Voltage and Op-amp Stages: PSpice Simulation

Figure 61 represents the experimental results of the controller. The op-amp is regulating at 5 V and controlled at 24 VAC.

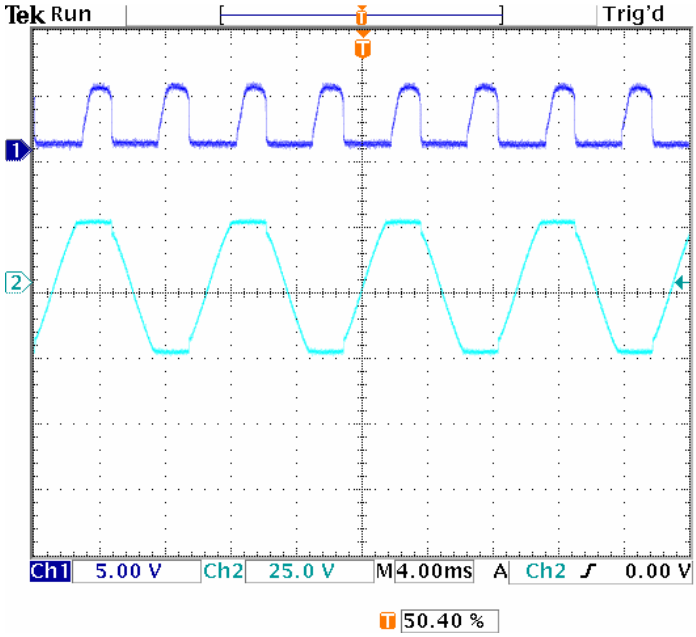

Figure 61. Op-Amp Stages and AC Control Voltage: Bench Testing

Figure 62 represents the PSpice simulation of the AC control voltage and the op-amp stages. As can be viewed below, the PSpice simulation results match the experimental results of Figure 61.

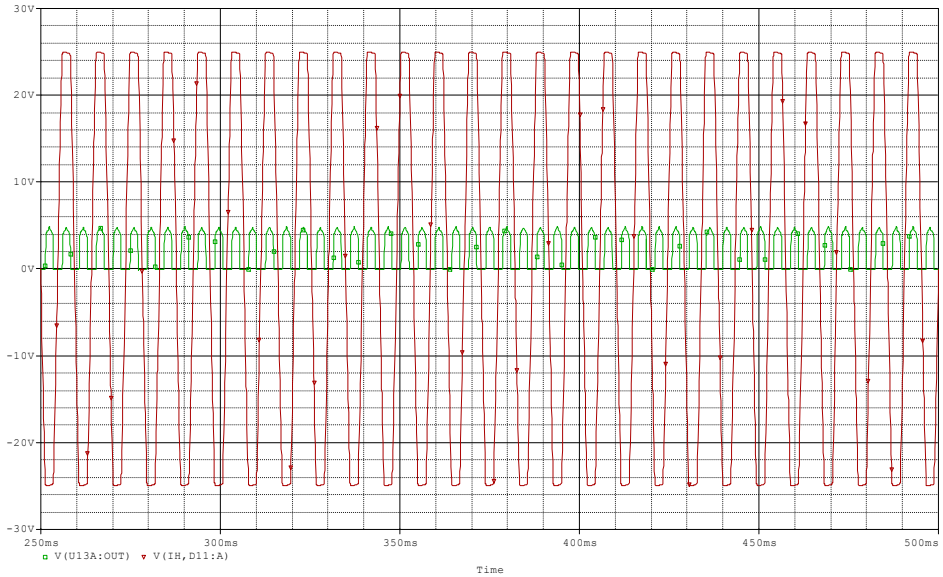

Figure 62. AC Control Voltage and Op-Amp Stage: PSpice Simulation

2.5.4 Conclusion

The PSpice simulation results match the bench testing results. This verifies that PSpice is an accurate tool for controller design. The results obtained in PSpice are accurate and can be used in order to verify controller operation before experimental testing.

2.6 Linear AC Controller Test on EE-35 SBIR 1 and 2 Convertors

The purpose of testing the linear AC regulator on the EE-35 convertors is to verify that the controller operates correctly and that the PSpice simulation accurately represents the performance of the controller with a stirling convertor.

2.6.1 Equipment

The following equipment was used to test the linear AC controller with the EE-35 stirling convertors: EE-35 SBIR 1, EE-35 SBIR 2, Linear AC Controller, Rack 6.

2.6.2 Procedure

The controller was connected to the linear alternator of the convertors. The voltage potentiometer was initially set to 5.44 in order to produce an output voltage of 22 V. Then the hot end temperature was increased to $300^{\circ}C$. The buzz convertors started on the AC bus and then were transferred to the linear AC regulator controller. The pot was adjusted to 6.53 in order to produce a piston stroke of 3.75 mm with Buzz 2 as the reference. The convertors ran at this temperature for approximately 5 minutes and then the temperature was increased to $400^{\circ}C$. As the hot end temperature increased the pot

setting was decreased. After approximately 5 minutes at $400^{\circ}C$, the temperature was increased to $470^{\circ}C$ and once again the pot was decreased. The final pot setting was 5.72.

2.6.3 Results

Table IV represents the alternator voltage, alternator current, power output, and DC output voltage of the convertors. This data was obtained at three operating temperatures. These parameters below are used in order to create a model in PSpice which accurately represents the operation of the controller at each of these temperatures.

	V_{AC} (V)	I (A)	P_{out} (W)	V_{DC} (V)
$300^{\circ}C$	24.25	0.66	11.99	25.78
$400^{\circ}C$	24.56	1.16	22.27	24.12
$470^{\circ}C$	24.3	1.42	27.41	23.24

Table IV. EE-35 SBIR 1 and 2 Run with Linear AC Regulator

Figure 63 and Figure 64 represent the alternator voltage data obtained from the operation of the convertors with the linear AC regulator controller at $470^{\circ}C$.

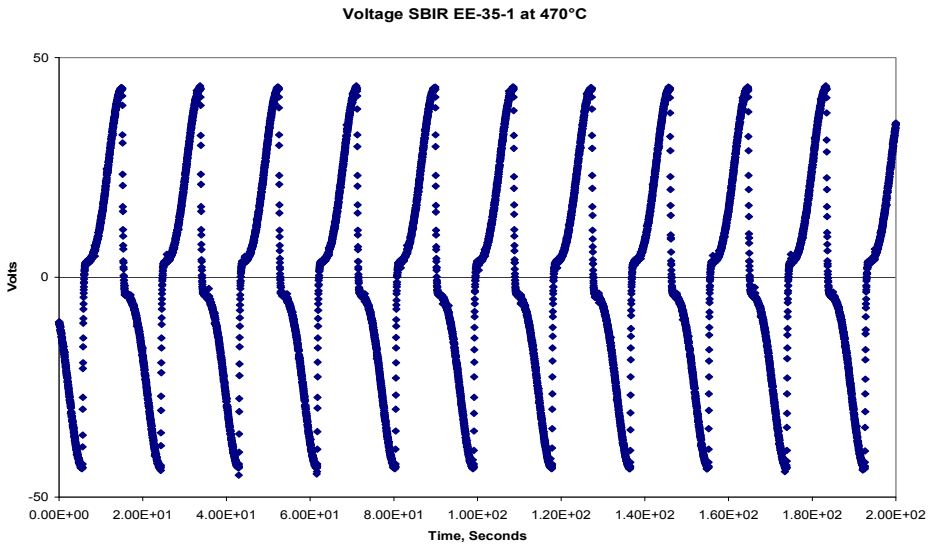

Figure 63. EE-35- 1 Alternator Voltage at $470^{\circ}C$

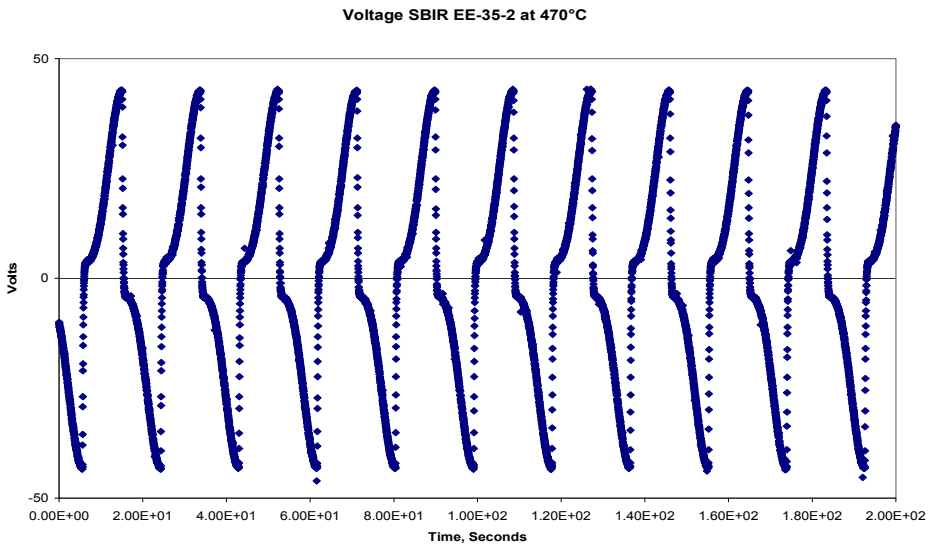

Figure 64. EE-35- 2 Alternator Voltage at $470^{\circ}C$

Figure 65 represents the PSpice simulation of the alternator voltage at $470^{\circ}C$. The open circuit voltage in PSpice was adjusted to 34.29 V and the output voltage potentiometer was set to 0.575. The open circuit voltage and voltage potentiometer were adjusted in order to meet the power output, current input, and DC output voltage obtained from the buzz run with the linear AC regulator controller. Table 4 lists the parameters that were obtained from the buzz run and therefore used to simulate at the corresponding temperature. PSpice does not have a temperature parameter. So in order to accurately compare the buzz run and the PSpice simulation their power output, current input, and DC voltage output need to match.

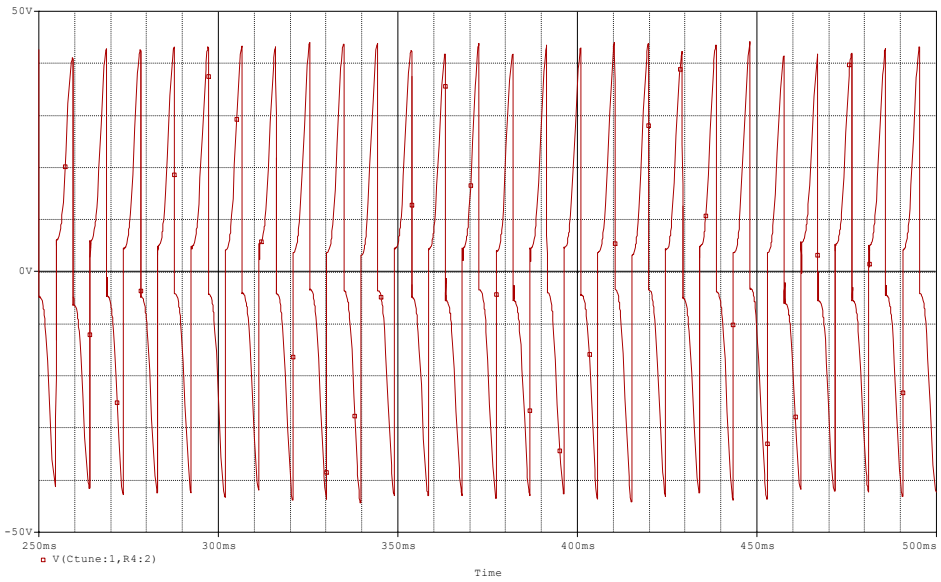

Figure 65. PSpice Simulation of Alternator Voltage at $470^{\circ}C$

Figures 66 and 67 represents the alternator voltage data obtained from the operation of the convertors with the linear AC regulator controller at $400^{\circ}C$.

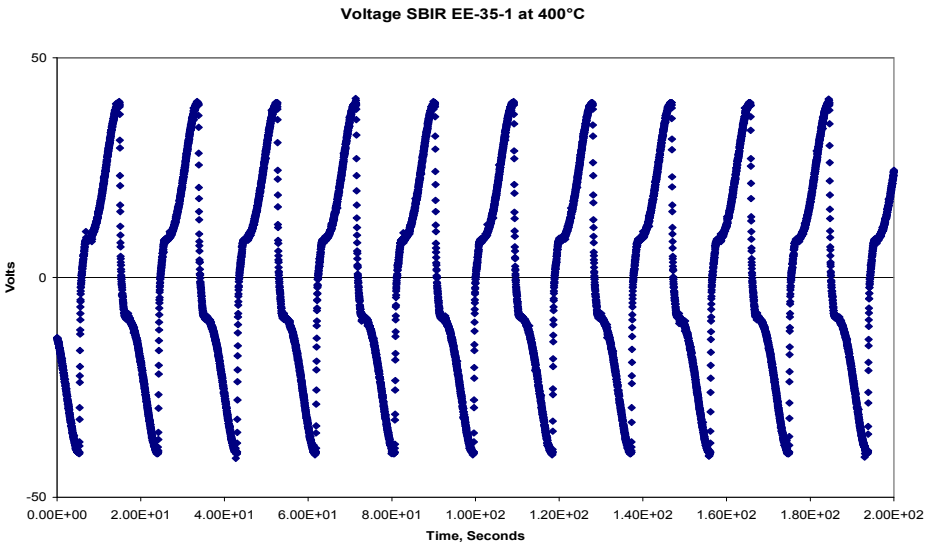

Figure 66. EE 35-1 Alternator Voltage at $400^{\circ}C$

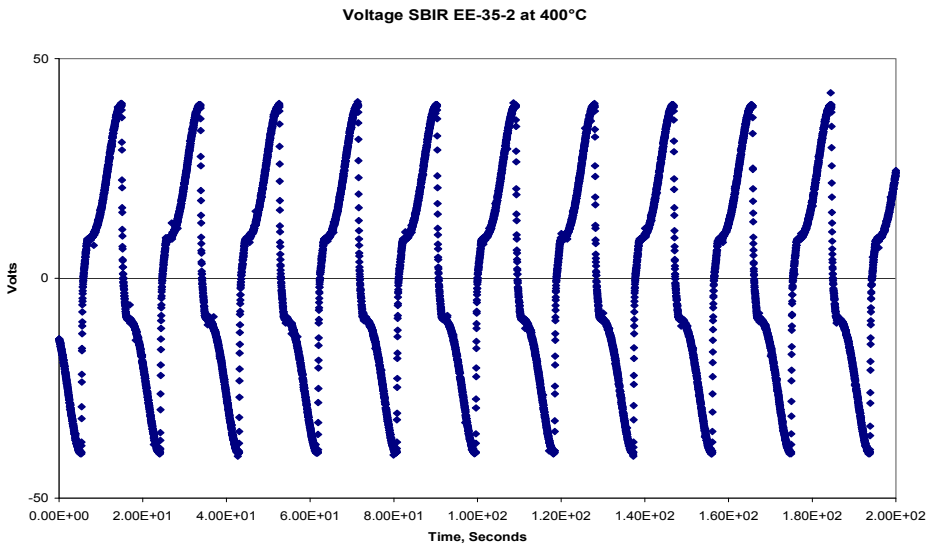

Figure 67. EE-35- 2 Alternator Voltage at $400^{\circ}C$

Figure 68 represents the PSpice simulation of the alternator voltage at $400^{\circ}C$. The open circuit voltage in PSpice was adjusted to 33.85 V and the output voltage potentiometer was set to 0.595.

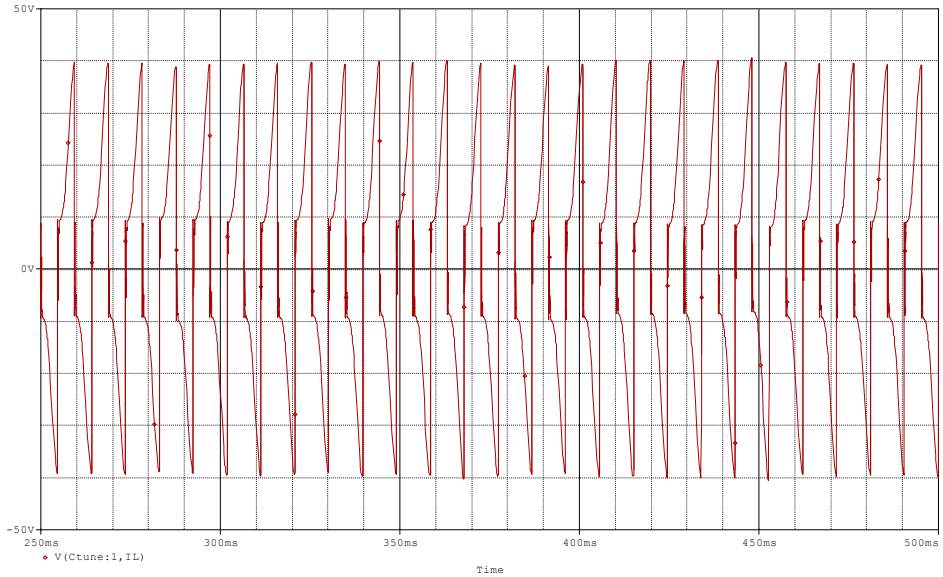

Figure 68. PSpice Simulation of Alternator Voltage at $400^{\circ}C$

Figure 69 and Figure 70 represent the alternator voltage data obtained from the operation of the convertors with the linear AC regulator controller at $300^{\circ}C$.

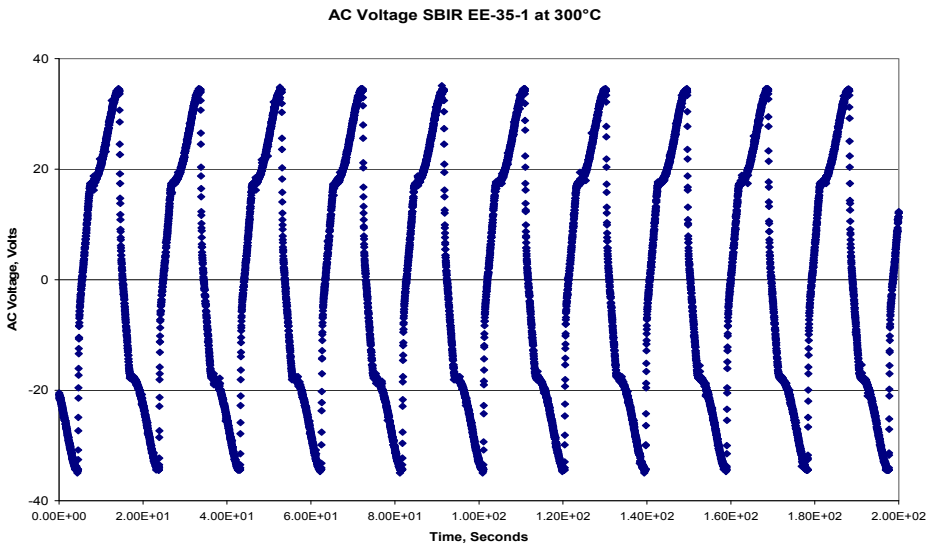

Figure 69. EE-35- 1 Alternator Voltage at 300° C

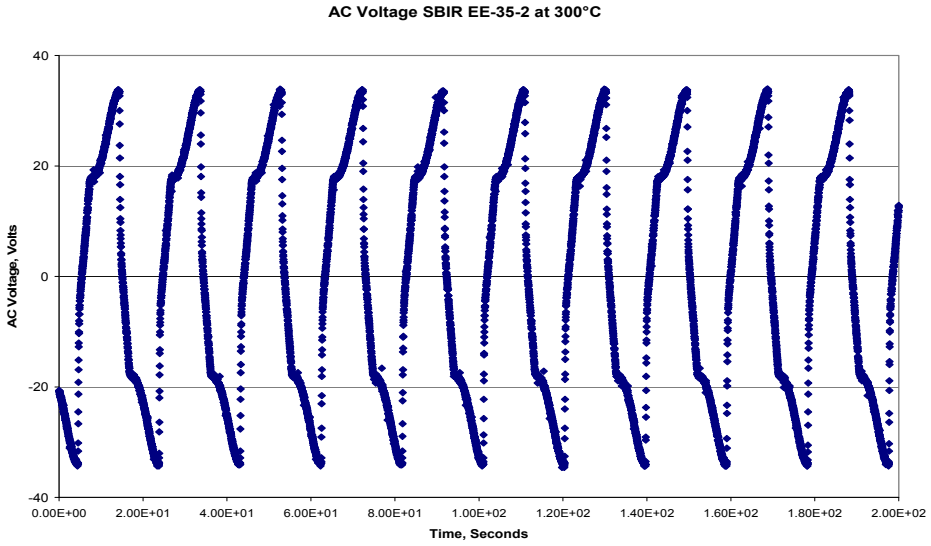

Figure 70. EE-35-2 Alternator Voltage at 300°*C*

Figure 71 represents the PSpice simulation of the alternator voltage at 300°*C*. The open circuit voltage in PSpice was adjusted to 33.1 V and the output voltage potentiometer was set to 0.625.

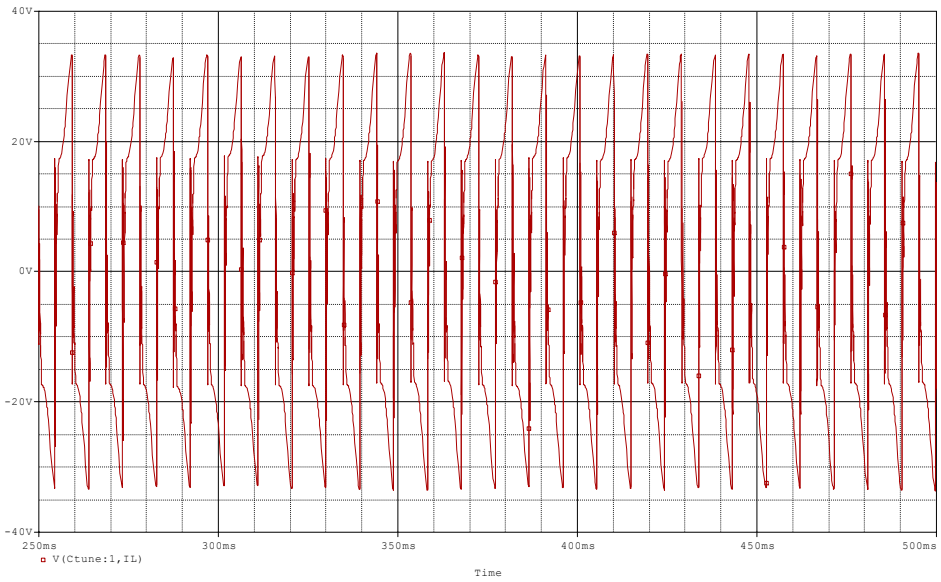

Figure 71. PSpice Simulation Alternator Voltage at $300^{\circ}C$

2.6.4 Test Summary

The PSpice simulation results match the operation of buzz SBIR 1 and 2 with the linear AC regulator controller. This verifies that PSpice is an accurate tool for controller design. The results obtained in PSpice are accurate and can be used in order to verify controller operation before experimental testing. The linear AC regulator controller was tested on a buzz SBIR 1 and 2, however it was designed for an ASC. As proved by the results listed above, the simulation of the controller for an ASC is accurate. So we can be certain that the operation of the controller with an ASC will resemble the results from the PSpice simulation.

2.7 Efficiency Test

An experiment was conducted to measure controller overall efficiency. Power was applied to the input of the controller using an AC voltage source to simulate convertor power. The voltage and current delivered to the input were measured to calculate power input. The voltage and current delivered to the loads were also measured to calculate

power output. The efficiency was then calculated as the ratio between the output and input power. True RMS meters were used for all measurements. True RMS meters measure the heating potential of an applied voltage. Unlike an "average-responding" measurement, a true RMS measurement is used to determine the power dissipated in a resistor. RMS amplitude measurement is the best way to relate AC quantities to DC quantities, or other AC quantities of differing waveform shapes. The output current of the linear AC regulator is not a pure sine wave. The output current meter was capable of measuring only up to 3 A, which limited the maximum power input to 41 W for this experiment. At this power level, the efficiency measured 98.6%. Table V lists the theoretical and experimental efficiencies. It should be noted that instrument error was not considered during experimental testing. The theoretical efficiency was calculated through PSpice simulation. The theoretical and experimental efficiencies were measured at the same point in the circuit. The output current was measured as the current through the four stages. The input current was measured before the diode bridge. The circuit model predicted a controller efficiency of 95.5% at approximately 130 W_e, which is the maximum output of the ASRG simulator.

	Experimental	**Simulation (low power)**	**Simulation (full power)**
Power Input (W)	44.33	40.00	129.41
Power Output (W)	43.72	38.27	123.88
Efficiency (%)	98.64	95.68	95.49

Table V. Linear AC Regulator Efficiency Summary

2.8 Linear AC Controller and ASRG Simulator Integration

Following successful checkout on the EE-35 convertors, the linear AC controller was integrated into the ASRG simulator electronics support. Stable operation of the FTB convertors was demonstrated up to their maximum combined power output of 130 W_e.

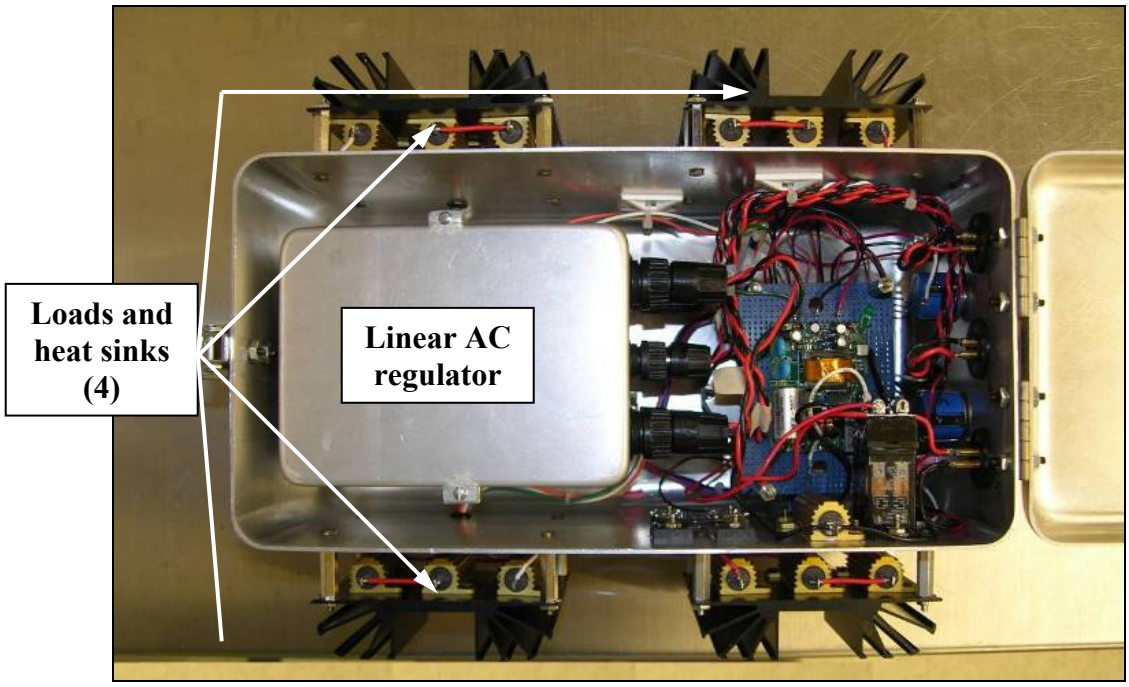

Figure 72. Linear AC regulator controller integrated into ASRG simulator support

Stability was qualitatively evaluated by observing the linear alternator voltage. While operating at full power, the alternator voltage did not deviate more than 1 mV. A photograph of the controller integrated into the support electronics can be seen in Figure 72. The controller occupies the left half of the container. The loads and their heat sinks are located on the outer surfaces of the container.

2.9 Conclusion

PSpice was the main instrument in designing the controller. Initially, six controllers were evaluated. After thorough analysis in PSpice of each of the controllers, tables of pros and cons were created in order to eliminate three of the six controllers. After three of

the controllers were eliminated, the linear AC regulator, digital hybrid, and buck converter with zener remained. A list of evaluation criteria were then developed; housekeeping power, reliability, complexity, stability, robustness, and size. The linear AC regulator was chosen for further design because it maximized the performance of the convertor. The linear AC regulator had the least amount of required housekeeping power, most stable, least complex and small in size. The completed controller can be viewed in Figure 73 below. The controller was housed in a box 4" X 5.5" X 4.37" minus the load modules.

Figure 73. Completed Linear AC Regulator Controller

The linear AC regulator was then assembled, bench tested, and run on the EE35 SBIR 1 and 2 convertors. After analyzing the bench testing and buzz run results, it can be concluded that PSpice accurately represents the behavior of the controller. So, since the controller was run on buzz convertors as opposed to ASCs, which it was originally designed for, it is safe to say that the simulations of the linear AC regulator controller with an ASC convertor resemble the actual performance of the controller with the convertors. The efficiency of the controller was measured to be 98.64%. Following successful checkout on the EE-35 convertors, the linear AC controller was integrated into the ASRG simulator electronics support. Stable operation of the FTB convertors was demonstrated up to their maximum combined power output of 130 W_e.

Plans have been made to replace the sensing diode bridge in the linear AC regulator with a true RMS-to-DC converter. This component computes the true root-mean-square value of a non-sinusoidal AC input signal and gives an equivalent DC output level. The true RMS value of a waveform is a more useful quantity than the average rectified value since it relates directly to the power of the signal. This modification theoretically eliminates the need for the user to constantly adjust the potentiometer.

CHAPTER III

CONSTANT POWER CIRCUIT

The circuit will maintain the stirling convertor output to its maximum, 130 W, while the Li-ion batteries provide additional power. When the load increases, the power from the stirling controller will reach its maximum and current will start to be drawn from the battery. The circuit design started with block diagrams and as knowledge was attained blocks were transformed into components.

3.1 DC-DC Converter

The DC-DC converter monitors the voltage and current provided by the stirling convertors. This voltage and current is monitored at the output of the linear AC controller. The TRM pin of the DC-DC converter adjusts the output according to the amount of power supplied by the convertors. The trim pin is driven by a 2N2222 BJT. The output of the DC-DC converter is between 24 and 28 V depending on the current and voltage. When the current required by the load exceeds the current available from the controller, then the DC-DC converter output will be 28 V. The Li-ion batteries supply the additional power required by the load.

A test was performed on the DC-DC converter, PAH350S24-28, in order to determine the value of the trimming voltage and internal resistors. The trim voltage is 1.225 V. The two internal resistors are 1 $k\Omega$ each. Figure 74 represents the test set-up provided by [10].

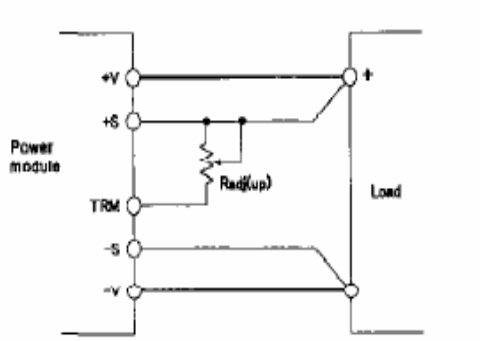

Figure 74. DC-DC Converter Trim Test Set Up

Table VI displays the data used to determine the value of the internal resistance.

Potentiometer	VIN (V)	Output Voltage Adjustment (V)	Trim (V)
200 Ω	18.218	14-15.26	0.110
1 $k\Omega$	19.374	14-18.64	0.405
10 $k\Omega$	18.535	14-25.67	1.020
500 $k\Omega$	19.49	29.36-37.11	1.3446-2.0223

Table VI. DC-DC Converter Adjustable Resistor Test

The following equation and graph from [10] in Figure 75 was also used to calculate the internal resistance and trim voltage. It can be verified from the formula that the measured value of voltage trim is correct as 1.225 V.

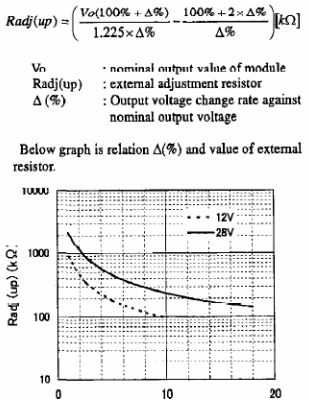

Figure 75. DC-DC Converter Trim Calculation

A component was created in PSpice after the voltage trim and internal resistors values were obtained. Currently, the PSpice part was written in code format and was created by [9]. This code can be viewed in the appendix.

3.2 Current Sensor

A current sensor is used to detect the current supplied to the load. The current sensor selected for the design is HY10-P. The current sensor output is 4 V for a 10 A input. A hierarchical model was created in PSpice. Figure 76 shows the model created for this component.

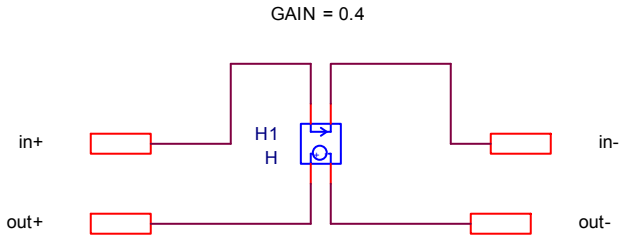

Figure 76. Current Sensor PSpice Hierarchical Model

The current sensor provides a voltage output proportional to the current through the load. This output signal is fed to one of two multiplier inputs.

3.3 Multiplier

A multiplier is used to measure the power supplied to the load. The voltage across the load and current through the load is multiplied. This is done with an analog multiplier integrated circuit (IC). The multiplier gives a voltage output proportional to the power supplied to the load. This will determine if the batteries should start producing power. The multiplier IC has been chosen as the AD734. The gains of the multiplier and the connections for the multiplier were completed with the help of [13]. The voltage input of the multiplier was scaled with a voltage divider. The output of the current sensor was

used as the second input to the multiplier. The current sensor and the voltage divider were both scaled based on the following transfer function provided by [13].

$$Output = \frac{(X1 - X2)(Y1 - Y2)}{10}$$

Where X is the current sensor output and Y is the scaled voltage across the load. The voltage was based a 28 VDC output from the DC-DC converter and was multiplied with the voltage divider to provide 9.6 V. The maximum current supplied by the output of the controller is 6.5 A. The conversion of the current sensor is 2.5 A/V. The current sensor input is 2.6 V. The output of the multiplier is 2.5 V.

$$Output = \frac{(9.6V)(2.6V)}{10V} = 2.5V$$

3.4 Design Process

3.4.1 First Step

At first, the constant power circuit design was implemented with block diagrams. The block diagram can be viewed in Figure 77. In this step blocks were used gain insight into the logic behind the constant power circuit. It was determined that the power would be measured by the voltage across the load and the current through the load. The amount of power would be controlled so an error amp would be needed to compare the desired to the actual.

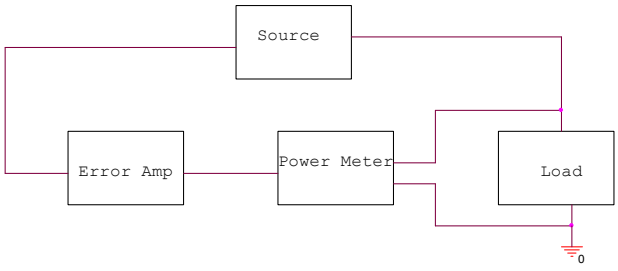

Figure 77. First Step Constant Power Circuit Design Process

3.4.2 Second Step

Each block was considered as to find a component that would perform that operation in the block. A multiplier was added to the block diagram as shown in Figure 78 because it is known that multiplying voltage and current gives power. A DC-DC converter would substitute the source block because it can be used to limit and control the voltage across the load.

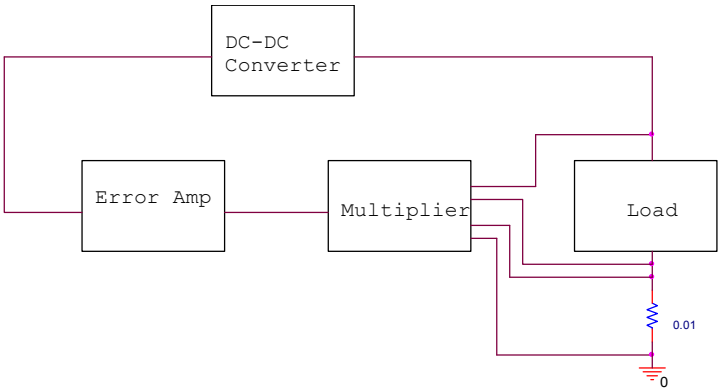

Figure 78. Second Step Constant Power Circuit Design Process

3.4.3 Third Step

PSpice was used to implement each of the blocks as shown in Figure 79. Components that had not been chosen were implemented in PSpice by the ABM library. A DC-DC converter model was inserted into PSpice to convert the voltage supplied by the controller to 24 VDC or 28 VDC. A sensing resistor was placed at the output of the DC-DC converter to measure the current through the load. The op-amp is connected as an error amplifier. A 2.5 V reference on the non-inverting terminal was used to compare the voltage and current across the load. The current and voltage across the load was multiplied by an ABM component. The output of the op-amp was fed to a limiter. The limiter started at 0 and allowed voltage adjustment up to 2.75 V. At this point, the exact trim voltage of the DC-DC converter was not known.

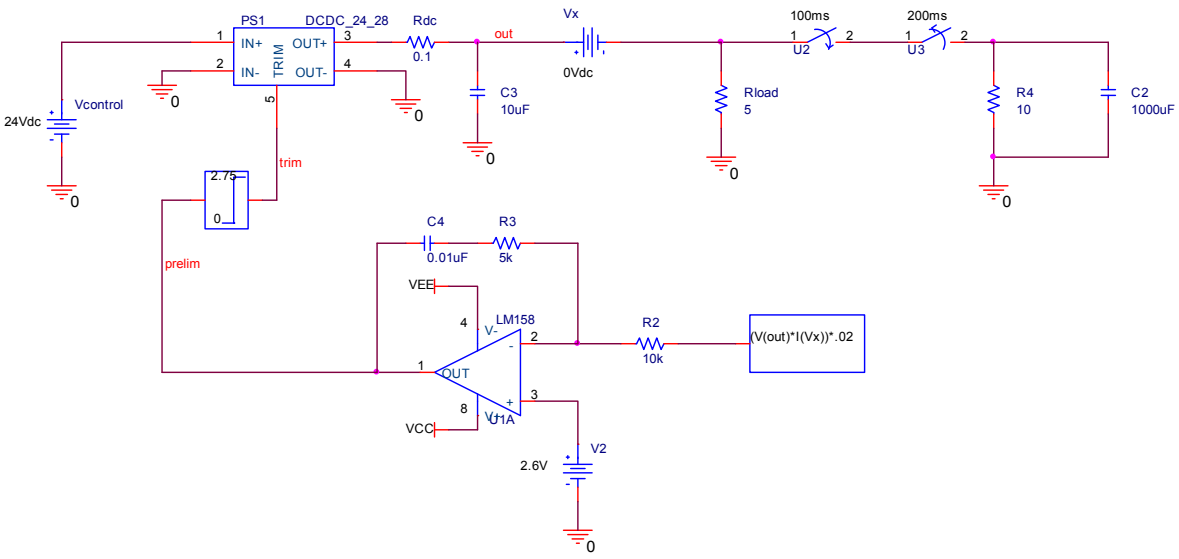

Figure 79. Third Step in Constant Power Circuit Design Process

3.4.4 Fourth Step

At this point the limiter was replaced with a MOSFET to control the trim voltage as shown in Figure 80.

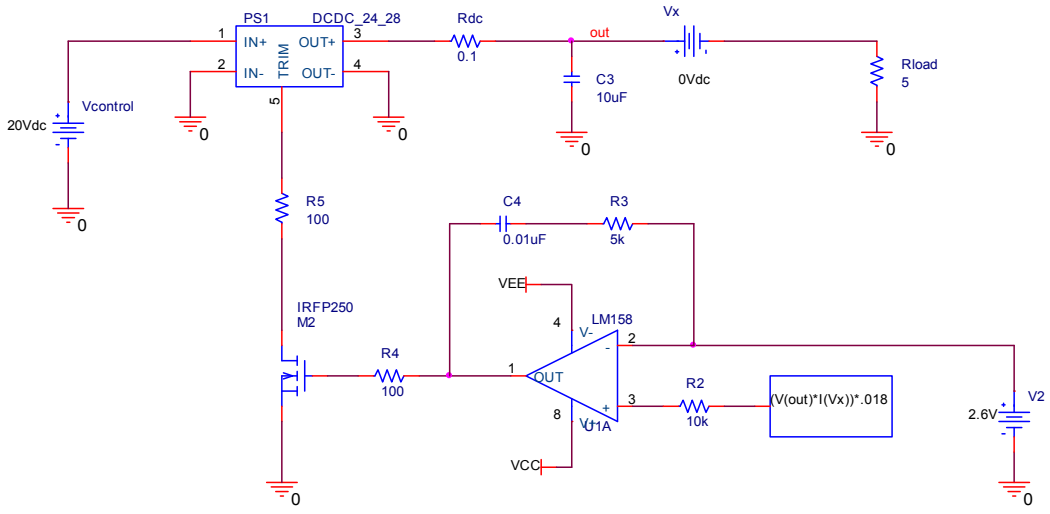

Figure 80. Fourth Step in Constant Power Circuit Design Process

3.4.5 Final Design

A signal from the DC output of the linear AC controller is fed to the input of the DC-DC converter. The output of the DC-DC converter changes between 24 and 28 V based

on the TRM pin. The TRM pin is activated by the collector of a transistor. As the power demand of the load changes, the TRM pin adjusts up or down to maintain the power at 130 W. The transistor is driven by an error amplifier which compares the power of the load represented by a voltage from the multiplier with a reference. The reference voltage is calculated based on the transfer function of the multiplier. The reference voltage was set to provide a maximum of 130 W and 6.5 A. The final design of constant power circuit can be viewed in Figure 81.

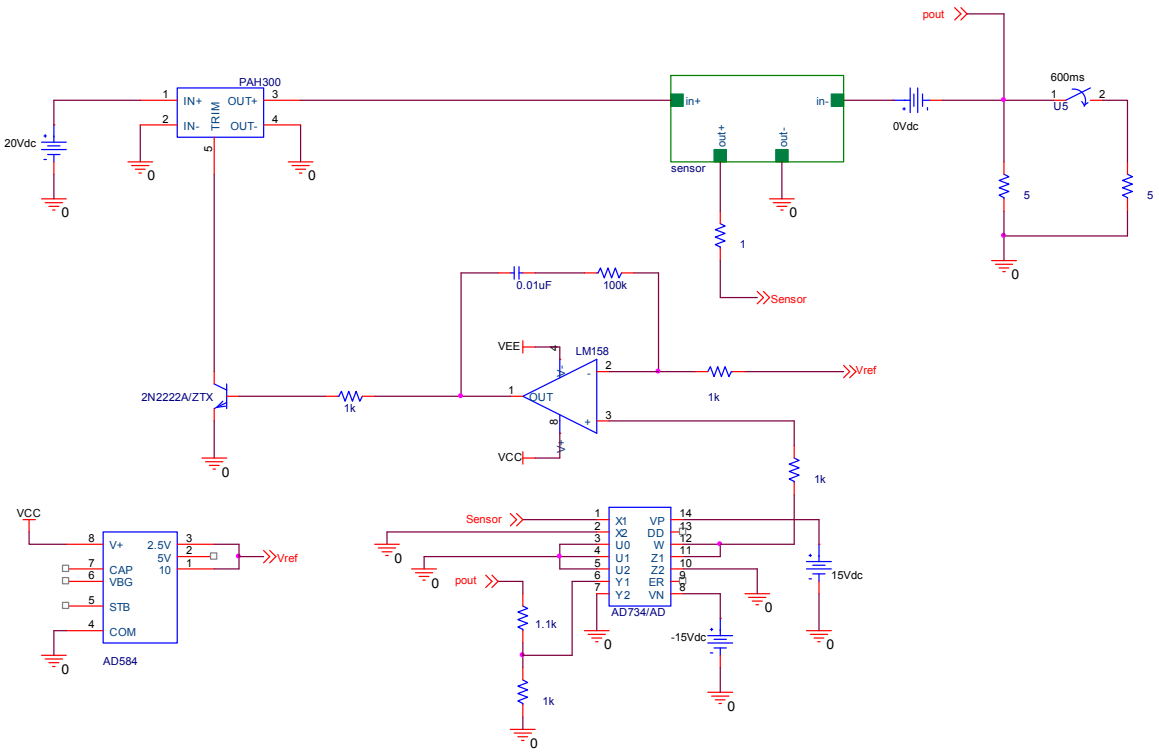

Figure 81. Final Design Constant Power Circuit

3.5 Simulation Results

Figure 82 represents the power output of the DC-DC converter for a 5 ohm load. The power output is maintained at approximately 132.85 W independent of an increase in load. This is the purpose of the constant power circuit; to maintain the power output of the linear AC controller when the load increases.

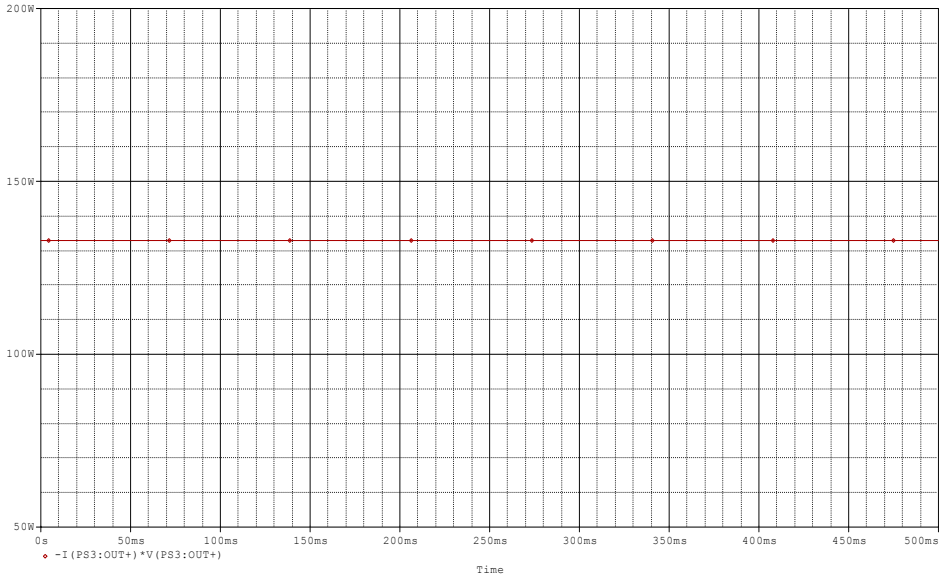

Figure 82. Constant Power Circuit Power

Figure 83 represents the output voltage of the DC-DC converter. The output voltage is 25.74 V for a 5 ohm load. The output voltage of the DC-DC converter changes based on the load. As the load is decreased, the output voltage of the converter increases. This voltage is adjusted between 24 and 28 V via the trim pin of the converter. The maximum converter output voltage is 28 V.

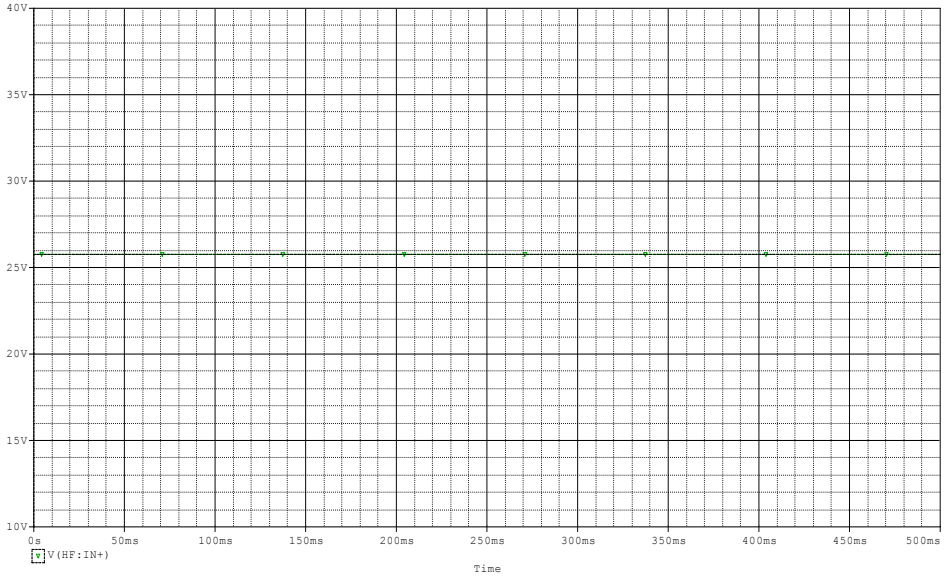

Figure 83. Constant Power Circuit Output Voltage

Figure 84 represents the output of the current sensor. The output of the current sensor is 2.06 V with a 5 ohm load. As the load decreases, the output of the current sensor increases.

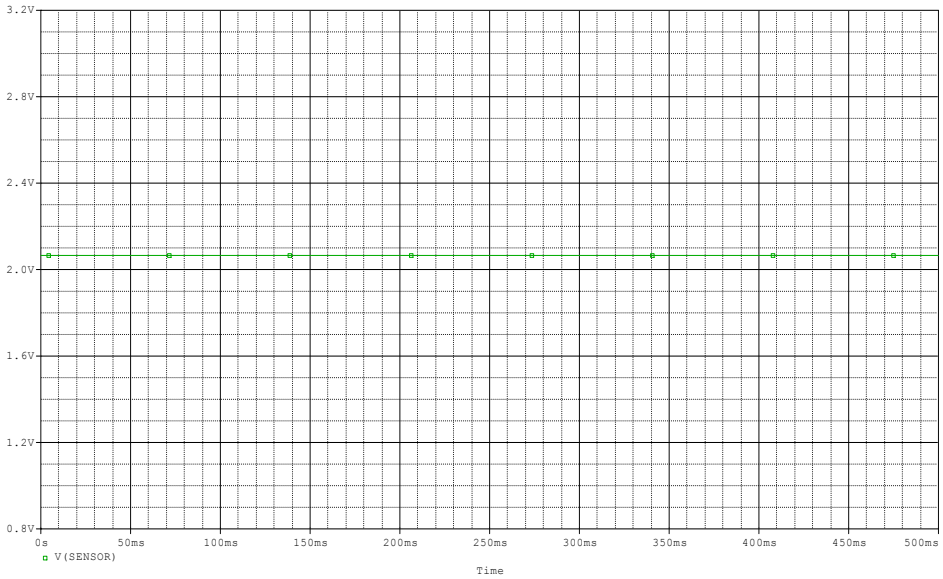

Figure 84. Constant Power Circuit Current Sensor Output

Figure 85 represents the output of the multiplier. The output of the multiplier is 2.5 V with a 5 ohm load. The output of the multiplier is scaled based on the current through the load and the voltage across it. The output of the multiplier is compared with the 2.5 V reference on the non-inverting terminal of the op-amp.

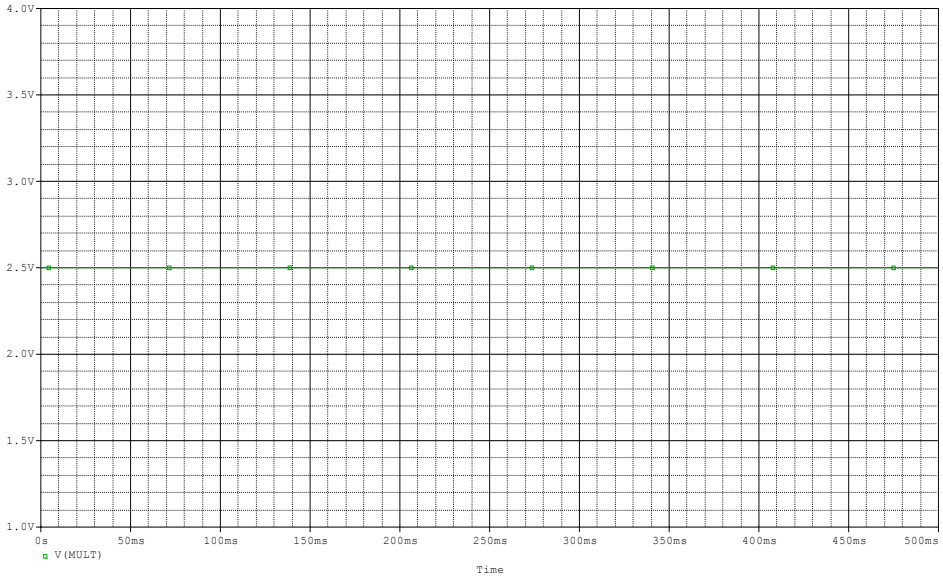

Figure 85. Constant Power Circuit Multiplier Output

Figure 86 represents the output of the op-amp. The output of the op-amp with a 5 ohm load is 0.568 V. This indicates that the difference between the multiplier output and the voltage reference is minimal. As the difference between the multiplier output voltage and 2.5 V reference on the op-amp increases, the op-amp reaches its rail voltage. The output of the op-amp is at plus or minus rail based on the multiplier output voltage.

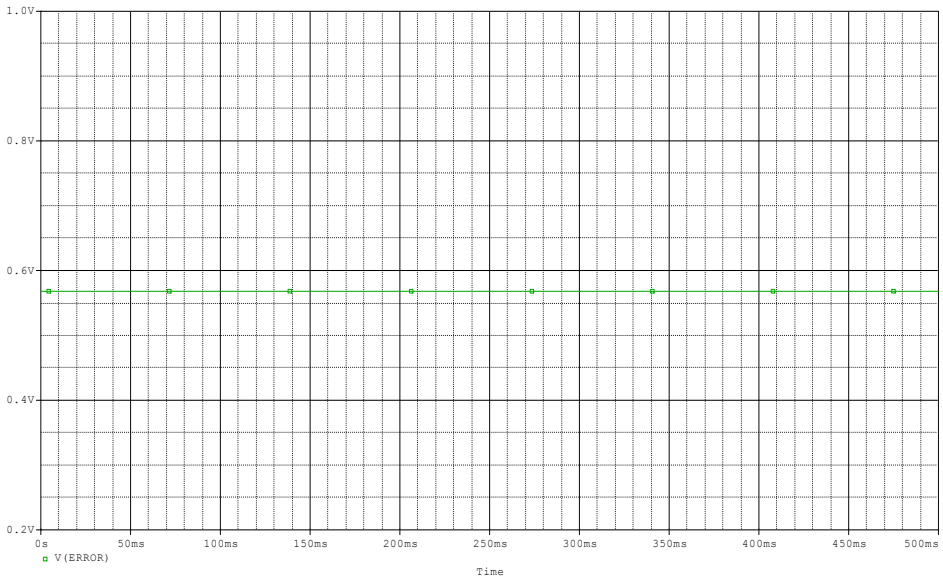

Figure 86. Constant Power Circuit Op-Amp Output

Figure 87 represents the trim voltage of the DC-DC converter. The maximum trim voltage is 1.225 V. This voltage is reached when the output of the converter is 28 V. The trim voltage of the constant power circuit is 1.03 V with a 5 ohm load. This trim voltage indicates that the DC-DC converter was adjusted above 24 V but did not reach 28 V. As the load decreases, the trim voltage increases to 1.225 V at a maximum.

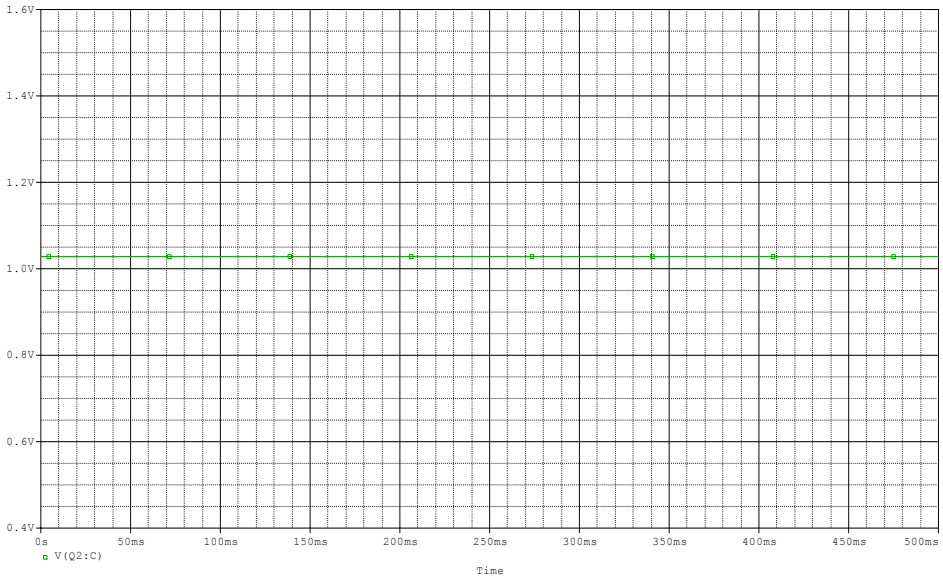

Figure 87. Constant Power Circuit Trim Voltage

Figure 88 represents the current produced by the load. The 5 ohm load current is 5.16 A.

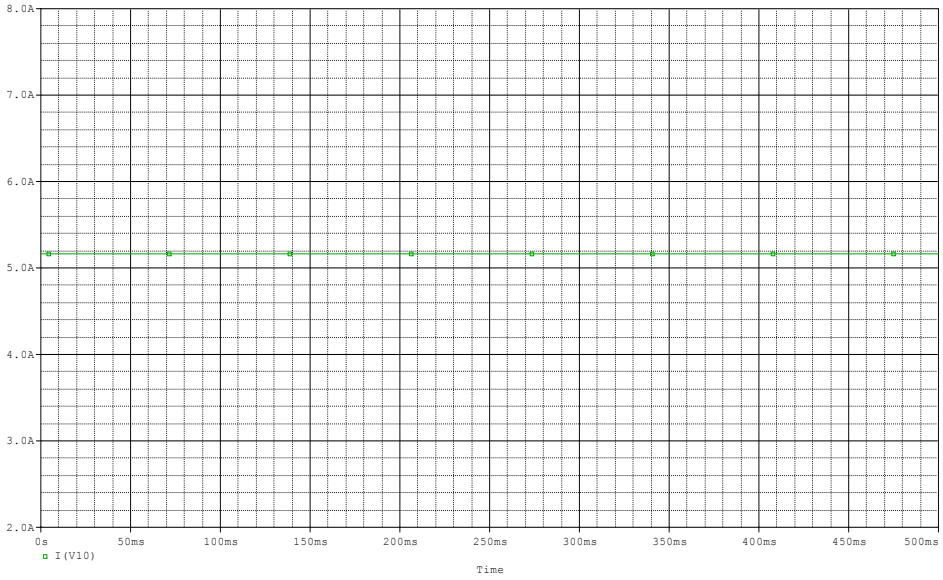

Figure 88. Constant Power Circuit Current

3.6 Constant Power Bench Test

A bench test was performed on the constant power circuit to verify that the simulations in PSpice accurately described the operation of the circuit.

3.6.1 Equipment

The following equipment was used for the constant power circuit bench test: Breadboard, Tektronix TDS3054 Oscilloscope, Dale 10 ohm load, Agilent 34401A multimeter, BK Precision 1760A DC Power Supply, Mastech HY3005C DC Power Supply, Fluke 77 multimeter, Fluke 87V multimeter, Fluke 76 multimeter.

3.6.2 Procedure

The constant power circuit was built up on a bread board according to Figure 81. The circuit was tested with a 10 ohm load. At 28 V this load produces 2.8 A of current. The

output of the DC-DC converter, output of the multiplier, output of the current sensor, output of the op-amp, and trim voltage were monitored on both multimeters and oscilloscopes.

3.6.3 Results

The circuit operated correctly and the waveforms were similar to those obtained through simulation in PSpice. Table VII displays the bench test data of the constant power circuit with a 10 ohm load. It should be noted that instrument error was not considered during experimental testing.

Load (ohms)	Vin (DCV)	Vref (DCV)	DC-DC Out (DCV)	Multiplier Out (DCV)	Trim (DCV)	Out Current Sensor (DCV)	Current (A)
10	20.0007	1.5	27.95	1.14	1.1171	1.0489	2.66

Table VII. Constant Power Circuit – Bench Test Data

Figure 89 represents the output voltage of the DC-DC converter with a 10 ohm load. The output is 27.95 V.

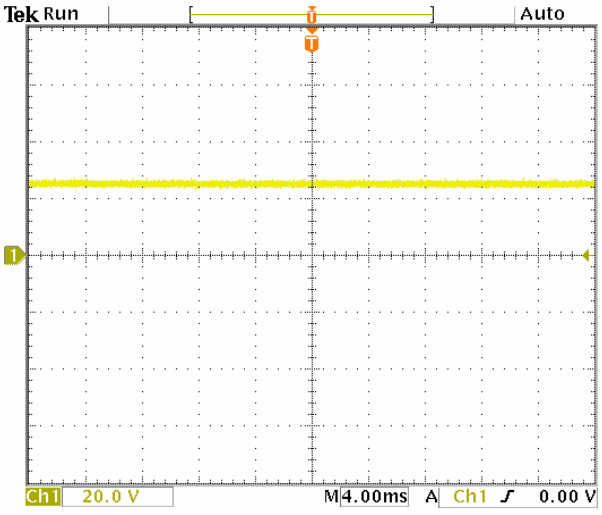

Figure 89. Constant Power Circuit Bench Test -DC-DC Output Voltage

Figure 90 represents the output of the multiplier with a 10 ohm load. The output of the multiplier was 1.14 V.

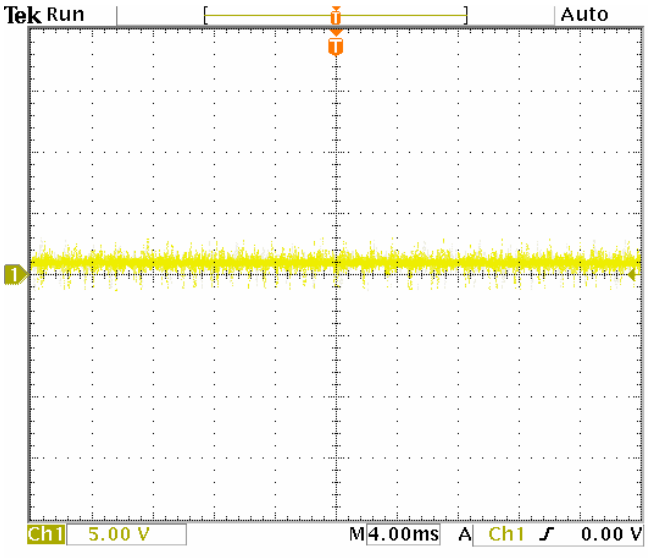

Figure 90. Constant Power Circuit Bench Test – Output of Multiplier

Figure 91 represents the trim voltage on the DC-DC converter with a 10 ohm load. The trim voltage was 1.12 V. The trim voltage changes as the load increases and decreases. The maximum trim voltage is 1.225 V. This is set by the internal circuitry of the DC-DC converter.

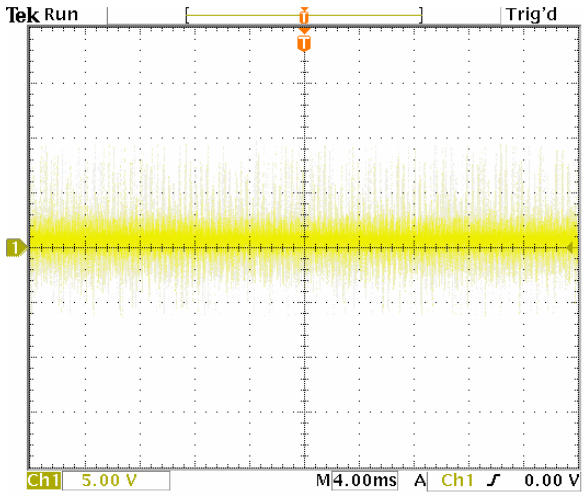

Figure 91. Constant Power Circuit Bench Test – Trim Voltage

Figure 92 represents the output of the current sensor with a 10 ohm load. The output of the current sensor was 1.05 V.

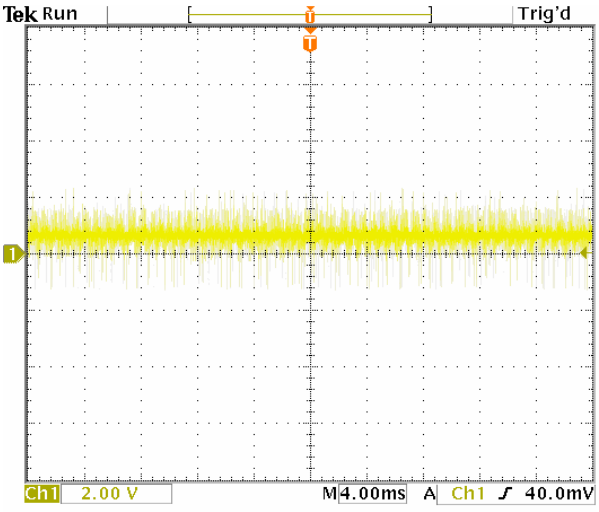

Figure 92. Constant Power Circuit Bench Test- Current Sensor Output

CHAPTER IV

LI-ION BATTERY CHARGER

The battery charger will be used to charge the Li-ion batteries. When the load increases and the stirling convertors are at maximum power, the batteries will supply the additional power needed by the load. Li-ion batteries require a specific charging scheme to operate effectively.

4.1 Lithium Ion Battery

The lithium ion cells are a high energy Lithium-ion chemistry that utilizes a mixed metal oxide cathode material and a graphitic intercalation anode. They have an organic solvent-based electrolyte with an inorganic lithium electrolytic salt. Lithium ion chemistry provides a much higher energy density and specific energy than other systems. The tolerance of a lithium ion battery is ± .05V/cell.

4.2 Charging Technique

A taper charge, constant voltage charge, with C/50 limit will be used to charge the Lithium ion batteries. The *C* refers to the capacity of the battery in Amp Hours (AH). The capacity of the battery is 55 AH. Based on the specifications in [4], the charger has a voltage limit of 4.1V/cell, a maximum charge current of C/5, a charge cutoff of C/50. Since there are 8 cells then charger voltage limit is equal to 32.8 V, charger current limit is equal to 3.5 A, and charger cutoff current is equal to 1.1 A. The charger will use a constant voltage, a current limit, and turn off when the current falls below 1.1 A. full charge is reached after the voltage has reached the upper voltage threshold and the current has dropped and leveled at 1.1 A. So, battery voltage rises slowly during the charge eventually the current tapers down, and the voltage rises to a float voltage level of 4.1 V/cell.

No trickle charge is used because the Li-ion battery is unable to absorb overcharge. Trickle charge could cause plating of metallic lithium, a condition that renders the cell unstable. Li-ion batteries are designed to operate safely within their normal operating voltage but become increasingly unstable if charged to higher voltages. Overcharging can also cause the cells to heat up.

4.3 Battery Life

Battery life can be improved by limiting the time at which the battery stays at 4.1 V/cell. Prolonged high voltage promotes corrosion, especially at elevated temperatures.

4.4 Design Process

4.4.1 First Step

At first, the battery charger was implemented with block diagrams. The block diagram can be viewed in Figure 93. Similar to the design process of the constant power circuit, the blocks were used to gain insight into the logic behind the battery charger. It was determined that the battery charger would require circuitry to limit the charge voltage of the battery and control the charge current. The Li-Ion battery charger must be turned off when the current reaches 1.1 A in order to prevent damage to the batteries. A block was implemented to designate this requirement. Based on experience from the constant power circuit, it was known that a DC-DC converter would be suitable for controlling the charge current and limiting the charge voltage.

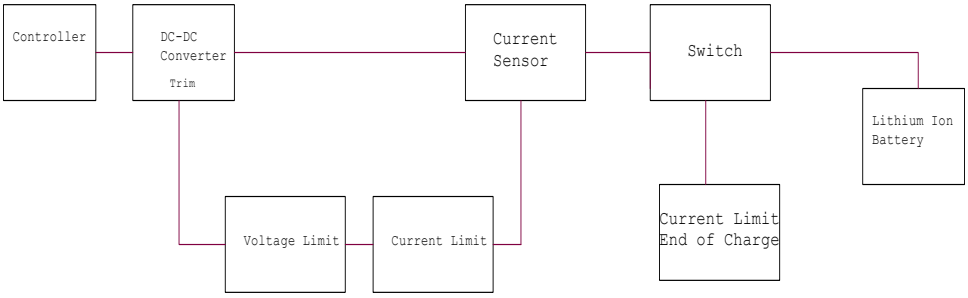

Figure 93. Battery Charger First Step

4.4.2 Second Step

Each block was considered as to find a component that would perform that operation in the block. The charge voltage can be limited by placing an adjustable resistor on the trim pin of the DC-DC converter. This was known based on the DC-DC converter test performed. This was discussed in Section 4.1. The charger current was controlled by an error amplifier. The output of the DC-DC converter adjusts to control the voltage at 3.5

A. An error amplifier is used to compare the actual current as measured by the current sensor to a reference voltage. This reference voltage is calculated as follows:

$$reference = \frac{3.5A}{2.5A/V} = 1.4V$$

When the current draw from the battery decreases, the transistor becomes an open circuit and the adjustable resistor is activated limiting the charge voltage to 32.8 V. The battery specifications limit a charge voltage to 4.1 V/cell. The battery has 8 cells giving a 32.8 V charge voltage. The vpulse component in PSpice was used to simulate the battery. This component simulates a battery effectively because it changes as a ramp function. The resistor in series with this component is used to represent the current draw of the battery.

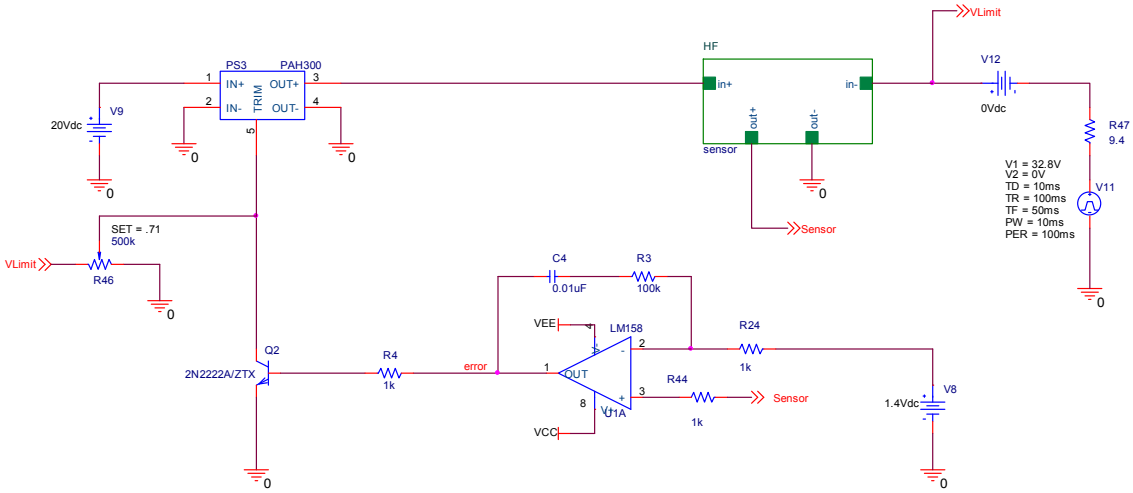

Figure 94. Battery Charger Second Step

4.4.3 Final Design

Figure 95 displays the final design of the battery charger. The final design includes the cut off circuit. The cut off circuit is designed to disconnect the battery from the battery charger when the current decreases to 1.1 A. A signal from the output of the

current sensor is connected to the non-inverting terminal of the op-amp. The op-amp compares the output of the current sensor with 0.44 V. The output of the current sensor is measured in voltage. A voltage of 0.44 V at the output of the current sensor is equivalent to 1.1 A. Initially, a push button must be pressed to energize the relay. Many options were considered to energize the relay such as a flip-flop or timer. However, the push button was the most efficient. The relay is connected between the current sensor and the battery. The relay is connected normally open. When the relay is energized then the switch is closed. When the relay is not energized then the switch opens. The op-amp is connected as a comparator so that the output of the op-amp is either at the positive or negative rail. This signal is sent to the base of the transistor which is used to energize or de-energize the relay.

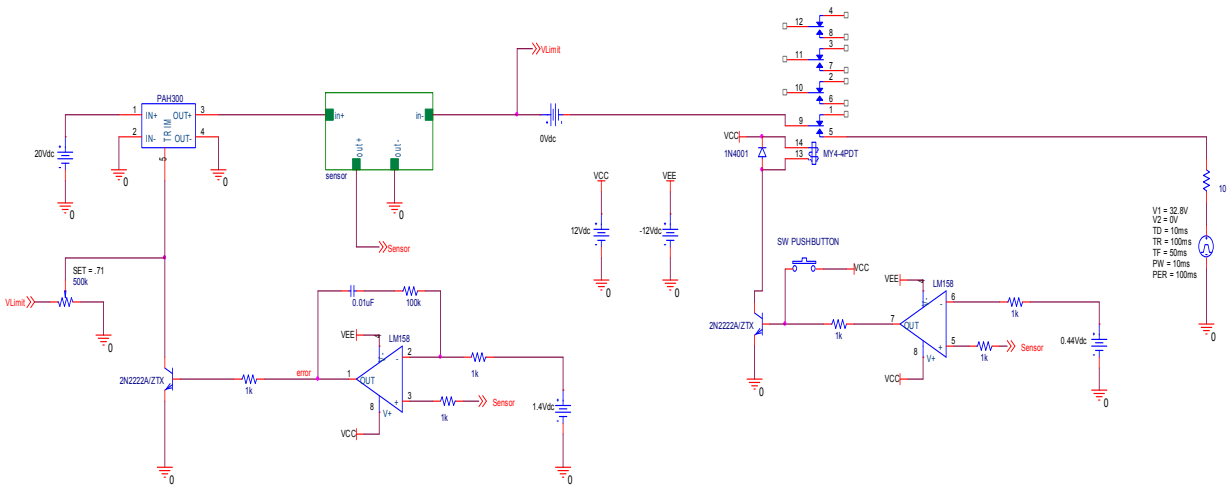

Figure 95. Battery Charger Final Design

4.5 Simulation Results

The battery charger was simulated in PSpice with a 5 and 25 ohm load. The cut off circuit of the battery charger was not simulated. The relay used in the design does not have a PSpice model and simulating a relay in PSpice is not reliable. The cutoff circuit was bench tested.

Figure 96 represents the PSpice simulation of the output of the DC-DC converter with a 25 ohm load. The output of the DC-DC converter is 32.806 V. The potentiometer is set so that the maximum output voltage of the DC-DC converter is 32.8 V. This voltage corresponds to the maximum charging voltage of the batteries. As the current draw of the battery decreases below 3.5 A the output of the DC-DC converter increases.

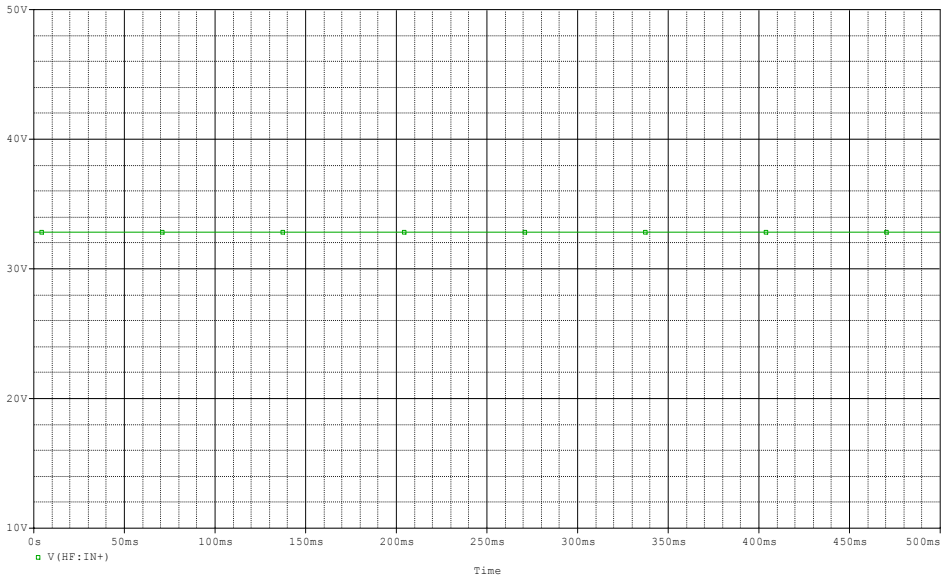

Figure 96. Battery Charger Simulation – Output of DC-DC Converter

Figure 97 represents the output of the DC-DC converter with a 5 ohm load. The output of the DC-DC converter was 17.501 V. The output of the DC-DC converter decreases as the load increases in order to maintain the current at 3.5 A.

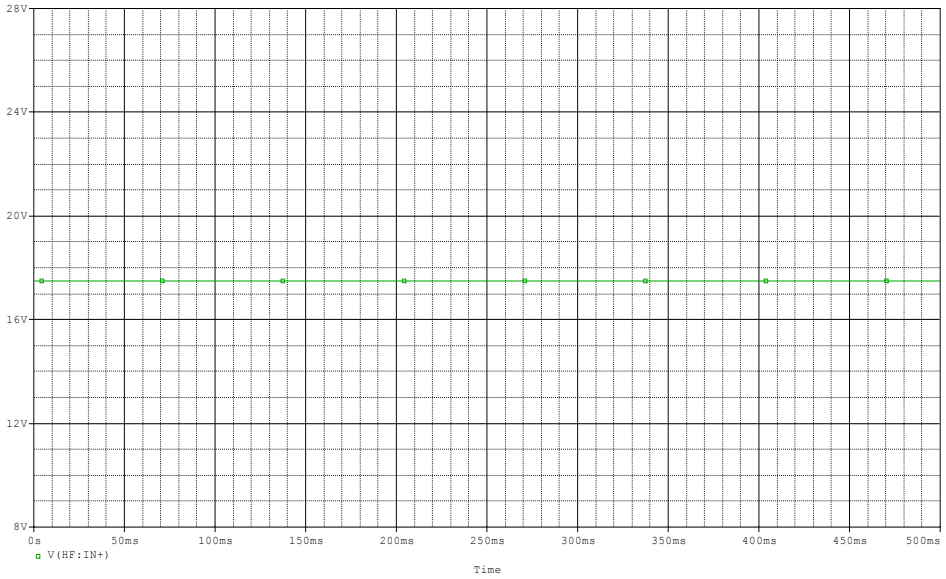

Figure 97. Battery Charger Simulation – Output of DC-DC Converter - 5 ohm load

Figure 98 represents the simulation of the output of the current sensor. The output of the current sensor was 0.524979 V with a 25 ohm load.

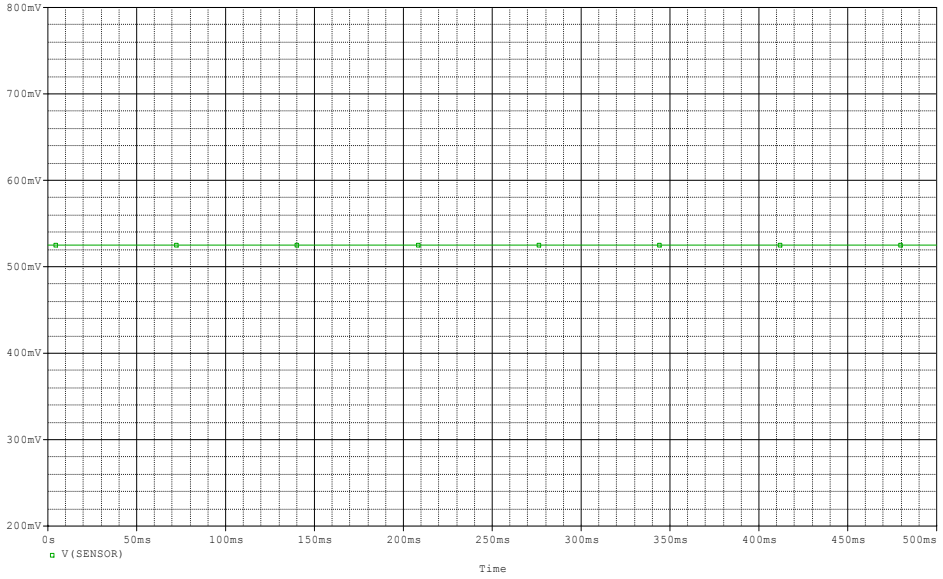

Figure 98. Battery Charger Simulation – Output of Current Sensor – 25 ohm load

Figure 99 represents the simulation of the output of the current sensor with a 5 ohm load. The output of the current sensor was 1.4 V.

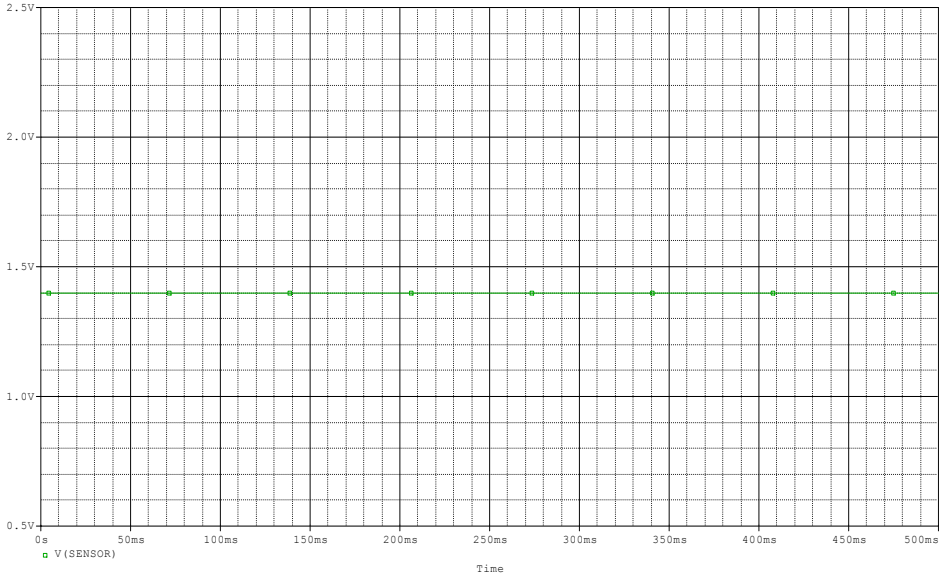

Figure 99. Battery Charger – Simulation – Output of Current Sensor – 5 ohm load

Figure 100 represents the simulation of the trim voltage. The trim voltage was 0.306 V with a 5 ohm load. The trim voltage will increase as the output of the DC-DC converter increases and will increase above 1.225 V due to the potentiometer.

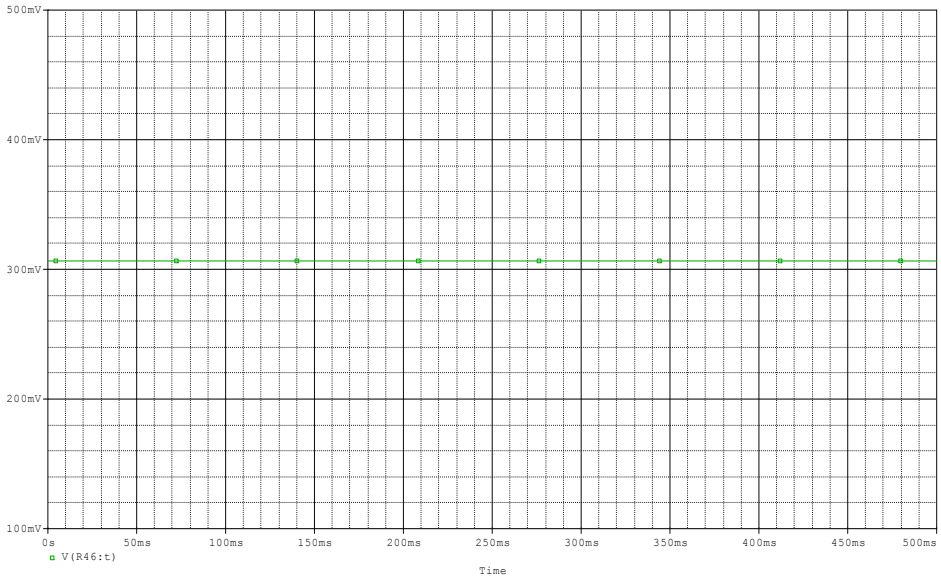

Figure 100. Battery Charger Simulation – Trim Voltage 5 ohm load

Figure 101 represents the simulation of the trim voltage with a 25 ohm load. The trim voltage was 1.65 V

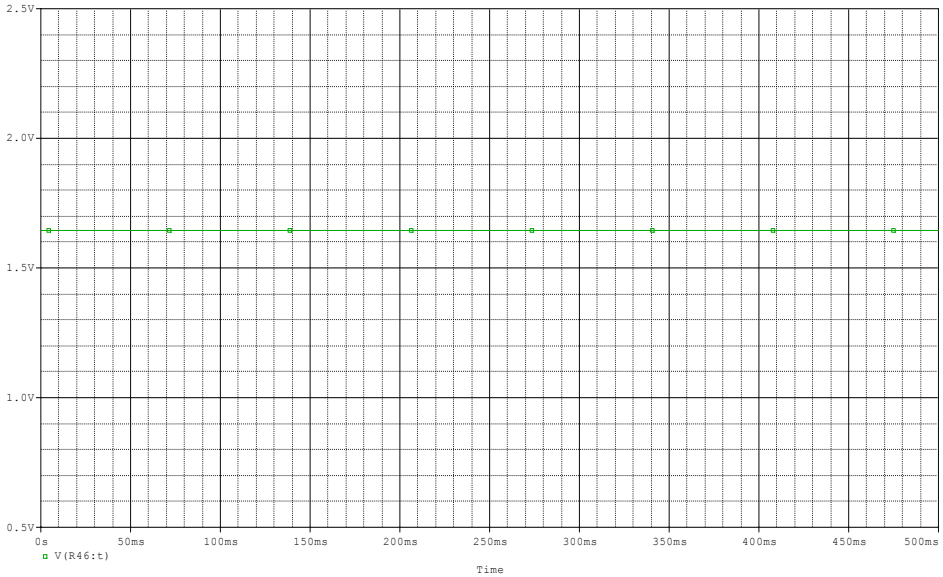

Figure 101. Battery Charger Simulation – Trim Voltage – 25 ohm load

Figure 102 represents the simulation of the current with a 25 ohm load. The current was 1.31 A.

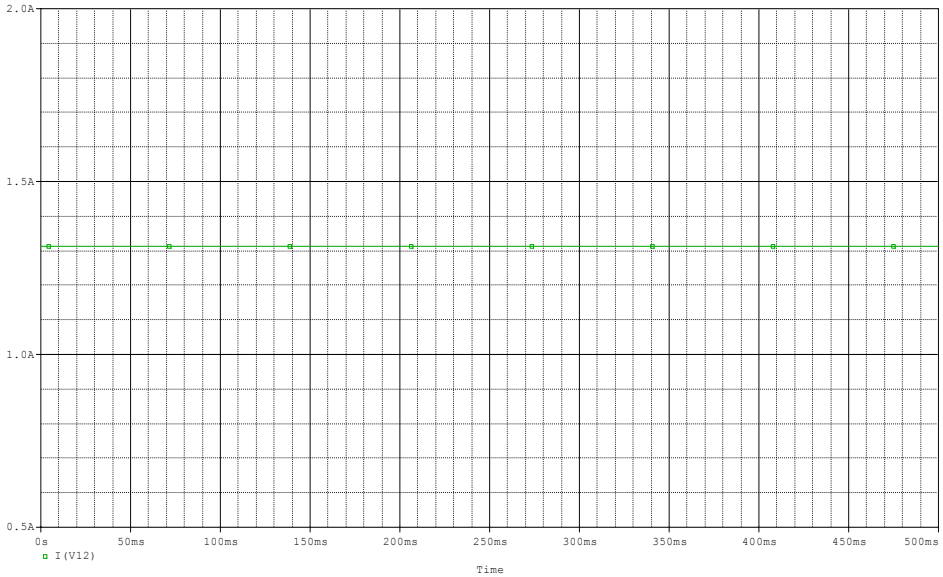

Figure 102. Battery Charger – Simulation- Current with 25 ohm load

Figure 103 represents the simulation of the current with a 5 ohm load. The current was 5 A.

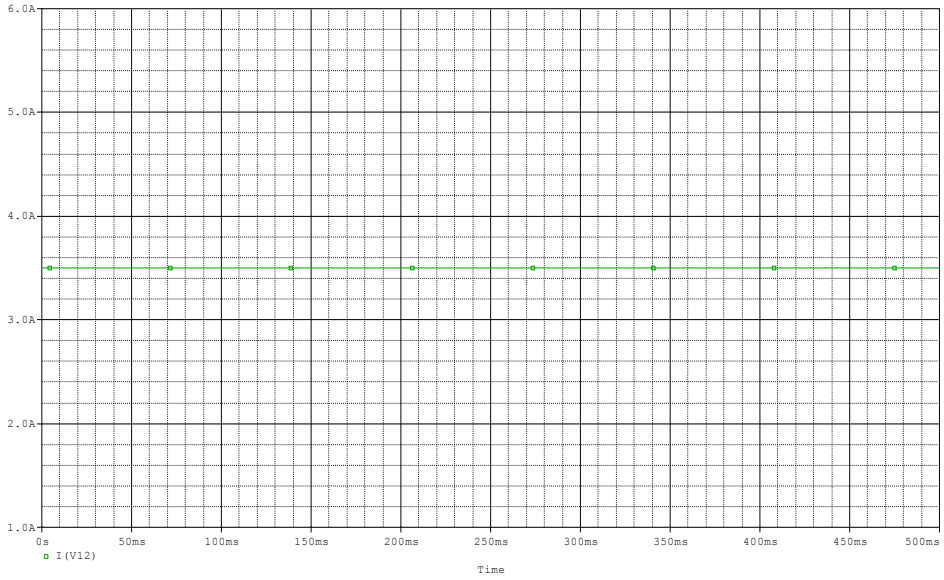

Figure 103. Battery Charger – Simulation – Current with 5 ohm load

4.6 Battery Charger Bench Testing

A bench test was performed on the battery charger to verify that the simulations in PSpice accurately described the operation of the circuit.

4.6.1 Equipment

The following equipment was used during the bench test of the battery charger: breadboard, Tektronix TDS3054 Oscilloscope, Hewlett Packard 6060B DC Electronic Load, Agilent 34401A multimeter, Kikusui PAD Regulated DC Power Supply, BK Precision 1760A DC Power Supply, Mastech HY3005C DC Power Supply, Fluke 77 multimeter, Fluke 87V multimeter, Fluke 76 multimeter.

4.6.2 Procedure

The battery charger was built up on a bread board according to Figure 87. The cutoff circuit was tested separately from the current control and voltage limit portion. The

circuit was tested with a DC electronic load. The load was changed between 4-20 ohms. At each of these loads, the output of the DC-DC converter, trim, current and output of the current sensor were monitored with multimeters and an oscilloscope.

4.6.3 Results

Table VIII represents the data obtained from each of the four multimeters at 5 load values. It should be noted that instrument error was not considered during experimental testing.

VIN (DCV)	Load (ohms)	Current Sensor Out (VDC)	Current (A)	DC-DC Converter Out (VDC)	Trim (VDC)
19.941	20	0.6508	1.609	32.48	1.546
19.941	15	0.8478	2.124	32.47	1.5217
19.941	10	1.2386	3.134	32.62	1.4768
19.941	8	1.3627	3.451	29.21	1.183
19.941	5	1.396	3.513	19.22	N/A

Table VIII. Battery Charger Bench Test Results

Table IX represents the bench test data taken with a 5 and 25 ohm load. These values can be used to compare the PSpice simulations with the bench test data.

Load (ohms)	Input Voltage (DCV)	Trim (V)	DC-DC Output (V)	Load Current (A)	Sensor (V)
25	19.603	1.5916	32.8	1.286	0.502
5	19.603	0.3318	19.44	3.478	1.369

Table IX. Experimental vs. Simulation Operation

The cutoff circuit was tested. The relay opened (disconnected the battery) when the current was at 1.1 A. The relay was closed when the current was greater than 1.1 A.

Figure 104 represents the DC-DC output voltage with a 5 ohm load. The output voltage is 19.44 V.

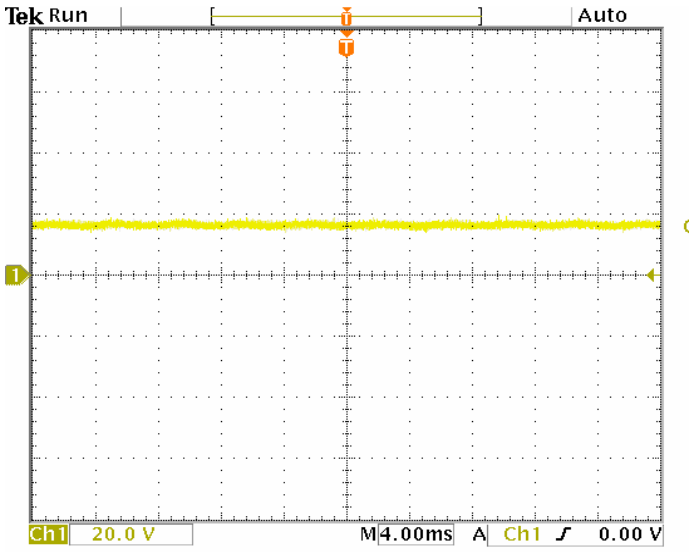

Figure 104. Battery Charger Bench Test – DC-DC Output Voltage – 5 ohm load

Figure 105 represents the output of the current sensor with a 5 ohm load. The output of the current sensor was 1.369 V.

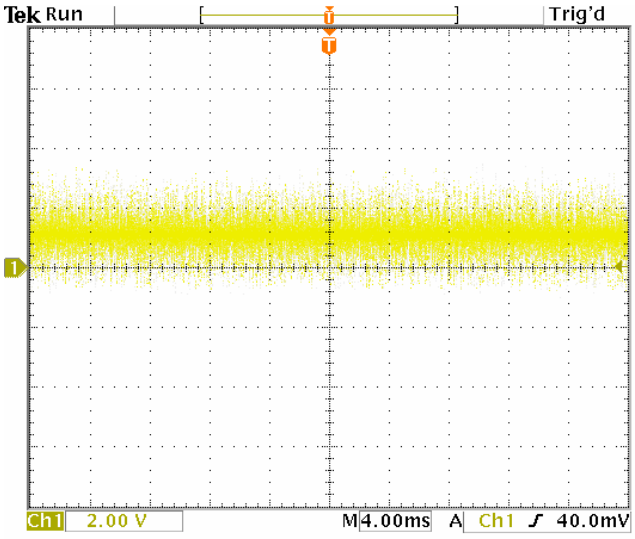

Figure 105. Battery Charger – Bench Test – Output of Current Sensor – 5 ohm load

Figure 106 represents the trim voltage with a 5 ohm load. The trim voltage was 0.33 V.

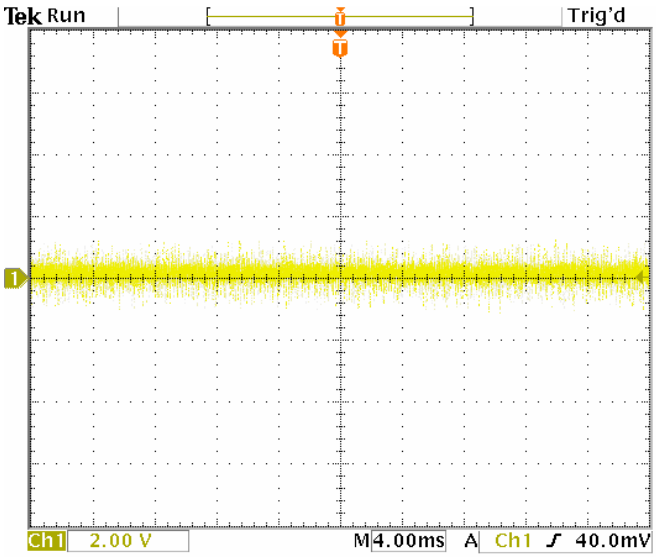

Figure 106. Battery Charger – Bench Test – Trim Voltage – 5 ohm load

Figure 107 represents the DC-DC converter output voltage with a 25 ohm load. The DC-DC converter output voltage was 32.8 V. This would be expected with a 25 ohm load because the current is decreasing and the voltage limit portion of the circuit is performing to maintain the charge voltage at 32.8 V.

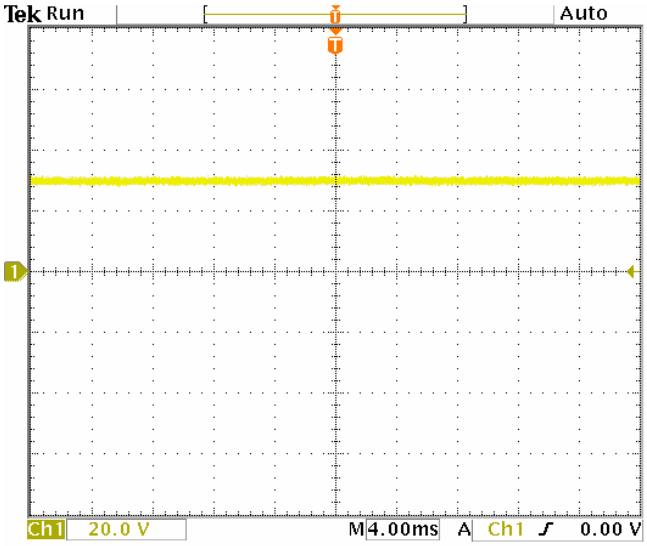

Figure 107. Battery Charger – Bench Test – DC-DC Converter Out – 25 ohm load

Figure 108 represents the trim voltage with a 25 ohm load. The trim voltage was 1.59 V because the DC-DC converter output is increasing to maintain the charge voltage.

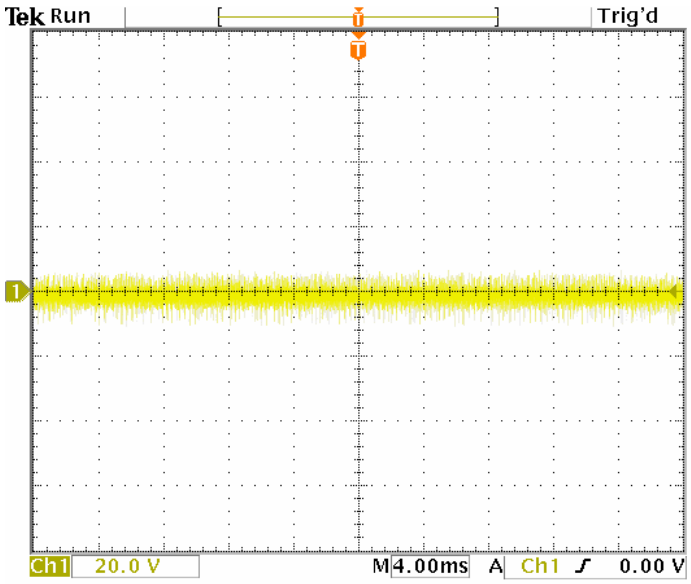

Figure 108. Battery Charger – Bench Test – Trim Voltage – 5 ohm load

Figure 109 represents the output of the current sensor with a 25 ohm load. The output of the current sensor was 0.5 V.

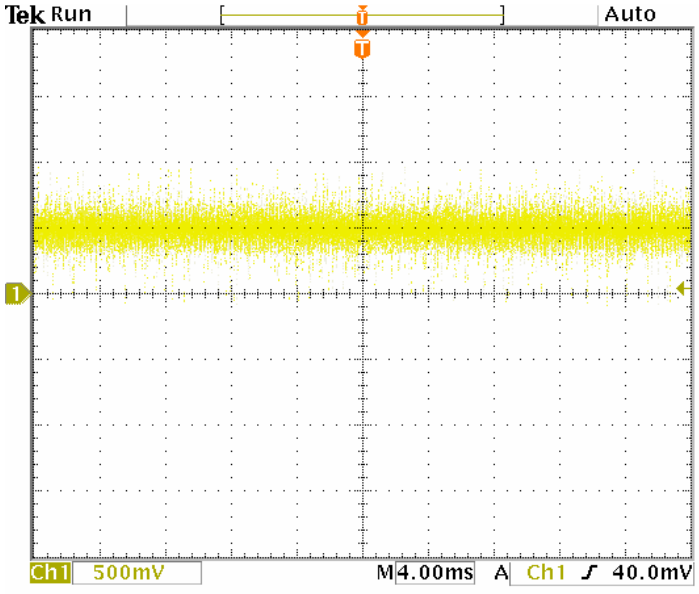

Figure 109. Battery Charger – Bench Test – Output Current Sensor – 25 ohm load

4.6.4 Summary

The data in Table VIII and Table IX verifies that the battery charger current control and voltage limit are operating correctly. The current is controlled when the current sensor output is at 1.4 V or above. This indicates that the battery is drawing less than 3.5 A. When the battery is drawing less than 3.5 A the battery is charging and the voltage limit circuit is operating. As indicated in Table VIII the DC-DC converter output voltage is 32.5 V when the current is less than 3.5 A. The PSpice simulations with a 25 and 5 ohm load match the bench test results.

CHAPTER V

SYSTEM INTEGRATION

5.1 Constant Power Circuit Pspice Integration

Figure 110 represents the constant power circuit integrated with the controller.

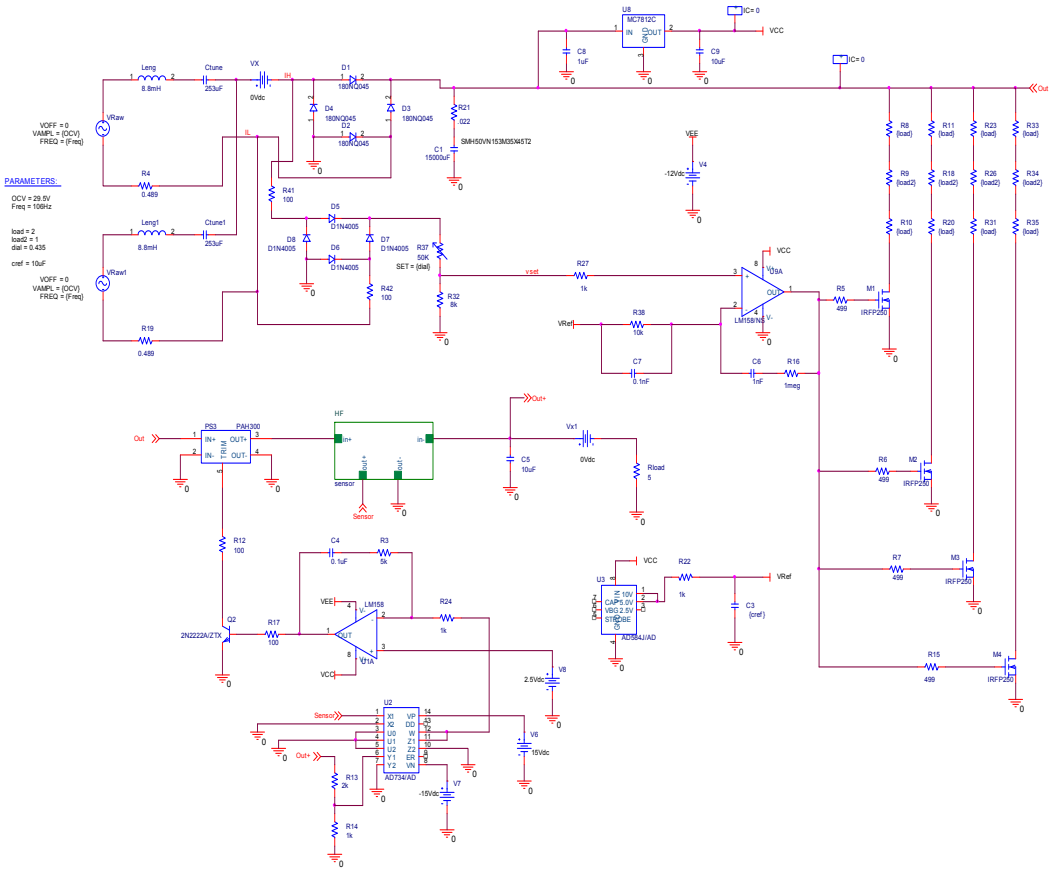

Figure 110. Integration of Constant Power Circuit and Linear AC Regulator

Figure 111 represents the output power of the DC-DC converter, input power of the linear AC regulator, DC-DC converter output voltage, and the DC output of the linear AC regulator. The power output of the linear AC regulator is 138.57 W and the constant power circuit maintains this power at 131.19 W even if the load demand increases. The figure below verifies that the constant power circuit is operating correctly and is compatible with the linear AC regulator. The DC output voltage of the linear AC regulator is 19.342 V. The output of the DC-DC converter is 25.65 V.

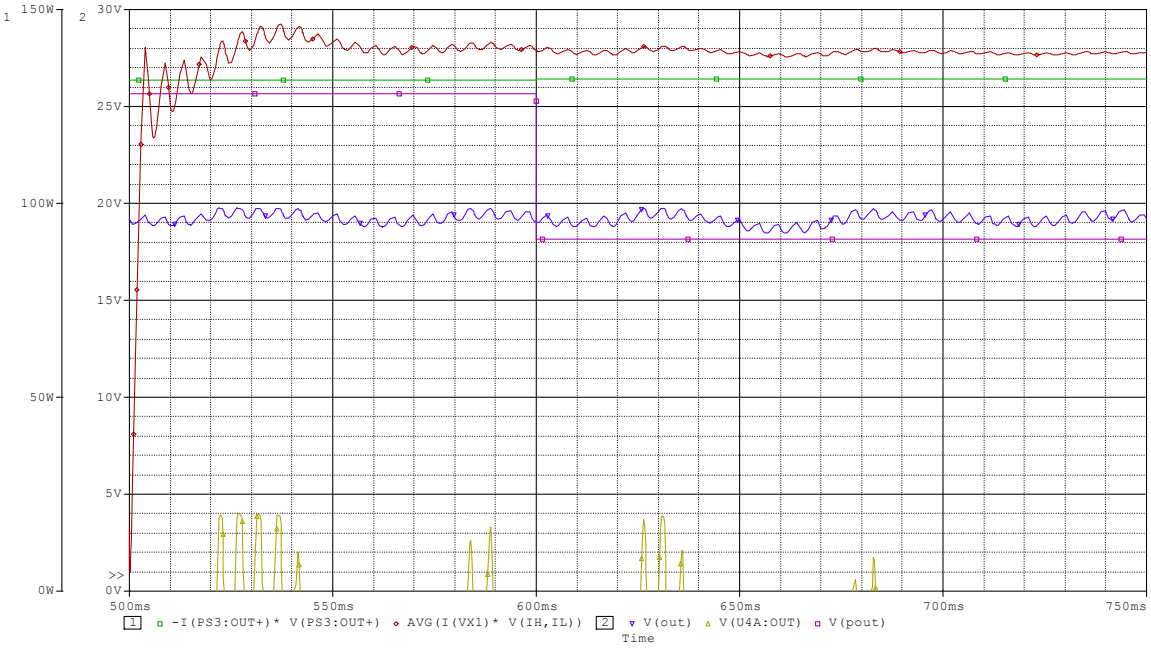

Figure 111. Simulation of Constant Power Circuit and Linear AC Regulator

5.2 System Integration Bench Test

The purpose of the system integration bench test is to verify that the constant power circuit and battery charger operate together properly.

5.2.1 Equipment

The following equipment was used for the integration bench test: breadboard, Tektronix TDS3054 Oscilloscope, Hewlett Packard 6060B DC Electronic Load, Agilent 34401A multimeter, Kikusui PAD Regulated DC Power Supply, BK Precision 1760A

DC Power Supply, Mastech HY3005C DC Power Supply, Fluke 77 multimeter, Fluke 87V multimeter, Fluke 76 multimeter.

5.2.2 Procedure

The integration test was set up according to Figure 7. The DC electronic load was placed between the two diodes in Figure 7 where it reads Rover World Power Bus. The Li-ion battery was represented by a DC power supply. To start, the voltage reference on the constant power circuit was changed to meet different power demands. The voltage reference was set to 0.75 V, which allows maximum power at 15 ohms. The voltage reference was also set to 1.12 V, which allows a maximum power at 10 ohms. Once the voltage reference was adjusted then the DC power supply voltage was adjusted to represent the voltage of a Li-ion battery. This voltage must be set below the maximum constant power circuit output voltage. The DC electronic load was set for resistances from 7-15 ohms. When the DC power supply started drawing current, this represented the Li-ion batteries supplying additional power to the load.

5.2.3 Results

Table X represents the integration test data with a constant power circuit reference voltage of 0.75 V. This set point limits the current to 1.399 A for a 20 ohm load.

$$sensor\_out = \frac{27.98V / 20ohms}{10A / 4V} = 1.399A$$

Constant Power Current (A)	Battery Current (A)	Constant Power Voltage (V)	Vref Constant Power (V)	Load (ohms)	Battery Voltage (V)	Vin (V)
1.3	0	27.98	0.75	20	25	19.67
0.99	0.59	25.73	0.75	15	25	19.67
1.86	0	25.27	0.75	15	20	19.67

Table X. Integration Test - Maximum Power at 15 ohm Load

Table X demonstrates that the integration of the constant power circuit and battery charger was successful because the battery voltage was greater than the constant power voltage when the battery drew current. It should be noted that instrument error was not considered during experimental testing.

Table XI shows the results of the integration test at higher power. This test was performed with loads from 7-12 ohms. The voltage reference was set so that a maximum power was reached at 10 ohms. The data shows that the battery voltage was set greater than the constant power circuit and the battery started supplying additional power. It can also be seen that when the maximum power of 10 ohms was reached then the batteries started supplying current. Table XI confirms that the constant power circuit maintains maximum power when the batteries supply additional power because this table shows that the constant power current and voltage remain constant as the load increases and the battery supplies additional power to the load.

Constant Power Current (A)	Battery Current (A)	Constant Power Voltage (V)	Vref Constant Power (V)	Load (ohms)	Battery Voltage (V)	Vin (V)
2.09	0	27.97	1.12	12	26.529	19.67
0.91	1.5	26.57	1.12	10	26.529	19.67
0.93	2.04	26.47	1.12	8	26.529	19.67
0.98	2.37	26.44	1.12	7	26.529	19.67

Table XI. Integration Test – Maximum Power at 10 ohm Load

5.2.4 Test Summary

The integration of the constant power circuit and the battery charger was successful. The battery supplied additional power when the linear AC regulator reached its maximum power output. It also demonstrated that the diodes in the circuit operated properly because the batteries did not supply power unless the battery voltage was greater than the constant power circuit output voltage.

CHAPTER VI

CONCLUSION

This paper discussed the design of support equipment for the ASRG simulator. The ASRG simulator and support equipment will be used on a lunar concept rover. At this time, a rover is in the process of being built. When it is completed, the ASRG simulator and Li-ion batteries will be used to power the rover.

The linear AC regulator will be used to control the ASRG simulator. A survey of six controllers was performed in order to choose a controller that would work effectively in a rover application. The initial evaluation of the six controllers included voltage monitoring, load staging, power dissipation technique, tuning, necessity of a DC-DC converter, and the power factor controller. When the initial evaluation was complete, three controllers were eliminated. The final evaluation included efficiency, number of components, and stability. The linear AC controller exceeded the other controllers in all categories. The linear AC regulator has the highest efficiency. This is important in this application. Various tests were performed on the linear AC regulator including bench testing, integration of controller and EE-35's, and efficiency testing.

A constant power circuit was designed to maintain the power at the output of the linear AC controller at its maximum when the batteries supply additional power to the load. The constant power circuit was designed and simulated in Pspice. The constant power circuit was bench tested on a bread board to verify that it was operating properly. This test also verified that the simulations in PSpice were accurate.

The battery charger was designed for constant voltage charging. The battery charger also protects the batteries by controlling the charger cut off current at 1.1 A. The battery charger was designed and simulated in PSpice. The battery charger was bench tested on a bread board to verify that it was operating properly. This test also verified that the simulations in PSpice were accurate.

An integration test of the constant power circuit and battery charger was performed. It was verified that the constant power circuit was maintained at maximum power while the batteries were supplying additional power. It also confirmed that the batteries supply additional power when the battery voltage exceeds the output voltage of the constant power circuit.

CHAPTER VII

FUTURE WORK

Plans have been made to add an adjustable resistor to the trim pin on the constant power circuit DC-DC converter. This will allow batteries greater than 28 V to be integrated into the system.

The battery charger design may be modified to accommodate other batteries than a Li-ion battery. Each battery requires a specific charging method.

The ASRG simulator and support equipment will be demonstrated on a lunar concept rover when the rover design is complete.

The tolerances of the instruments used during experimental testing were not considered. These tolerances will be considered in the future. This will aid in explaining the large difference between the experimental and theoretical efficiency of the linear AC regulator.

REFERENCES

[1] Thermal Energy Conversion Branch, Operation of a Free-Piston Stirling Convertor, http://www.grc.nasa.gov/WWW/tmsb/stirling/intro_stirling/Slidepage_1.html

[2] Jeffrey Schreiber, "Developmental Considerations on the Free-Piston Stirling Convertor for Use in Space", International Energy Conversion Engineering Conference, San Diego, 2006

[3] Richard Shaltens, Wayne Wong, "Advanced Stirling Technology Development at NASA Glenn Research Center", NASA Science Technology Conference, Maryland, 2007

[4] Salvatore Oriti, Gina Blaze, "Advanced Stirling Convertor Testing at NASA Glenn Research Center", International Energy Conversion Engineering Conference, St. Louis, 2007

[5] Douglas K Leland, Joel F. Priest, Douglas Keiter, Jeffrey G. Schreiber, "Development of a Power Electronics Controller for the Advanced Strirling Radioisotope Generator", International Energy Conversion Engineering Conference, 2007

[6] Timothy Regan, "Free Piston Stirling Convertor Controller Development at NASA Glenn Research Center", International Energy Conversion Engineering Conference, 2003

[7] Henry W. Brandhorst, Jr., "Future NASA Multi-kilowatt Free Piston Stirling Applications", International Energy Conversion Engineering Conference, 2006

[8]Paul C. Schmitz, L. Barry Penswick, Richard K. Shaltens, "Stirling Isotope Power Systems for Stationary and Mobile Lunar Applications", International Energy Conversion Engineering Conference, 2006

[9] Michael H. Brace, Electrical Engineer, NASA Glenn Research Center, Michael.H.Brace@nasa.gov

[10] PAH 300 Series Instruction Manual, Densei Lambda, http://www.densei-lambda.com/products/sps/ps_pm/pah350s/indexe.html

[11] PAH 300 Series Specification Sheet, Densei Lambda, http://www.lambdapower.com/ftp/Specs/pah300-450.pdf

[12] Operating Procedure for NCP55-2 Lithium-Ion Cell, Lithion Inc., Thomas.B.Miller@nasa.gov

[13] 10 MHz 4- Quadrant Multiplier/Divider, Analog Devices, http://www.analog.com/UploadedFiles/Data_Sheets/66167428AD734_c.pdf

[14] Power Mesh II MOSFET, International Rectifier, http://www.vishay.com/docs/90277/90277irf.pdf

APPENDIX

APPENDIX A
(PSpice Code for DC-DC Converter Model)

The following code was written in the PSpice model editor.

```
Rover PHA300 24V to 28V DC-DC Convertor
* ideal spice model
* active input and output
* 7/30/2007
* modified trim circuit
*
usage:      name  in+ in- out+ out- trim
.subckt PAH300 1 2 3 4 5
GIN 2 1 VALUE={((V(3)-V(4))/(V(1)-V(2)))*I(EOUT)}
VTRIM 6 4 DC 1.225V
EOUT 3 4 Value={22.857*(v(7)-v(4))}
RTRIM1 6 7 1K
RTRIM2 7 5 1k
.ends PAH300
```